2018

RIPK1 and Myosin IIA-dependent Ceramidosomes form Plasma Membrane Pores to Mediate Blebbing and Necroptosis

Rose N. Nganga
Medical University of South Carolina

RIPK1 and Myosin IIA-dependent Ceramidosomes form Plasma Membrane Pores to Mediate Blebbing and Necroptosis

By

Rose N. Nganga

A Dissertation submitted to the Medical University of South Carolina in partial fulfillment of the requirements for the degree of Doctor of Philosophy in College of Graduate Studies.

Biochemistry and Molecular Biology Department

Medical University of South Carolina

May 2018

Approved by,
Advisory committee

Besim Ogretmen, PhD, Chairman

Alan Diehl, PhD

Robert Gemmill, PhD

Christina Voelkel-Johnson, PhD

Vamsi Gangaraju, PhD

Table of Contents

ACKNOWLEDGEMENTS

First and foremost, I would like to thank Dr. Besim Ogretmen for his invaluable support and mentorship through the course of my PhD training. Without you, this work would not have been accomplished. I truly appreciate you for the support and guidance you have provided for me in my professional career. I am also grateful to my committee members, Drs. Alan Diehl, Robert Gemmill, Christina Voelkel-Johnson, and Vamsi Gangaraju, their scientific input and guidance was invaluable and I would not be where I am without their guidance and support in my scientific journey.

I would like to thank Drs. Cynthia Wright, Edward Krug, Sue Hennigan, Laura Kasman and the whole IMSD group. I would also like to thank my collaborators, Dr. Eric Bieberich (U. of Kentucky), Dr. Robert Stahelin (Purdue U.), Kristen Johnson (UT South Western) Jason Pierce, Barbara Rembiesa, Silva Tersiva and Aiping Bai (MUSC lipidomics)

Much regards to my lab mates, former and current, Natalia Oleinik, Jisun Kim, Mohammed Dany, Raquela Thomas, Kyla Baron, Silvia Vaena-Avalos, Shanmugam Panneer Selvam, Salih Gencer, Braden Roth and Ryan De Palma. Through your support, assistance and feedback, I have been able to get this far.

Words cannot describe how grateful I am to my family, my mother, Mary K. Mutiso, my rock and my number one cheerleader, my brothers George and Christopher Ndeto, my constant motivators. My loving husband Martin K. Nganga, my love, thank you for your love, support and your continuous encouragement.

Finally, I thank God, for being the light to my path and for teaching me to trust his timing.

LIST OF TABLES

LIST OF FIGURES

LIST OF ABBREVIATIONS

AML- Acute Myeloid Leukemia

Bstatin-Blebbistatin

BSA- Bovine Serum Albumin

CDase-Ceramidase

CerS- Ceramide Synthase

CERK- Ceramide Kinase

CERT- Ceramide Transfer protein

CML- Chronic Myelogenous Leukemia

DES- Dihydroceramide Desaturase

DMSO: Dimethyl sulfoximide oxide

EDTA- Ethylene diamine tetra acetic acid

ER- endoplasmic reticulum

FB1- Fumonisin B1

FBS-Fetal Bovine Serum

GFP-Green Fluorescent Protein

GPMV-Giant Plasma Membrane Vesicles

GSC- Germline Stem Cells

HPV-Human papilloma virus

I2PP2A-Inhibitor 2 of PP2A

LC/MS- liquid chromatography mass spectrometry

LDH- Lactase Dehydrogenase

LPA- Lipoprotein A

MLKL- Mixed Lineage Kinase Like protein

NSCLC- Non-small cell lung cancer

Nec-1-Necrostatin-1

NMIIA- Non-Muscle Myosin IIA

NSA- Necrosulfonamide

PBS: Phosphate Buffered Saline

PCR- polymerase chain reaction

PI- Propidium Iodide

PM-Plasma Membrane

PP2A- Protein phosphatase 2 A

RIPK1-Receptor Interacting Protein Kinase 1

RIPK3- Receptor Interacting Protein Kinase 3

ROS-Reactive Oxygen Species

SCLC-small cell lung cancer

scr-scramble

SEM-Scanning Electron microscopy

S1P-Sphingosine 1 phosphate

S1PRs- Sphingosine 1-phosphate receptors

shRNA-Short hairpin RNA

siRNA-Small interfering RNA

SK/SphK-Sphingosine Kinase

SM- Sphingomyelin

SMase- sphingomyelinase

SPT/SPTLC- Serine pamitoyl transferase

TEM-Transmission Electron Microscopy

TNFα- Tumor Necrosis Factor alpha

WT-Wild type

ZVAD-FMK- carbobenzoxy-valy-alanyl-aspartyl-o-methyl-fluoromethylketone

ABSTRACT

Sphingolipids have over the years, been explored as cancer therapy targets. FTY720 (Fingolimod, Gilenya) is a sphingosine analogue drug used for the treatment of multiple sclerosis. FTY720 is phosphorylated by sphingosine kinase 2, to generate P-FTY720 to exert its immunosuppressive properties through binding to sphingosine -1 phosphate receptors (S1PRs). FTY720 also exhibits anti-cancer properties. Our previous studies indicated that FTY720's anti-cancer property is through induction of necroptosis. FTY720 directly binds to I2PP2A/SET (Inhibitor 2 of PP2A), consequently activating the tumor suppressor protein phosphatase 2A (PP2A). The activated PP2A then induces cell death by activating Receptor-Interacting Protein kinase-1 (RIPK1), involved in necroptosis signaling. Little is known about the roles of FTY720 in ceramide signaling and regulation of necroptosis in lung cancer. We therefore, sought to investigate the mechanisms of FTY720 in inducing necroptosis with regard to ceramide signaling. Our data indicate that C16-ceramide is crucial for FTY720-induced cell death. Interestingly, FTY720 does not induce ceramide generation but leads to the formation of specific ceramide-multi-protein complexes at the plasma membrane involved in plasma membrane disruption and necroptosis. Here we show D147, N148 and N169 residues in RIPK1 are important for RIPK1- ceramide binding and cell death. In addition, we show a novel role for non-muscle Myosin IIA (NMIIA) in trafficking these complexes to the plasma membrane to promote membrane rupture. We identify RIPK1 L112 and C256 residues as critical for RIPK1-NMIIA interaction. We hereby propose that these novel

ceramide complexes form non-selective pores supported by RIPK1 and NMIIA. Our data suggest that these structures are very specific and are important in the execution of necroptosis independent of RIPK3 and MLKL. Additionally, preliminary data suggest that these novel structures can also form *in-vivo*, without external stimulus, indicating a possible role in non-pathological conditions.

CHAPTER ONE: INTRODUCTION AND LITERATURE REVIEW

1. Sphingolipids metabolism

Sphingolipids are a class of structural lipids that are found in membranes. In addition to their structural role, some sphingolipids have been shown to play key roles in signal transduction in cells [1]. These bioactive sphingolipids like ceramide, sphingosine and sphingosine 1 phosphate (S1P) have been shown to have roles in cell death, cell proliferation, cell migration and inflammation. Studies have indicated that ceramide and S1P mainly play opposing roles in cells. Because of this, there exist a balance between levels of ceramide and S1P, in what has been referred to as sphingolipid rheostat [2]. An imbalance in this rheostat determines the cell's fate whether it is towards proliferation or cell death.

Ceramide, the central molecule in the sphingolipid metabolism is generated in cells by three main pathways (**Figure 1**); the *de novo* synthesis pathway, the salvage pathway and sphingomyelin breakdown. In *de novo* synthesis, Serine Pamitoyl Transferases (SPT/SPTLC), catalyze the condensation of serine and pamitoyl-CoA to generate 3-ketosphinganine, which is rapidly reduced to dihydrosphingosine by 3-ketosphinganine reductase. Through the activity of (dihydro) ceramide synthases (dihydro-CerSs/CerSs) the dihydrosphingosine is acylated to dihydroceramide. Dihydroceramide is then desaturated by Dihydroceramide desaturase (DES) to yield ceramide [1, 3].

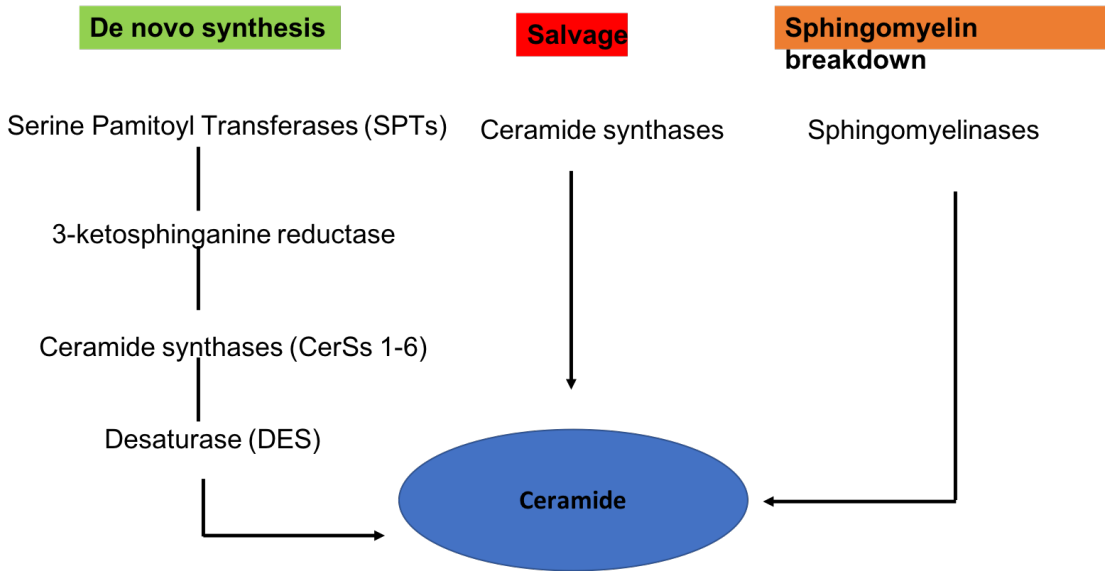

Figure 1 : Ceramide synthesis pathways

Ceramide is generated by multiple pathways including *de novo* synthesis, sphingosine recycling (salvage pathway) and breakdown of complex sphingolipids including sphingomyelin.

There are six known mammalian Ceramide Synthases (CerS1-6) **(Table 1)**. Different CerSs generate ceramides of varying fatty acid lengths [4]. Ceramide Synthase 1(CerS1) is known to generate C18-ceramide. Studies show that C18-ceramide functions as a pro-death ceramide, accumulation of this ceramide species has been linked to induction of apoptosis [5], autophagy [2] and mitophagy [6-8]. Ceramide Synthase 2 (CerS2) is known to catalyze the generation of longer-chain ceramide species C22-24 ceramide [9]. Conversely, C24-ceramide is known to inhibit rather than induce cell death in cancer cells [10]. Ceramide Synthase 3 (CerS3) is mainly localized in testis and tissues and is the less studied ceramide synthase. CerS3 generates ceramides with very long chain lengths

>C26, these very long ceramides are critical for forming the water barrier in the skin [11] . Ceramide synthase 4 (CerS4), like CerS1, generates C18- ceramide. In addition to C18-ceramide, it also produces C20-ceramide. Lack of CerS4 and its products has been implicated in cell migration and hair growth cycle [12, 13]. Ceramide synthase 5 (CerS5) and ceramide synthase 6 (CerS6) both generate mainly C12, C14, and C16 ceramides [14]. CerS6 and its product C16 ceramide have been implicated in induction of ER stress [15]. The role of C16 ceramide varies depending on the cell type and conditions as it has been shown to have both pro-apoptotic [16] and pro-proliferative [17]. Several groups have shown the significance of the chain length of the fatty acid in ceramide molecules in conferring their functions. Because of this, it is important for investigators to not generalize the effect of ceramide as different ceramide species can have opposing roles.

Table 1: Divese biological roles of Ceramide Synthases 1-6

Ceramide synthase isoform	Ceramide product	Biological Role
Ceramide synthase 1 (CerS1)	C18 ceramide	• Induces cancer cell death [5] • Decreases tumor growth [18] • CerS1 mutant mice have neurological disorders [19]
Ceramide synthase 2 (CerS2)	C22-24 ceramide	• C24 ceramide can protect from cell death [20] • CerS2 knockout mice exhibit liver damage [21]
Ceramide synthase 3 (CerS3)	Ultra-long chain ceramides >28	• CerS3 knockout leads to trans-epidermal water loss leading to death after birth [22]
Ceramide synthase 4 (CerS4)	C18 and C20 ceramide	• CerS4 knockout mice exhibit severe alopecia with alterations in sebaceous glands and sebum contents [12]
Ceramide synthase 5 (CerS5)	C12, C14, C16 ceramide	• Implicated in induction of autophagy mediated hypertrophy of cardiac myocytes [23]
Ceramide synthase 6 (CerS6)	C12, C14, C16 ceramide	• Increases cancer cell proliferation [17] • Increased expression associates with positives lymph nodes status [15] • Induces chemotherapy mediated apoptosis [10] • CerS6 knockout mice exhibit neurological/behavioral alterations [24]

Table adapted from Mohammed Dany and Besim Ogretmen, Ceramide induced mitophagy and tumor suppression [25].

The salvage (recycling) pathway involves the conversion of sphingosine, a breakdown product of ceramide, back to ceramide. Ceramide is broken down to sphingosine and a fatty acid through the activity of ceramidases [26]. Sphingosine, a bioactive molecule can then be phosphorylated by sphingosine kinases, sphingosine kinase 1 (SK1) and sphingosine kinase 2 (SK2) to generate sphingosine 1 phosphate (S1P), which is known to be involved in many cellular pathways [27]. Excess sphingosine can also be converted back to ceramide by ceramide synthases, hence the name salvage pathway [3]. It should be noted therefore that inhibition of ceramide synthases not only inhibits the *de novo* synthesis pathway, but also the salvage pathway, unlike the inhibition of serine palmitoyl-CoA transferases, which target only the *de novo* ceramide synthesis. S1P can also be metabolized into ethanolamine-1 phosphate and hexadecanal through the activity of S1P lyase.

Ceramide can also be generated through the breakdown of complex sphingolipids like glycosphingolipids [28, 29]. Glycosphingolipids have been shown to serve crucial roles in cells including regulating cell growth, differentiation and neoplastic transformation [30]. Additionally, sphingomyelins can be broken down to generate ceramide and phosphatidylcholine, through the activity of sphingomyelinases (SMases).

Ceramide can also be modified to generate different sphingolipid molecules. Ceramide kinase (CERK) [31] or SM synthase (SMS) [32] generate ceramide-1-phosphate (C1P) and sphingomyelin, respectively (**Figure 2**). Ceramide is also utilized by glucosylceramide synthase (GCS) as a precursor for the generation of GlcCer [33]. GlcCer

is then transported from early Golgi to distal Golgi compartments by four-phosphate adaptor protein (FAPP2) for the synthesis of glycosphingolipids, determining the lipid composition of the plasma membrane [34]. Non-vesicular C1P trafficking between membranes is regulated by a transporter protein GLTPD1 (renamed as C1P transporter protein, CPTP), which then controls prostaglandin signaling and inflammation [35].

Ceramide is hydrolyzed by ceramidases (CDases) to yield sphingosine, which is phosphorylated by sphingosine kinase 1 or 2 (SK1 or SK2), to generate sphingosine-1-phosphate (S1P). S1P engages with S1P receptors (SIP $_{1\text{-}5}$/S1PR1-5) in an autocrine/paracrine manner for oncogenic signaling [36]. S1P is usually rapidly (within 10-20 min in cells/tissues) metabolized by S1P phosphatases [37] or S1P lyase [38], yielding ethanolamine 1-phosphate and hexadecanol (C16-fatty aldehyde) **(Figure. 2).**

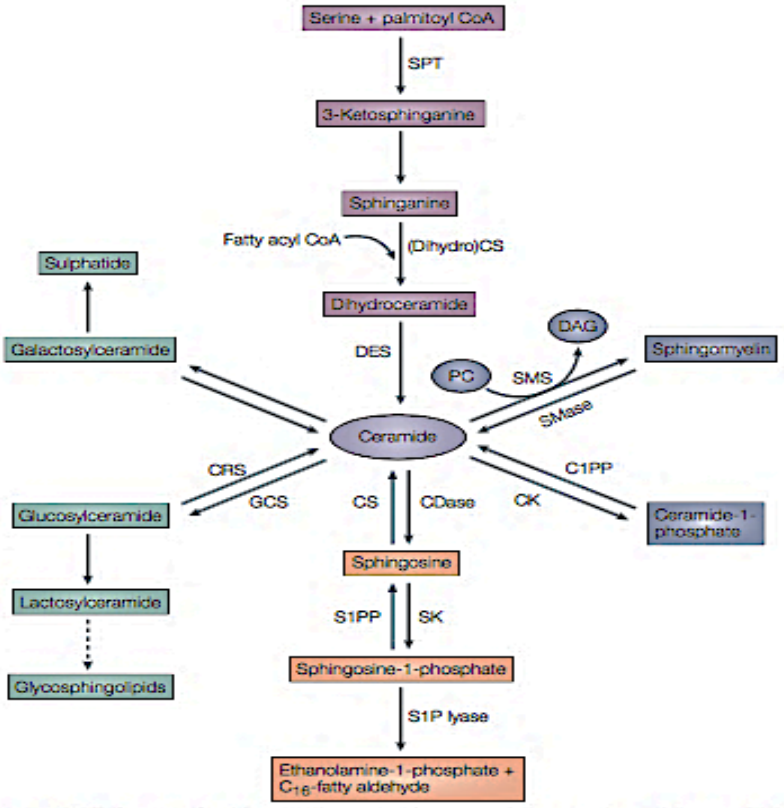

Figure 2 : Sphingolipid metabolism pathway

Ceramide can be formed de novo (pink) or from hydrolysis of sphingomyelin, SM (blue) or cerebrosides (green). Ceramide can be phosphorylated by ceramide kinase to yield ceramide 1 phosphate (C1P) or can serve as a substrate for the synthesis of SM or glycolipids. Ceramide can be metabolized (orange) by ceramidases (CDases) to yield sphingosine, which in turn is phosphorylated by sphingosine kinase (SK) to generate sphingosine-1-phosphate, S1P. S1P can be cleared by the action of specific phosphatases that regenerate sphingosine or by the action of a lyase that cleaves S1P into ethanolamine-1-phosphate and a C16-fatty aldehyde. C1PP, ceramide 1-phosphate phosphatase; CRS, cerebrosidase; CK, ceramide kinase; CS, ceramide synthase; DAG, diacylglycerol; DES, dihydroceramide desaturase; GCS, glucosylceramide synthase; PC, phosphatidylcholine; S1PP, S1P phosphatase; SMS, sphingomyelin synthase; SMase, sphingomyelinase; SPT, serine palmitoyl transferase.

Figure adapted from Besim Ogretmen and Yusuf Hannun, Biologically active sphingolipids in cancer pathogenesis and treatment [3].

2. Ceramide in programmed cell death and tumor suppression

Induction of cell programmed cell death in cancer cells has been applied as one means to induce tumor suppression. Some of the programmed cell death implicated in tumor suppression include apoptosis, autophagy and programmed necrosis (necroptosis) [39]. Addition of exogenous ceramide analogs and/or induction of endogenous ceramide accumulation have been implicated in the induction of caspase dependent as well as caspase independent programmed cell death. It has been shown that cells generate ceramide and sphingosine during cytotoxic stress.

a) Apoptosis

Apoptosis is a form of programmed cell death involving the activation of cysteine proteases known as caspases [40]. Cellular phenotypes known for cells undergoing apoptosis include DNA fragmentation, cell shrinkage, chromatin condensation and membrane blebbing. Induction of apoptosis is well studied in cancer as a regulated form of clearing cancerous cells without triggering the inflammatory response.

Ceramide has been implicated in apoptosis induction in cancer cells. Ceramide was initially reported to induce apoptosis in leukemia cells [41]. Since this initial report ceramide-mediated apoptosis has been intensively investigated and reported in many other different cancer types [1]. C2 and C16-ceramides have been shown to form large channels (ceramide channels) in mitochondrial membranes. Formation of these types of channels promoted mitochondrial outer membrane permeabilization (MOMP) and apoptosis [42, 43]. Interestingly, very long ceramides and dihydroceramides have been

shown to greatly destabilize these channels [44, 45], showing a possible mechanism of how these channels and ceramide-mediated apoptosis are regulated. C16-ceramide, generated by CerS6 has also been shown to be increased in TRAIL (tumor necrosis factor-related apoptosis-inducing ligand) induced apoptosis [46]. This study found that SW620 colon cancer cells, which were resistant to TRAIL, had low levels of CerS6 and elevation of this enzyme increased their sensitivity to TRAIL, leading to apoptosis.

Resisting cell death is one of the hallmarks of cancer [47] and cancer cells have evolved ways to evade apoptosis. One known way is by modulating the sphingolipid rheostat, leading to decreased ceramide and increased S1P generation, which has been associated with proliferation (reviewed in [48]). Manipulation of the sphingolipid metabolism pathway to increase ceramide generation and promote apoptosis has been one way to induce cell killing in apoptosis- resistant cancer cells.

b) Autophagy

Autophagy, from the Greek word meaning, "self-eating" is a cellular process whereby the cell digests some of its organelles, during starvation conditions to provide nutrients to itself [49]. In some instances, autophagy has been shown to promote caspase independent cell death, also known as lethal autophagy.

As in the case with apoptosis, ceramide has also been shown to play critical signaling roles in autophagy. Accumulation of ceramide induces both types of autophagy [25, 50, 51]. In lethal autophagy, ceramide leads to autophagy by modulating the expression of autophagic proteins like Beclin-1 [52]. In another study, ceramide was shown to induce autophagy in amino acids deprivation through mTOR suppression [2]. Additionally, dihydroceramide has also been shown to induce autophagy. In glioma cells, Tetrahydrocannabinol (THC, the active component of marijuana) triggered dihydroceramide accumulation in the endoplasmic reticulum (ER), promoting autophagosomal and lysosomal membrane permeabilization, leading to cathepsin release and apoptosis [53]. Expectedly, sphingomyelin accumulation, by silencing SMPD1, has been correlated with aggregation of elongated and unclosed autophagic membranes with reduced association of ATG9A in cancer cells [54] **(Figure 3)**.

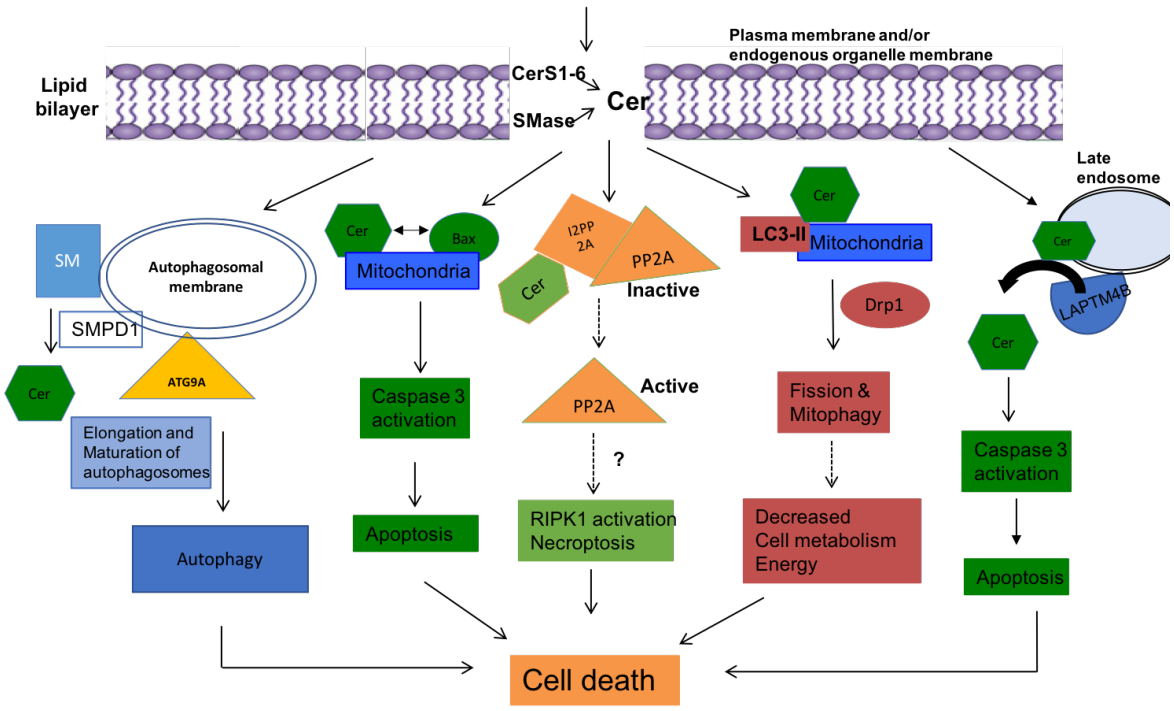

Figure 3 : Ceramide involvement in cell death

Ceramide has been implicated in multiple cell death pathways in cancer. Ceramide can induce apoptosis through caspase activation, necroptosis through PP2A and RIPK1 activation and mitophagy through targeting autophagolysosomes to the targeted organelles or by macro-autophagy by promoting maturation of autophagosomes.

Ceramide has also been implicated in a more organelle specific type of autophagy known as mitophagy. Mitophagy is the digestion of cell's mitochondria to provide nutrients to the cell during starvation or in some instances to induce cell death [55]. Accumulation of C18-ceramide, exogenously added or induced through CerS1 activation, was shown to specifically accumulate in the mitochondria and propagate mitophagy through tethering of LC3B to the mitochondria in head and neck (HN) cancer cells [8] **(Figure 3**). This phenomenon has also been observed in AML (acute myeloid leukemia) cells. Interestingly, the addition of exogenous C18 pyridinium ceramide (LCL461), which is specifically targeted to the mitochondria because of the positively charged pyridinium ring, induced mitophagy and this overcame FLT-3 mediated chemoresistance [7]. It was also shown that ceramide-dependent lethal mitophagy was regulated by the activation of DRP1 and mitochondrial fission, involving PKA inhibition and decreased phosphorylation of DRP1 at S637 in FLT3+ AML cells [7]. In addition, HPV/E7 protein has been shown to confer its sensitivity to chemotherapy through increased C18-ceramide levels which promotes mitophagy in HN cancer cells [6].

c) Necroptosis

Necroptosis is a form of programmed cell death that involves the activity of receptor interacting proteins (RIPKs) **(Figure 4).** Necroptosis has been shown to play a role in both physiological and pathological settings [56]. In cells, RIPK1 is typically poly ubiquitinitated via K63-linked ubiquitin chains by CIAPs (cytoplasmic inhibitors of apoptosis) and signals for NFkB activation [57]. In canonical necroptosis, activation of

death receptors leads to activation of RIPK1 through de-ubiquitination by CYLD [58], De-ubiquitination of RIPK1 increases its affinity for RIPK3 and other adaptor proteins to signal for necroptosis as opposed to pro-survival NFkB signaling [57-60] . Activated RIPK1 recruits and phosphorylates RIPK3. Phosphorylated RIPK3 (active) then phosphorylates MLKL (mixed-lineage Kinase domain-like) a pseudo kinase. Phosphorylated MLKL oligomerizes and the oligomers translocate to the plasma membrane where they form pores and lead to plasma membrane rupture [61, 62, 63].

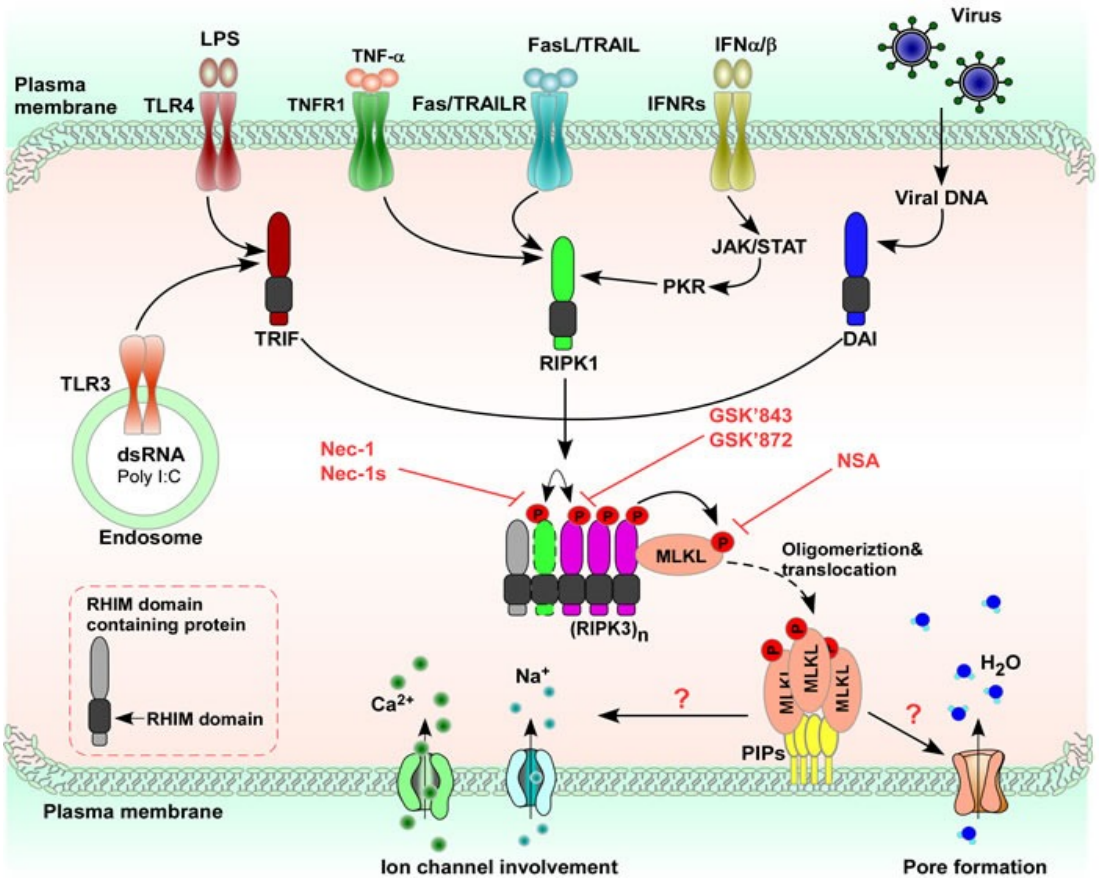

Figure 4 : Necroptosis signaling

Activation of RIPK1 from extracellular and intracellular stimuli leads to activation of RIPK3 followed by recruitment and activation of MLKL and plasma membrane disintegration.

Figure was taken from Meng et.al, Necroptosis in tumorigenesis, activation of anti-tumor immunity, and cancer therapy [64].

Ceramide has been shown to be involved in necroptosis in lung and ovarian cancer. In lung cancer, studies indicate that C18-ceramide binds I2PP2A/SET **(Figure 3)**, an endogenous inhibitor of tumor suppressor PP2A, leading to the activation of PP2A, which leads to RIPK1 activation, through unknown mechanism [65]. However, the exact mechanisms of this activation remain unclear. In ovarian cancer, exogenous ceramide, through ceramide nanoliposomes was shown to activate MLKL [66]. U937 lymphoma cells treated with a combination of TNFα and ZVAD underwent necroptosis and exhibited a significant increase in the levels of C16-ceramide, indicating a role of this ceramide species in necroptotic signaling [67].

Although in this dissertation study, I focused on the role of ceramide in necroptosis, it is important to note that, in addition to programmed cell death, ceramide has also been implicated in other cellular mechanisms that lead to tumor suppression. These include ER stress and cell cycle arrest, discussed below.

d) Ceramide and ER Stress

Induction of ceramide-associated ER stress was reported as an upstream regulator of autophagy [68]. Melanoma differentiation associated gene-7 (mda-7) regulated IL-24 induced ER stress, leading to ceramide-mediated lethal autophagy in glioblastoma cells [69]. Methotrexate-induced folate stress in lung cancer cells increased the formation of ER stress aggregates with CerS6 accumulation, which was associated with the activation of p53 [70].

e) Ceramide and cell cycle arrest

Ceramide's inhibition of cancer progression has also been shown to occur through cell cycle arrest. In MOLT4 leukemia cells, ceramide and its metabolite sphingosine led to the dephosphorylation Retinoblastoma protein (Rb), which led to cell cycle rest in Go/G1 and growth suppression [71]. Exogenously added C6 ceramide was shown to arrest rhabdomyosarcoma (RMS) cells in G2 phase and eventual apoptosis of these cells [72]. Additionally, exogenously added C2 ceramide also induced cell cycle arrest in Bel7402 hepatocarcinoma cells [73].

3. Ceramide generation in chemotherapy/radiation-mediated tumor suppression

CerS-generated ceramide was linked to daunorubicin-induced apoptosis in various cancer cells [74]. Vorinostat and sorafenib combination was efficacious in the inhibition of gastrointestinal tumor and pancreatic tumor-derived xenograft growth in mice. The mechanism involved activation of CD95 through the generation of Ca^{+2} and CerS6-dependent ceramide, leading to PP2A and ROS signaling [75]. In a phase II clinical trial in patients with recurrent HN cancers, elevation of serum C18-ceramide was significantly associated with improved response to gemcitabine plus doxorubicin combination therapy, which induced CerS1/C18-ceramide [76].

In intestinal stem cells, Ataxia telangiectasia (ATM) kinase regulates target switching to escalating doses of radiation via activation of ceramide synthesis, without affecting microvascular response [77]. Interestingly, neutralizing ceramide signaling by anti-ceramide antibody prevented gastrointestinal damage in response to radiation, relieving gastrointestinal syndrome mortality [78]. Measurement of plasma ceramide levels

during the treatment of 35 patients with hypo-fractionated stereotactic body radiation therapy showed that elevated total ceramide was associated with positive response [79]. Moreover, ABC294640, a pharmacological inhibitor of SK2, which was shown to also inhibit DES, resulting in the accumulation of dihydro-ceramides [80], has been successfully tested in a phase I clinical trial for the treatment of patients with advanced solid tumors [81]. Thus, these data suggest that increased (dihydro) ceramide generation in cancer cells in response to chemotherapy or radiation play important roles in tumor suppression.

4. Ceramide metabolism in tumor immunology and immunotherapy

In addition to its roles in chemo/radiotherapy, ceramide signaling is implicated in the regulation of tumor immunology and immunotherapy. C16-Ceramide inhibited the growth of myeloid derived suppressor cells (MDSCs) by activating lysosomal cathepsin B/D and inducing autophagy in these cells [82]. Induction of autophagy and ER stress in MDSCs enhanced cytotoxic T cell lymphocyte function for tumor suppression [82]. In Gaucher's disease patients, who are susceptible to myeloma, clonal immunoglobulin was reactive against lyso-glucosylceramide, which is highly elevated in these patients due to deficiency in glucocerebrosidase [83]. These data suggested that lyso-glucosylceramide might be involved in the origin of myeloma and/or Gaucher's disease-associated gammopathy [83]. Interestingly, in Gaucher's disease complement signaling via C5a/C5aR1 induced GlcCer accumulation and tissue inflammation [84]. Recently, Sofi et.al demonstrated that CerS6/C16-ceramide enhanced T-cell response to alloantigens during allogeneic hematopoietic cell transplantation (allo-HCT), an effective immunotherapy for

various hematologic malignancies [85]. The data revealed that genetic loss of CerS6 prevented graft versus host disease (GVHD), a major toxicity limiting the anti-leukemic efficacy of allo-HCT [85]. Thus, these data suggest that ceramide metabolism/signaling plays key roles in the regulation of anti-cancer immunotherapy.

5. Targeting sphingolipid metabolism and signaling for cancer therapy.

Given the importance of sphingolipids in promoting cancer progression or inhibition, sphingolipids have become great targets for cancer therapy. Highly soluble pyridinium-ceramides, selectively accumulating in cancer cells' mitochondria, induced lethal mitophagy [7, 8] and tumor suppression in HN, AML and prostate cancers [86, 87]. Inhibition of survivin by nanoliposomal ceramide (NLC) resulted in complete remission of the natural killer type of aggressive large granular lymphocytic leukemia [88]. NLC is now tested in a phase I clinical trial for the treatment of patients with advanced solid tumors (NCT02834611).

The table below shows some of the anticancer that target the sphingolipid metabolism that have been developed and being studied for clinical purposes.

Table 2: List of anticancer drugs targeting sphingolipid metabolism

Name	Target or activity	Stage of Development
Ceramide inducers and analogues		
C8 CPC (C8-cyclopropenylceramide)	DES	Preclinical [89]
CHC (3-chloro 8β-hydroxycarapin-3,8-hemiacetal)	CERT: ceramide trafficking, sphingomyelin synthesis	Preclinical [90]
NVP-231	CERK	Preclinical [91]
LCL 521 and LCL 204		Preclinical [92-94]
Pyridinium ceramide (LCL-124 and LCL-461)		Preclinical [86, 87]
Nanoliposomal ceramide	Surviving, MLKL	Preclinical [66, 88]
Targets of S1P metabolism and signaling		
FTY720	S1PR1;I2PP2A	FDA-approved for multiple sclerosis [65, 95-97]
JTE013	S1PR2	Preclinical [98]
AB1	S1PR2	Preclinical [99]
SK1-I	SK1	Preclinical [100]
PF543	SK1	Preclinical [101]
VPC03090	S1PR1;S1PR3	Preclinical [102]
Sphingomab (sonepcizumab)	S1P	Phase II [103]
ABC294640	SK2; DES	Phase 1b and II [81, 104]

Modified table adapted from Besim Ogretmen, Sphingolipid metabolism in cancer signaling and therapy [1].

6. FTY720

The US Food and Drug Administration (FDA) approved FTY720 (Fingolimod/Gilenya, Novartis, Inc), for the treatment of relapsing MS [105, 106]. Mechanistically, FTY720 is phosphorylated in cells by one of the two sphingosine kinases, sphingosine kinase 2 (SK2) [105, 106] to generate P-FTY720. P-FTY720 is

trafficked to outside the cell by SNSP2 [107], the same transporter that traffics S1P. On the plasma membrane P-FTY720 binds S1P receptors (S1PRs) where it acts as a functional antagonist **(Figure 5).** There are five S1PRs ($S1PR_{1-5}$), and P-FTY720 binds all of them except $S1PR_2$ [108]. Binding of P-FTY720 to the S1PRs leads to their internalization and degradation. Degradation of S1PRs after P-FTY720 binding disrupts the S1P gradient, usually maintained to allow T cells egress from lymph nodes to the bloodstream, hence conferring its immune suppressive property.

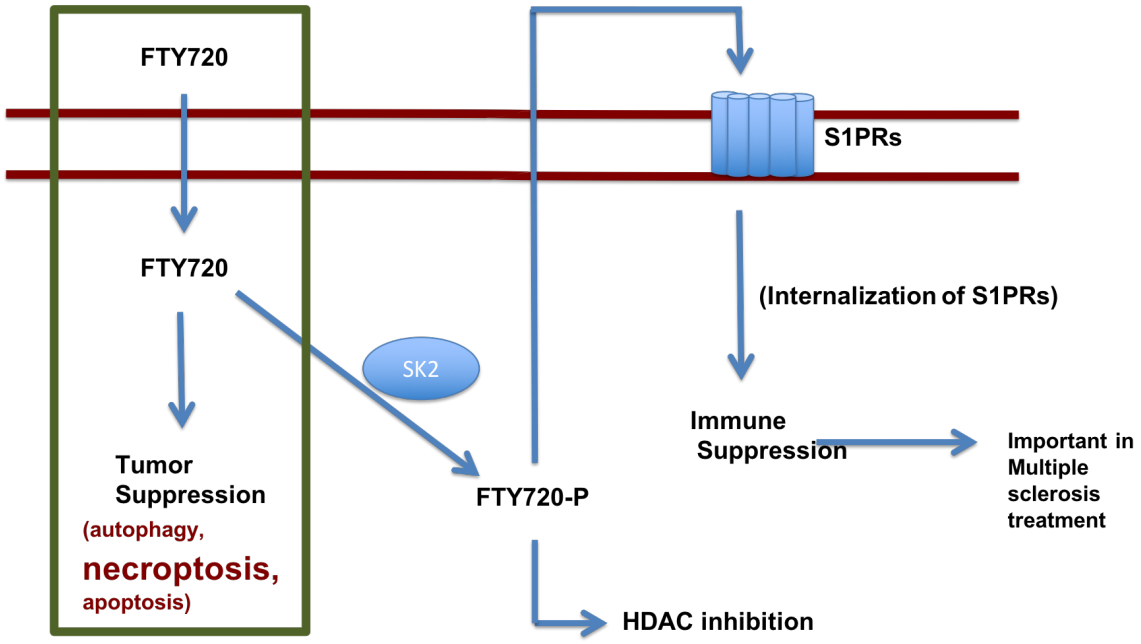

Figure 5 : FTY720 signaling in multiple sclerosis and cancer

To induce immune suppression, important for multiple sclerosis, FTY720 is phosphorylated by SK2 to generate P-FTY720 which binds S1PRs and leads to their degradation. In cancer, the prodrug, FTY720 (without phosphorylation) induces different types of cell death depending on cell type and other conditions.

FTY720 (prodrug) also exhibited tumor suppression via S1PR-dependent [109] and receptor-independent [65] mechanisms **(Figure 5).** Receptor-independent mechanism involves inducing necroptosis via inhibition of onco-protein SET and activation of tumor suppressor PP2A signaling in various cancer types, including lung, oral and colon cancers [65, 110, 111]. Another tumor-suppressor mechanism results in inhibition of CML stem cell proliferation/expansion, reversing CML drug resistance [97]. FTY720 has also been shown to induce apoptosis in multiple myeloma through down regulation of anti-apoptotic protein, MCL-1 [112] and activation of caspases 8, 9 and 3 [113]. Intriguingly, FTY720 induced apoptosis even in cells that were known to be resistant to common chemotherapeutic agents [113]. In glioblastoma, FTY720 was shown to induce tumor suppression by activating more than one type of cell death [114], demonstrating the diversity in the different mechanisms of cell death induced by FTY720 in different cell types. These data suggest that sphingolipid metabolism and signaling present a valuable target for cancer therapy. Although cancer cell death activity of FTY720 requires micro molar (10-20 μM) concentrations to be effective in cell culture studies, tumor suppression in human lung cancer xenografts grown in mice was achieved using physiologically relevant concentration (3 mg/kg/day) via induction of necroptosis *in vivo* [65].

FTY720 has also been shown to either increase cancer cells' sensitivity to chemotherapeutic agents, or radiation, when used in combination with other chemotherapeutic agents in multiple cell lines. In multiple myeloma, when used together with bortezomib [112], dexamethasone, or anti-Fas antibody [113] the cells exhibited increased apoptosis. When used in combination with Cisplatin, FTY720 was shown to induce autophagy-related apoptosis in non-small cell lung carcinoma, sensitizing cells initially

resistant to cisplatin [115]. In triple negative breast cancer model, FTY720 was used in combination with an EGFR inhibitor, leading to tumor suppression [116] and also sensitized breast cancer cells to radiation [117].

In addition, FTY720 has been used as a lead compound in developing inhibitors for specific ceramide synthases: ST1060 inhibited CerS2, ST1072 inhibited CerS4 and CerS6, while ST1058/1074 inhibited CerS2 and CerS4 [118]. These chemicals provide valuable preclinical tools to distinctly regulate various CerS enzymes and their specific ceramide products in different cancer models. In fact, inhibition of CerS6 by ST1072 reduced T cell activation in response to allogeneic stimulation in mouse and human T cells, preventing GVHD toxicity during allo-HCT for anti-leukemia therapy [85]. Inhibition of GCS by PDMP (D-thereo-1-phenyl-2-decanoylamino-3-morpholino-1-propanol) sensitized CML cells expressing mutant Bcr-Abl (T315I) to tyrosine kinase inhibitors by inducing glycogen synthase kinase-3 (GSK-3)-dependent apoptosis [119]. Overall these studies show the potential of FTY720 and its analogues as chemotherapeutic agents, as stand-alone or in combination with other agents.

7. FTY720 modulation of sphingolipid metabolism

FTY720 has been shown to modulate different sphingolipid molecules by interacting with the enzymes of the sphingolipid pathways to induce cell death. Multiple studies have shown, in colitis and cancer models, that FTY720 reduced the expression of SK1 [109, 120]. Another study on the contrary, found that FTY720 also inhibited S1P lyase [121], the enzyme known to cleave S1P. This suggested FTY720 was cleaved and dephosphorylated by other enzymes. This led to further studies that identified several

enzymes that metabolize FTY720. CYP4F hydroxylates and oxidizes FTY720 for elimination [122], while Lipid phosphate phosphatase, LPP3 [123] and LPP1a [124] dephosphorylate P-FTY720. Moreover, FTY720 has been shown to inhibit ceramide synthases and lead to dihydrosphingosine 1-phosphate accumulation in human lung endothelial cells [125]. Accumulation of dihydrosphingosine-1 phosphate shows this inhibition is of the *de-novo* synthesis pathway of ceramide generation. Interestingly, another study by Lahiri, S. *et. al.*, found that FTY720 could also modulate Ceramide syntheses activity via a mixture of uncompetitive and noncompetitive inhibition [126]. As before-mentioned, ceramide accumulation in cells has been implicated in caspase independent cell death [7, 25] including necroptosis [127] and mitophagy [128]. However, whether FTY720 has any implication for ceramide generation and/or signaling during necroptosis in lung cancer is a question that still remains unanswered.

8. Ceramide signaling in stem cells

Sphingolipids have also been implicated in normal and cancer stem cells biological activities. In Glioblastoma, S1P signaling was found to be crucial for maintenance of stemness in glioblastoma cells [129]. In non-pathological context, ceramide and S1P have been shown to play key roles in embryogenesis by regulating stem cell differentiation [130, 131]. In one study, ceramide generated from neutral sphingomyelinase and *de novo* synthesis propagated primary ciliogenesis and promoted differentiation in embryonic stem cells and neuroprogenitors [132]. This study showed that inhibition of ceramide generation significantly reduced ciliogenesis, which was restored with addition of

exogenous ceramide [132]. These studies further illustrate the key roles played by sphingolipids in both physiological and pathological conditions.

9. Ceramide signaling in *Drosophila melanogaster*

To study ceramide signaling in-vivo, *Drosophila melanogaster* (*D. melanogaster*) ovaries are a great model as they contain different types of stem cells [133]**.** In *D. melanogaster*, ovary development (oogenesis) begins with the formation of cyst of interconnected germ cells, produced by germline stem cells, enveloped by somatic follicle cells [134]. Oogenesis in insect cells requires a complex mechanism for differentiation of germ line and somatic cells [135]. The Drosophila ovary contains three types of stem cell populations, germline stem cells (GSC), somatic stem cells (SCC) and escort stem cells (ESC), which are contained in a well-defined anatomical structure called germarium [136-138]. Thus, insect ovaries present an ideal model to study the roles of various mechanisms in the regulation of stem cell development and signaling. As opposed to mammals, *D. melanogaster* has only one isoform of ceramide synthase, known as *schlank* [139]. Predictably, knocking out *schlank* in *D. melanogaster* is lethal [139], emphasizing the importance of ceramide and sphingolipids signaling in embryogenesis and development.

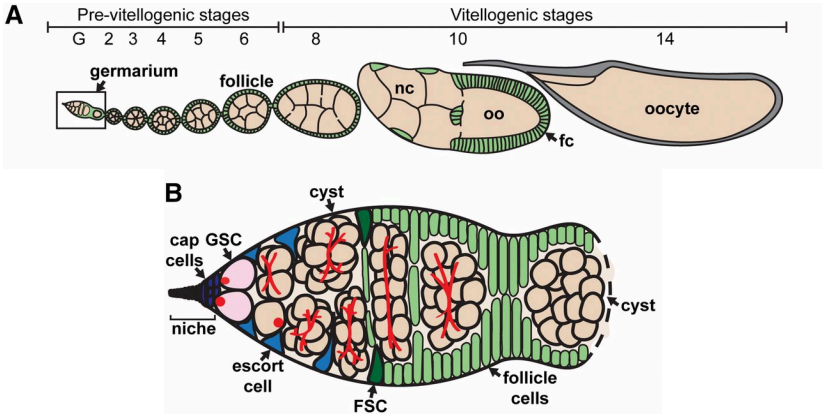

Figure 6 : Drosophila melanogaster oogenesis

A. Drosophila oogenesis is fueled by the activity of germline stem cells. The Drosophila ovary is composed of 14–16 ovarioles, each harboring a germarium and older follicles that progress through 14 distinct stages of development. **B.** shows the germarium. The germarium contains germline stem cells (GSCs; pink) that are juxtaposed to cap cells, the major cellular component of the somatic niche (purple), and a subset of escort cells (blue). GSCs divide to form daughter cells (cystoblasts), which divide four additional times to form 16-cell germline cysts (peach) composed of nurse cells and an oocyte. Follicle stem cells (FSC; dark green) divide to form pre-follicle cells, which surround the 16-cell germline cyst, and pinch away from the germarium, forming a follicle. Pre-follicle cells give rise to a variety of specialized follicle cells (fc; green) that reside in an epithelial monolayer around each cyst.

This figure was adapted from Abels *et. al.*, A Genetic Mosaic Screen Reveals Ecdysone-Responsive Genes Regulating Drosophila Oogenesis [140].

Given the importance of ceramide in programmed cell death tumor suppression and with the knowledge that FTY720 induces RIPK3-MLKL independent necroptosis in lung cancer cells, in this study, I sought to investigate if FTY720- induced necroptosis was ceramide dependent. It is important to note that FTY720-induced necroptosis in lung cancer cells differs from the canonical necroptosis, in that it is RIPK3 and MLKL dependent. This leaves a gap in knowledge of how the plasma membrane integrity is compromised during this type of necroptosis. FTY720 has been shown to modulate ceramide signaling and this could also be occurring during the induction of necroptosis. Putting this knowledge together, I investigated the potential of ceramide modulation by FTY720 to affect the plasma membrane integrity, independent of MLKL. Additionally, I investigate the role of ceramide-enriched macrodomains in a non-pathological context, using *drosophila melanogaster* as my model.

CHAPTER TWO: MATERIALS AND METHODS

Cell lines and Reagents

A549, and H1341 human lung cancer cells were grown in DMEM containing 10% FBS (Cellgro) and 1% penicillin/streptomycin (Cellgro), WT MEFs and NHFL were grown in DMEM with 10% FBS and 1% Pen/Strep. Cells were treated with the following reagents: FTY720, P-FTY720, NBD-FTY720, Latrunculin A (Cayman Chemical Company), OSU-2S (was a gift from Dr. Chen, Ohio State University), Myriocin (Sigma), LPA (Santa Cruz Biotechnology), Brefeldin A (Sigma), AZ10606120, ARRY 520, K858, Ciliobrevin (Tocris), Blebbistatin (Selleckchem), Necrosulfonamide, NSA (EMD Millipore), Sphingosine, (Avanti Polar Lipids), Fumonisin B1, FB1 (Enzo) Biotinylated C6-ceramide (Echelon Biosciences). Full length recombinant RIPK1 was purchased from Origene. The antibodies used were Ceramide MB154 (Enzo), cholesterol (US Biological) RIP-1 (Cell Signaling), non-muscle Myosin IIA, β-Actin (Sigma), GM130, Calnexin, Eaa1, CD63, Caveolin-1, CerS5, CerS6, Acid Ceramidase (Santa Cruz Biotechnology). Nanogold Gold- antibody Conjugates, (mouse and Rabbit) were from Nanoprobes. α1B1 (University of Iowa, Developmental Studies Hybridoma Bank). Rhodamine phalloidin and YO-PRO-1 were purchased from Life sciences (Thermo Fisher Scientific). DUOLINK Proximity Ligation Kit and streptavidin-coated 96 well plates were purchased from Sigma.

Plasmid constructs and shRNAs

The shRNA lentiviral plasmids were purchased from sigma-Aldrich. The TRC numbers and sequences are as follows: shMYH9 (gene ID: 4627), TRCN0000285480, sequence: CCGGGCCAAGCTCAAGAACAAGCATCTCGAGATGCTTGTTCTTGAGCTTGGC

TTTTTG, shRIPK1, (gene ID 8737), TRCN0000200006, sequence: CCGGCGGAACAGATTCTGGTGTCTTCTCGAGAAGACACCAGAATCTGTTCCG TTTTTTG, shCerS1 (gene id: 10715), TRCN0000168211, sequence: CCGGCTACTTCTTCTTCAATGCGCTCTCGAGAGCGCATTGAAGAAGAAGTAGT TTTTTG, shCers2 (gene id: 29956), TRCN000276376, sequence: CCGGCCTGCCTTCTTTGGCTATTACCTCGAGGTAATAGCCAAAGAAGGCAGG TTTTTG, shCerS4 (gene id: 204219) TRCN0000016986, sequence: CCGGGTTACATGATTCCTCTGACTACTCGAGTAGTCAGAGGAATCATGTAACT TTTT, shCerS5 (gene id: 91012) TRCN0000022221, sequence: CCGGGTGGGCTTTATCACTATTATACTCGAGTATAATAGTGATAAAGCCCACT TTTT, shCerS6 (gene id: 253782) TRCN0000344342, sequence: CCGGGAACTGCTTCTGGTCTTACTTCTCGAGAAGTAAGACCAGAAGCAGTTCT TTTTG, shSPT1 (gene ID:10558) TRCN0000303825 sequence: CCGGGCTATTCCTGCTTACTCTAAACTCGAGTTTAGAGTAAGCAGGAATAGCT TTTTG, shSPT2 (gene ID: 9517) TRCN0000286903, sequence: CCGGGCTCATACCAAAGAAATACTTCTCGAGAAGTATTTCTTTGGTATGAGCT TTTTG, shSPT3 (gene ID: 55304) TRCN0000136363, sequence: CCGGCAAACATCTCATGGGCAACTACTCGAGTAGTTGCCCATGAGATGTTTGT TTTTTG, shSMPD3/nSMase2 (gene ID: 55512) TRCN0000048943 sequence:CCGGCCCAACAAGTGTAACGACGATCTCGAGATCGTCGTTACACTTG TTGGGTTTTTG, SMPD4/nSMase 3 (gene ID: 55627) TRCN0000245620, sequence: CCGGCCTGAAAGCTGACTCTATAAACTCGAGTTTATAGAGTCAGCTTTCAGGT TTTTG, shSK2 (gene ID: 56848) TRCN0000036973, sequence:

CCGGCTACTTCTGCATCTACACCTACTCGAGTAGGTGTAGATGCAGAAGTAGT TTTTG, RIPK3 (gene ID: 11035) TRCN0000002261, sequence: CCGGCTACAGCTTCGGGATCCTAATCTCGAGATTAGGATCCCGAAGCTGTAG TTTTT, pMD2.G (Addgene plasmid #12259) and pCMV-psPAX2 (Addgene plasmid # 12260) were gifts from Dr. Didier Trono. Non-targeting shRNA (shSCR) was used as control.

Stable shRNA knockdown studies

CerS1, CerS2, CerS4, CerS5, CerS6, SPT1, 2, 3, nSMase 1, 2, 3, SK2, RIPK1, RIPK3, MYH9 and non-targeting shRNA containing plasmids (purchased form the MUSC shRNA shared Technology Resource) were co-transfected in HEK293 packaging cells with together with pCMV-psPAX2 and pMD2.G plasmids to generate lentiviral particles. The lentiviral particles were collected after 48Hrs. These were added to H1341/A549 cells, together with 10μg/mL polybrene. After 48 hours, the lentiviral particles were removed and cells were selected for approximately 14 days with 2μg/mL puromycin.

Site Directed Mutagenesis

RIPK1 D147A, N148A, N169A, N186A, L112A, C256A, R258A, L293A, E295A mutants were generated using Q5 site-directed mutagenesis kit (New England Biolabs) per manufacturer's instructions. Primers were designed using NEBaseChanger (New England Biolabs) and are listed in the table below.

Table 3: List of Primers used to generate RIPK1 mutants

RIPK1 mutant	Forward sequence (5'-3')	Reverse sequence (5'-3')
D147A	TATCCTTGTTGCTAATGACTTCCAC	TTTTCAGGCTTCAGGTCC
N148A	CCTTGTTGATGCTGACTTCCACATTAAG	ATATTTTCAGGCTTCAGG
N169A	GAGCAAACTGGCTAATGAAGAGCACAATG	CACATCTTAAAGGAGGCAAG
N186A	CGCTAAGAAGGCTGGCGGCACCC	GTGCCGTCCACTTCCCTC
L112A	GAGTACTCCGGCTTCTGTAAAAGGAAGG	ATCTCGGCTTTCAGCACG
C256A	CACTGAGTACGCCCCAAGAGAAATTATC	ATGTCATCCACATCTGGC
R258A	GTACTGCCCAGCAGAAATTATCAGTC	TCAGTGATGTCATCCACATC
L293A	TTTAAGTCAAGCAGAAGAAAGTGTAGAAG	TAAAAAGGCCTAAATTTTTCTTC
E295A	TCAATTAGAAGCAAGTGTAGAAGAG	CTTAAATAAAAAGGCCTAAATTTTTC

Immunofluorescence Labeling

Cultured cells were incubated the respective treatment, washed two times with 1X PBS, fixed with pre-warmed 4% paraformaldehyde (PFA) for 15 minutes at room temperature, permeabilized for 10 minutes with 0.01% Triton X-100, blocked for 20 minutes with 1% BSA before incubation with primary antibody in blocking solution overnight at 4°C. The following day the cells were incubated with secondary antibody (Alexa fluor-488 anti-mouse) and Rhodamine phalloidin. The coverslips were mounted on slides with a drop of Prolong anti-fade reagent (Invitrogen), and sealed with nail polish. Labeling patterns were observed using Olympus FV10i Laser Scanning confocal microscope. Images were analyzed by Flouview Fv10i software. Ceramidosomes quantification was performed using Fiji (ImageJ).

Proximity Ligation Assay

Proximity ligation assays were performed using Duolink in situ red kit (Olink Biosciences, Sigma) per manufacturer's instructions. Antibodies were used at 1:100 dilution, probed overnight at 4° C. Images were analyzed as described previously [141].

Co-Immunoprecipitation and Western blotting

For immunoprecipitation, cells were grown to 70% confluency, treated with FTY720 or vehicle, cells were rinsed with cold 1X PBS, scrapped off and lysed in Pierce IP lysis buffer (non-denaturing) with protease inhibitor cocktail and phosphatase inhibitor. Immunoprecipitation was done with RIPK1 or Myosin IIA antibody. Lysates were precleared with 40µl of protein A/G beads and control IgG and incubated in a rotatory shaker for 1 hr at 4°C. Samples were centrifuged at 2,000Xg for 5 minutes. The supernatant was collected and incubated with the respective antibody at 4°C for 1 hr before adding 40µl agarose beads and rotating overnight. The following day, samples were centrifuged at 2,000 g for 5 minutes; the beads were washed with cold 1X PBS four times, followed by the addition of 2X loading dye. The samples were boiled using a heating block before western blotting. For assays cells were homogenized in RIPA buffer (25mM Tris-HCl pH7.4, 150mM NaCl, 1% TritonX-100,1% sodium deoxycholate, EDTA (20µl of 0.5M stock) including protease inhibitor cocktail using a gauge (26.5G) syringe five times, incubated for 20 minutes on ice. The samples were centrifuged at 12,000Xg for 15 minutes at 4ºC. The supernatant was collected and proteins were quantified with Bradford method. 4X loading dye was added to sample and boiled using a

heating block at 95ºC for 5 minutes before loading. SDS gradient gels 4%-20% were used to run the samples with Bio Rad Criterion apparatus, followed by semi-dry transfer onto PVDF membrane. Blocking was done with 5% milk in 0.1% PBST. Primary antibodies were used at 1:2000 dilution overnight at 4ºC. Proteins were analyzed by Western blotting using the following antibodies: the rabbit RIPK1 (Cell signaling), β-actin (Sigma, St. Louis, MO), anti-GFP (Santa Cruz), Non-muscle Myosin IIA (Sigma).

Quantitative RT-PCR

RNA was extracted from cell pellets using RNeasy kit (Qiagen) per the manufacturer's instructions. cDNA was generated using equal amounts of RNA from each sample and iScript cDNA synthesis kit (Bio-Rad) per manufacturer's instructions. The thermal cycler protocol used was as follows; Priming (5 min at 25°C) followed by Reverse transcription (20 min at 46°C) and RT inactivation (1 min at 95°C). Reactions were carried out using SsoAdvance universal probes mix (Bio-Rad) and TaqMan primer probes (ThermoFisher Scientific) in a BioRad CFX96 RealTime system. The thermal cycling protocol used was as follows: Polymerase activation and DNA denaturation at 95°C for 30 sec, followed by 40 amplification cycles (denaturation at 95°C for 10 sec and annealing/extension and plate read at 60°C for 30 sec).

Membrane permeability/Dead cell apoptosis kit with YO-PRO-1 and PI

Cells were cultured to 70-80% confluency, and then treated with 20μM FTY720 or vehicle. The cells were collected by scrapping off the dishes, rinsed with cold 1X PBS, resuspended in 1 mL cold PBS dyes were then added at 1μl/mL concentration. The

samples were kept on ice for 20-30 minutes before analysis by flow cytometry on LSRFortessa/X-20. For live cell imaging, cells were treated with 20μM FTY720 or vehicle and incubated with the dyes (1μl/mL). Pictures were taken every 30 minutes for a period of 3 hrs. For the RIPK1 mutants, membrane permeability was analyzed by propidium iodide only in GFP positive cells.

Trypan blue exclusion assay

Cells were seeded in 6-well plates and allowed to adhere for 20 hours. Treatment was with 20μM FTY720 in DMSO, or corresponding amount of vehicle control. Medium containing dead cells was pelleted with trypsinized cells, then re-suspended in 1X PBS then counted with a hemocytometer after addition of trypan blue dye (Sigma-Aldrich) at a 1:10 dilution.

Lipidomics analysis

Cells were collected by scrapping off from the dishes and washed twice with cold PBS. Further preparation of samples and measurement of endogenous ceramides by LC-MS/MS followed the protocol described previously [142]. Briefly, samples were supplemented with internal standards, and 2 ml of isopropyl alcohol:water:ethyl acetate (30:10:60; v:v:v) was added to the extracts. Samples were subjected to two rounds of vortex and sonication followed by a 10-min centrifugation at 4000 rpm. The supernatant or top layer was used as lipid extract and subjected to LC-MS/MS for analysis of ceramide species. Lipid extraction and analyses were performed by the MUSC

Lipidomics Shared Resources. Inorganic phosphates (Pi) were used for normalization. Detailed protocol for inorganic phosphates analysis can be found in the Appendix.

Isolation of Ceramide-enriched membrane pores

We followed previously published protocol for isolating Giant Plasma membrane vesicles [143, 144]. In summary, cells were grown in 100 mm dishes to 80% confluency. These cells were treated with Vehicle/ FTY720. The cells were rinsed twice with GPMV buffer (10 mM HEPES, 150 mM NaCl, 2 mM $CaCl_2$, pH 7.4) and incubated with vesiculation buffer (25 mM PFA/2 mM DTT in GPMV buffer, to prepare add 18µl of 4%wt/vol PFA solution and 2µl of 1M DTT solution to 1mL GPMV buffer) for 1hr at 37ºC incubator. GPMV (ceramidosomes) were collected and processed for electron microscopy.

Ceramide Docking to RIPK1

Using the software MOE from CCG [145], a complete contiguous model of the kinase domain from RIPK1 was created based on Xray-derived coordinates PDB:4NEU and 5HX6 [146, 147]. The protein was protonated at T=310K, pH 7.3, salt at 200mM, and using GB/VI electrostatics. The final structure was energy minimized using the AMBER12: ETH forcefield. C16-ceramide was docked to the RIPK1 monomer using the entire surface as a target. Initial placement calculated 100 poses using triangle matching with London dG scoring, the top 50 poses were then refined using forcefield and Affinity dG scoring, as we described previously [8, 141].

Molecular interaction analysis

The heterodimer structures from pdb:3L82 and the best heterodimer output from ClusPro for Fbxo4:Fxr1 were interrogated for intermolecular contacts. Protein contact thresholds were 4.5 for hydrophobic interactions, 4.2 for ionic bonds, 2.5 for disulfide bonds with a sequence separation of 4 and a network separation of 0. Molecular images were prepared using MOE, as we described previously [8, 141].

Molecular modeling of ceramidosomes forming membrane pores

The theoretical model was created in several steps, as we have previously described. First the top C16-RIPK1 results from the i*n-silico* probe was duplicated in order to make a symmetric RIPK1 homodimer containing two molecules of ceramide. Two mode ceramides were added per molecule of RIPK1 and placed along the active site as a stack in order to create homodimer of RIPK1 with six total ceramides. Finally, the CBD of NMIIA was attached to each molecule of RIPK1. This was done using a prediction derived from a CluPro protein-protein interaction simulation. Part of the recognition domain of CBD from myosin molecules is defined and uses a conserved amphipathic helix (E^{1547}-K^{1555} in the case of NMIIA). A NMIIA (also known as MYH9) CBD domain homology model was created using the CBD (also known as a globular tail domain GTD)) from MyoVa (PDB:4KP3) [148]. Using the structural file for RIPK1 and the CBD of NMIIA, bimolecular docking was performed. Using the docking servers ClusPro server, the RIPK1 structure (as described above) was uploaded as the ligand and the NMIIA CBD structure was uploaded as the receptor. The binding residues were not selected nor were any residues selected to block docking and default settings were used to allow

maximum freedom of docking poses. The best pose and four of the top 10 poses indicated an interaction with the E^{1547}-K^{1555} helix and indicated it is favored interaction site. Using protein superposition between the CluPro results and the aforementioned RIPK1 dimer, the CBD was attached to each molecule of RIPK1.

Quantitative detection of ceramide-RIPK1 binding

H1341 cells were transfected with GFP-tagged RIPK1 WT, RIPK1 N169A, or empty vector (pEGFP.N1). Cells were lysed by freeze-thawing in non-denaturing buffer: 50mM Tris (pH7.4), 150 mM NaCl, 1mM EDTA, 0.5% NP-40 and 1:500 protease inhibitor cocktail. Lysates (2 mg protein) were precleared with 40µl agarose beads. The precleared lysates were incubated with GFP-magnetic beads at 4ºC for 18 hrs with gentle agitation. The beads were then washed with 1X PBS and incubated with unlabeled ceramide or biotin ceramide in 200µl of binding buffer. RIPK1-biotin-ceramide complexes were quantified using competitive ELISA with streptavidin coated plates. The results were analyzed using GraphPad Prism 7 software, as we previously described [8, 141].

Ultrastructural analysis using Transmission Electron Microscopy (TEM)

A549 cells were collected by scrapping off tissue culture plates. Rinsed with 1X PBS and fixed in 2% glutaraldehyde in 1X PBS. After post-fixation with 2% (vol/vol) osmium tetroxide, specimens were embedded in Epon 812, and sections were cut orthogonally to the cell monolayer with a diamond knife. These sections were visualized with a JEOL1010 transmission electron microscope.

Immunogold analysis using transmission electron microscopy

H1341 cells were treated with FTY720/vehicle, collected by scraping the cells off the plate using cell lifter. The cells were washed with 1X PBS and fixed for 15 minutes with 4% paraformaldehyde. The cells were washed again 2X with 1X PBS, and permeabilized with 0.01% saponin. The saponin was rinsed off 2X with 1X PBS, followed by blocking for 20 minutes with 1% BSA (in 1XPBS) and incubated with primary antibody (1:100) at 4ºC for 18 hrs. After primary antibody incubation, the cells were pelleted by centrifuging for 5 minutes at 1,300 rpm. The pellets were then rinsed 2X with 1% BSA, before incubation with secondary antibody (gold-conjugated Donkey anti-mouse/rabbit) at 1:200 dilution for 1 hr at room temperature. Finally, the cells were washed 2X with 1% BSA and post-fixed with 1% glutaraldehyde (in 1XPBS) for 10 minutes, then kept in ddH_2O. The staining was enhanced by silver staining before imaging.

Scanning Electron Microscopy (SEM)

Post treatment, samples were fixed with primary fixative (2% glutaraldehyde, 2% paraformaldehyde in 0.1 M cacodylate buffer pH 7.35). Secondary fixation was achieved with 1% osmium tetroxide in 0.1 M cacodylate buffer. After both fixation steps, samples were washed three times with ddH_2O then dehydrated with increasing ethanol concentrations (20% to 100%). Samples were submerged in 100% ethanol and critical point drying was achieved with a Tousimis Autosamdri-931 (Rockville, MD). Before imaging, 3-6 nm iridium was applied to samples and images were acquired with a

Magellan 400 field emission scanning electron microscope (FEI) (Hillsboro, OR) at the Notre Dame Integrated Imaging Facility.

Germline knockdown of *zipper*

Fly stocks were obtained from Bloomington Drosophila Stock Center and maintained at 25°C. *zipper* was knocked down in the germline by driving *zipper* shRNA using Gal4-nos.NGT. Adult ovaries in F1 progeny from this cross were rudimentary.

***Drosophila* ovaries immunostaining and microscopy**

Immunostaining of ovaries was performed as described earlier [149]. α-Ceramide was used at 1:100 [150]. α-1B1 was obtained from Developmental Studies Hybridoma Bank, Iowa and used at 1:50 dilution. Confocal images were taken using Zeiss LSM 880 NLO microscope and Plan-Apochromat 63x/1.40 Oil DIC objective. Images were analyzed using Fiji (ImageJ).

Immuno-gold labeling of *Drosophila* ovaries

Isolated ovaries from *D. melanogaster* flies were stained with gold-labeled ceramide as described in [151]. Briefly, paraformaldehyde tissues were sliced into ultra-thin sections using a microtome. The sections were mounted on carbon-coated copper grids. The grids were then rinsed, blocked and incubated with ceramide antibody, then gold labeled antibody before contrast staining with uranyl acetate and imaging.

FB1 exposure of *D. melanogaster*

10-15 adult male and female OregonR flies were exposed to food containing 100 μM FB1. Flies not exposed to FB1 were used as control. F1 generation flies from exposed and not exposed parents were used for immunostaining adult ovaries using α-1B1 and α-Ceramide.

Statistical analysis

Data were reported as mean ± standard deviation. Statistical analysis was performed by ANOVA or Student's t-test using Prism/GraphPad software version 7; $p < 0.05$ were considered statistically significant, as described previously [8, 141].

CHAPTER THREE: RESULTS

1. FTY720 induces loss of PM integrity, which can be inhibited by Blebbistatin

To confirm that FTY720-mediated necroptosis was associated with plasma membrane alteration, a known occurrence in necroptosis, we carried out live cell imaging, transmission electron microscopy (TEM), and scanning electron microscopy (SEM) studies. We treated GFP-expressing A549, non-small cell lung cancer cells with FTY720 or vehicle (DMSO) and carried out live cell imaging over a period of 240 minutes. Our data showed that FTY720 induced membrane blebbing, followed by plasma membrane rupture and necroptosis in a time dependent manner **(Figure 7A-B).** Using A549 cells without GFP, we were also able to detect compromised plasma membrane with YO-PRO1 [152] and propidium iodide (PI) dyes **(Figure 7C),** used to detect plasma membrane breaks and cell death. We further detected the plasma membrane breaks and/or holes using transmission electron microscopy and scanning electron microscopy in cells treated with FTY720 **(Figure 8 A-B).**

Interestingly, FTY720-mediated blebbing and plasma membrane rupture was largely abrogated when the cells were pretreated with blebbistatin [153], a known inhibitor of non-muscle myosin IIA (NMIIA)-mediated blebbing in A549 cells detected using live cell imaging **(Figure 9A-B)** and trypan **(Figure 9C).** Concurrently, Blebbistatin pretreatment inhibited the plasma membrane breaks/holes in cells, detected by SEM **(Figure 10).** Thus, these data suggest that FTY720-mediated necroptosis is linked to NMIIA-mediated blebbing, resulting in membrane rupture and cell death.

Moreover, alterations of the plasma membrane integrity and induction of necroptotic cell death in response to FTY720 were also evident with YOPRO-1 and PI dyes in H1341, a small cell lung cancer cell line, using live cell imaging **(Figure 11A)**

and flow cytometry **(Figure 11 B-C).** This was confirmed using trypan blue exclusion assay **(Figure 11 D).**

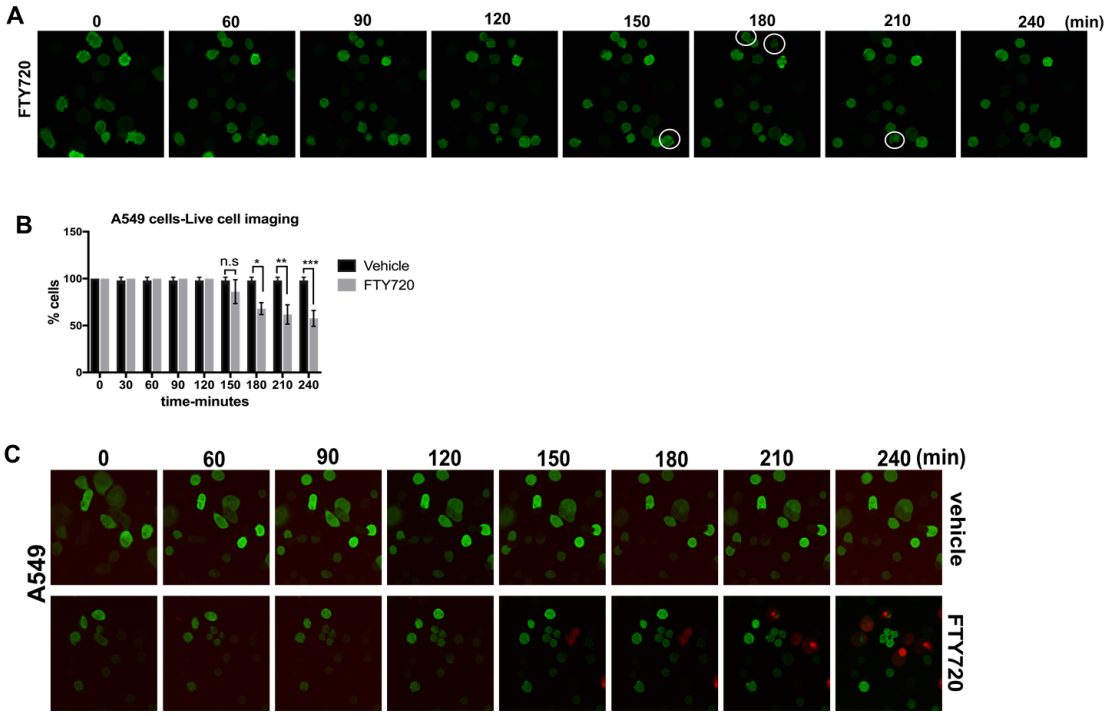

Figure 7 : Loss of plasma membrane integrity in A549 cells in response to FTY720

A. A549-GFP cells were treated with 20µM FTY720 and their morphological changes monitored over a period of 240 minutes. Frozen frames of the time lapse experiment show plasma membrane blebbing before rupture and disintegration of cells treated with FTY720, quantified in **B**. Data are means ± SD from three independent experiments, analyzed by paired student t-test (n=3, *P= 0.002**P=0.004***P=0.002). **C**. Effect of FTY720 on cells' plasma membrane integrity. Live cell imaging in A549-GFP cells shows plasma breakage as evidenced by incorporation of propidium iodide dye (red) in A549 cells.

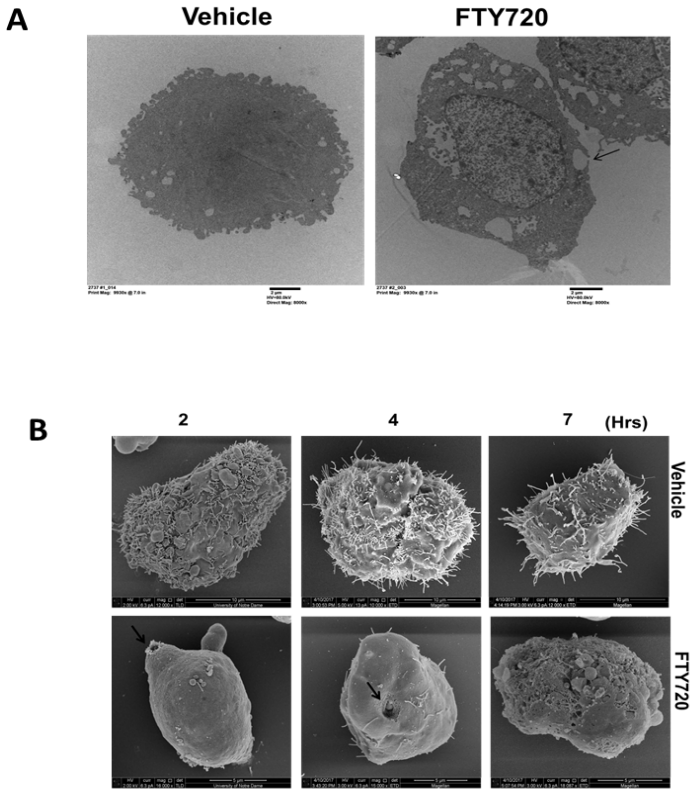

Figure 8 : Electron microphotographs A549 and H1341 cells after FTY720 treatment

A. TEM micrographs show plasma membrane breaks (compromised plasma membrane, shown with black arrow) in FTY720 (20μM) treated A549 cells. **B.** SEM micrographs show pores (shown with black arrows) and compromised plasma membrane in H1341 cells after FTY720 treatment (20μM), in a time-dependent manner.

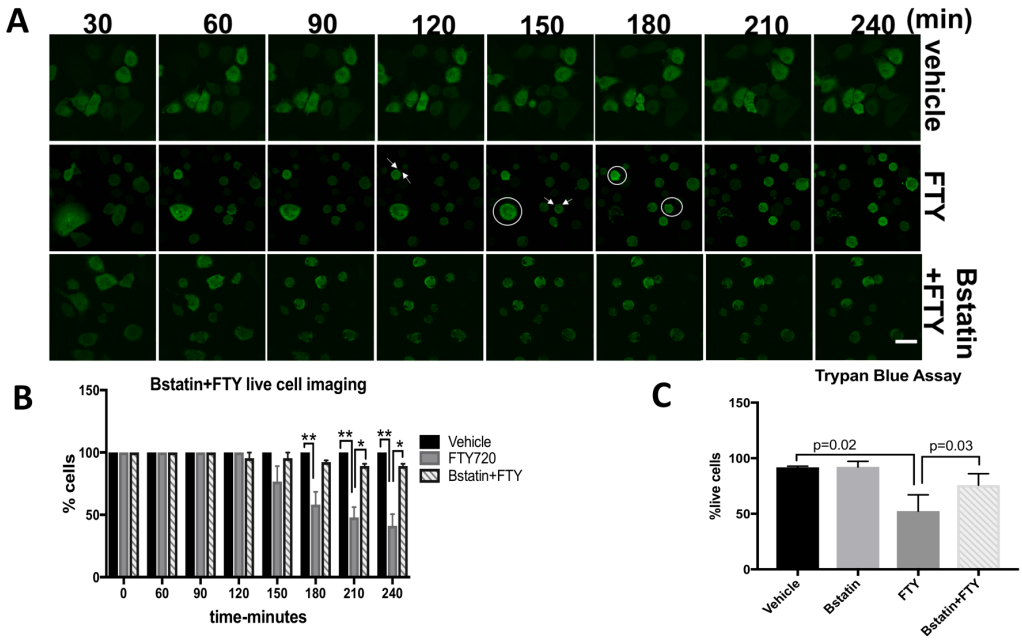

Figure 9 : Blebbistatin protects cells from FTY720-induced necroptosis

A. A549-GFP cells were pretreated with blebbistatin (12.5μM for 2hr) before FTY720 treatment shows and time lapse images were taken to monitor changes in morphology. Blebbistatin treated cells showed protection from plasma membrane rupture induced by FTY720, quantified in **B,** Data are means ± SD from three independent experiments, analyzed by paired student t-test (n=3, *P=0.03**P<0.0008). **C.** Trypan blue in A549 cells pretreated with blebbistatin before FTY720 treatment.

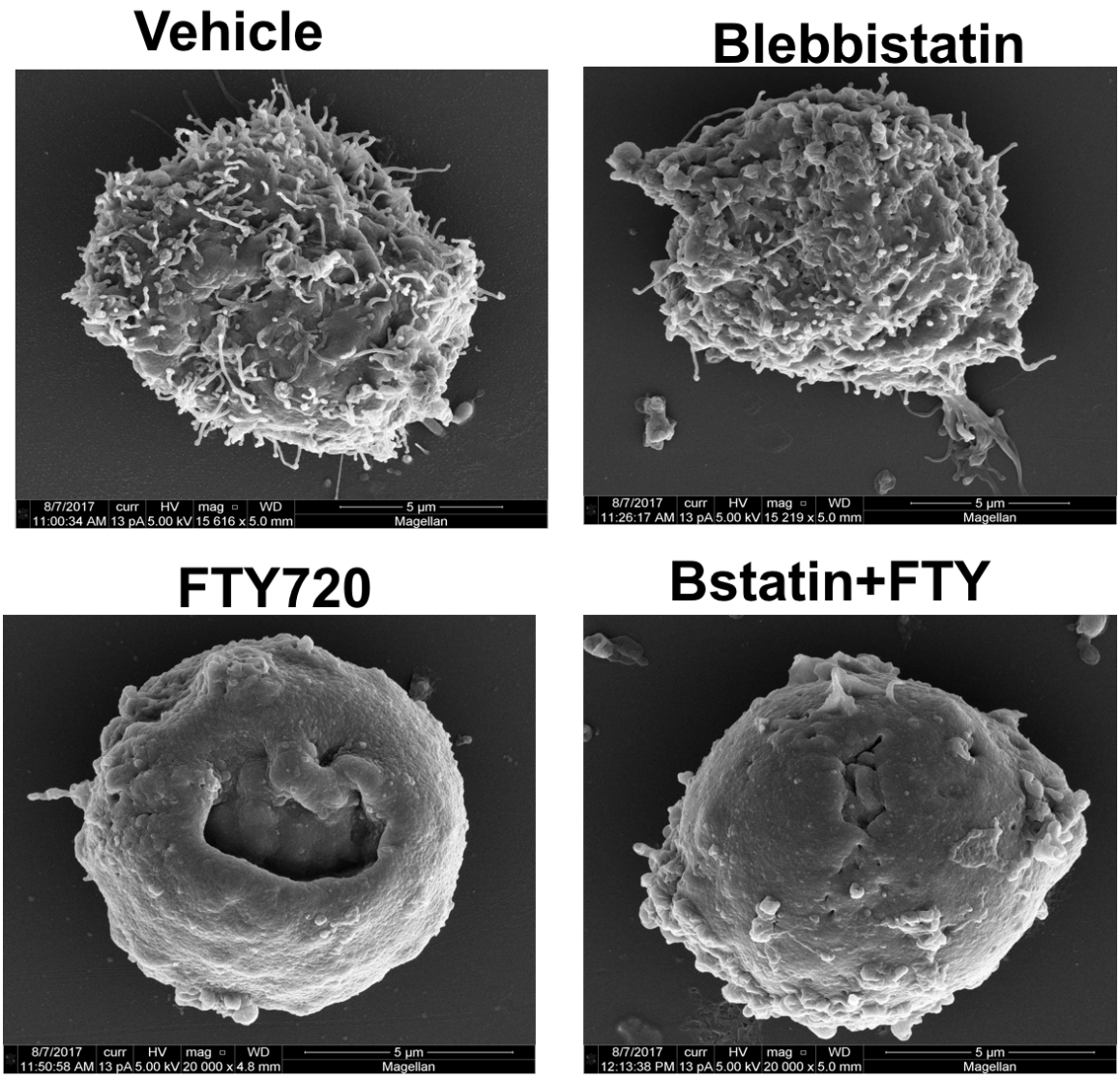

Figure 10 : Blebbistatin pretreatment inhibits FTY720-induced plasma membrane holes

SEM micrographs show protection of the hole punctures in plasma membrane in cells pretreated with blebbistatin (12.5 μM, 2 hr) before FTY720 treatment.

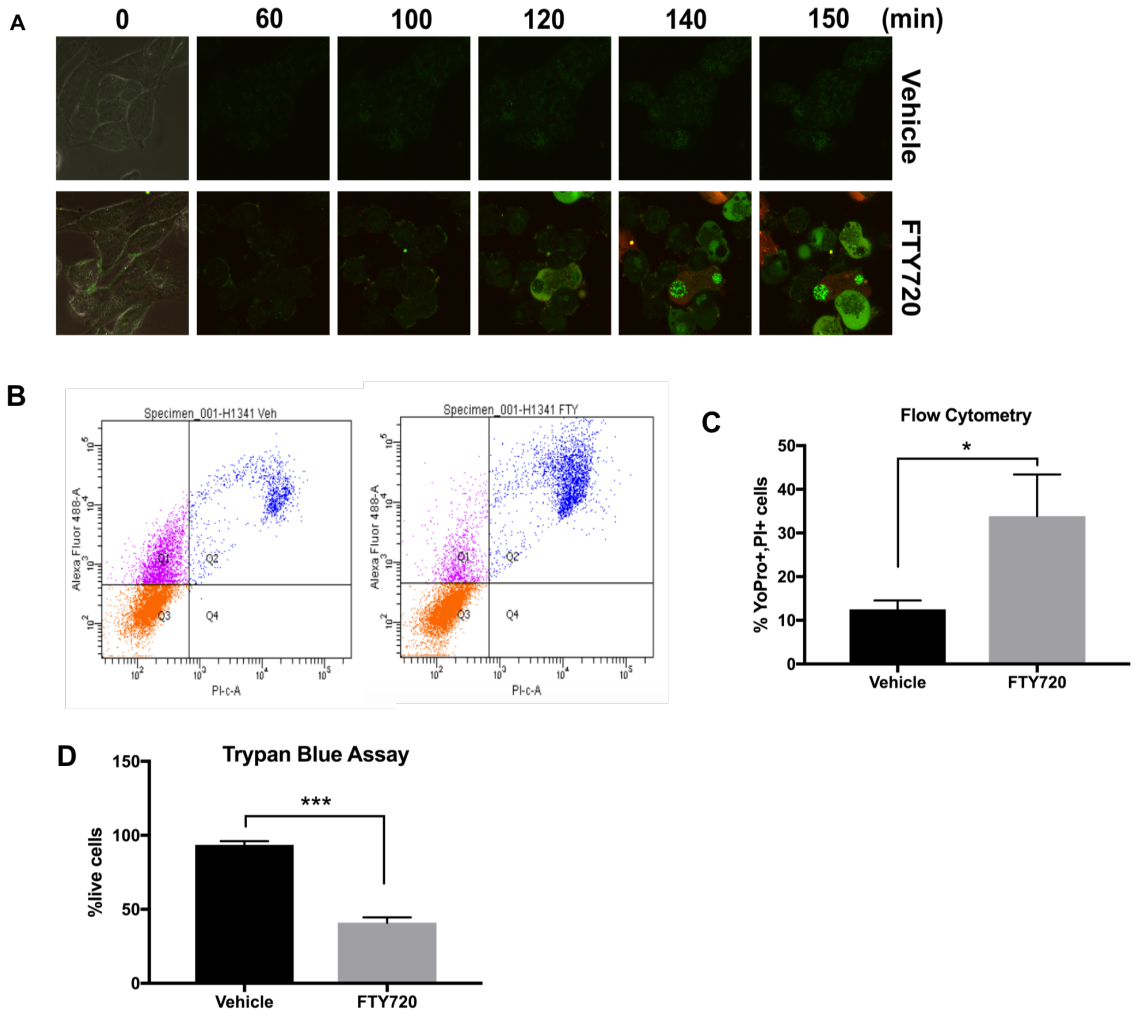

Figure 11 : FTY720 treatment induces plasma membrane permeability and cell death in H1341 cells

A. H1341 cells were imaged with YOPRO-1(green) and PI (red) dyes after exposure to FTY720. **B.** Flow cytometry indicate increased necroptosis in cells treated with FTY720 versus vehicle (DMSO). Flow cytometry data is quantified in **C**. Data represents means ± SD from three independent experiments, analyzed by paired student's t-test (n=3, *P=0.02). **D**. Trypan blue exclusion assay shows significant trypan blue inclusion with FTY720 treatment. Data represents means ± SD from three independent experiments, analyzed by paired student's t-test (n=3, ***P<0.0001).

2. FTY720 induces ceramide-enriched macrodomains on the PM

Because FTY720-induced necroptosis was independent of RIPK3 and MLKL [65], and FTY720 is known to modulate ceramide synthesis, we investigated whether FTY720-mediated necroptosis is linked to ceramide generation, a bioactive lipid that is known to alter membrane integrity and induce blebbing [154]. Surprisingly, there were no detectable changes in the overall abundance of ceramides in response to FTY720, measured by LC/MS/MS in A549 total cell lysates **(Figure 12).**

In addition to the amounts of sphingolipids, their localization, also confers their role in the cell [6-8, 155]. Because of this, we investigated whether FTY720 exposure resulted in the changes in ceramide subcellular localization. Interestingly, in A549 cells, FTY720 led to the formation of ceramide platforms/macrodomains on the plasma membrane, as detected by immunofluorescence using two distinct anti-ceramide antibodies [150, 156] **(Figure 13 A-B).** There was no accumulation of S1P or cholesterol on the plasma membrane, as detected by anti-S1P or anti-cholesterol antibodies respectively [157,158] **(Figure 13 C-D**). Moreover, treatment of cells with NBD-FTY720, a fluorescently tagged FTY720, showed no sign of drug accumulation on plasma membrane of A549 cells **(Figure 13 E),** suggesting that FTY720 itself does not accumulate in ceramide-enriched membrane macrodomains, which appear to be around 1-2 microns in diameter.

To confirm the presence of ceramide in the FTY720-mediated membrane macrodomains, we depleted ceramides in H1341 cells by overexpressing acid ceramidase (AC) [92, 159], an enzyme that hydrolyzes ceramide to sphingosine and fatty acid. Ectopic expression of AC using adenoviral particles (Ad-GFPAC), reduced total ceramide levels **(Figure 14 A)** and abrogated the formation of ceramide-enriched membrane

macrodomains **(Figure 14 B-C). Figure 14 D** Shows the expression levels of AC compared to Ad-GFP control. Taken together, these data suggest that FTY720 exposure induces the formation of membrane pores, which are enriched in endogenously generated ceramides, altering plasma membrane integrity and inducing necrotic cell death.

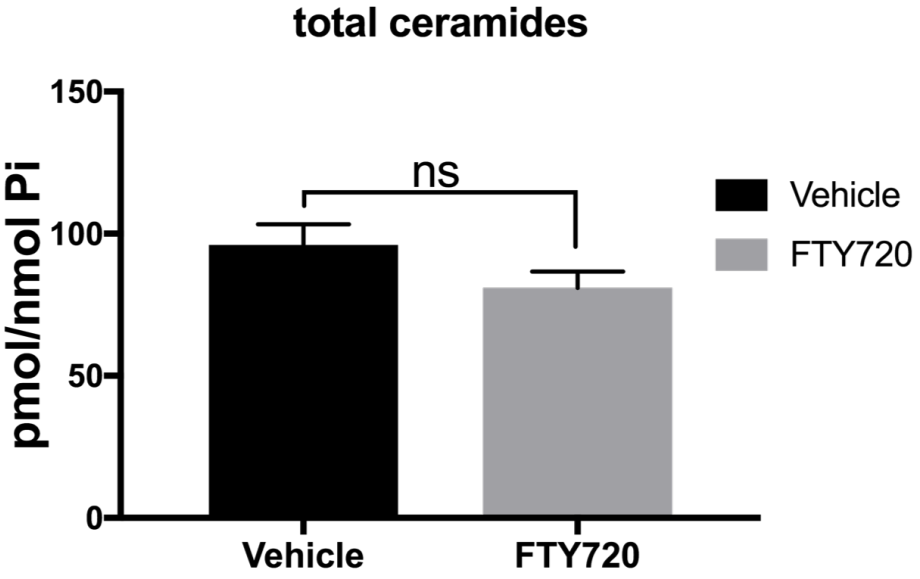

Figure 12 : FTY720 does not alter ceramide generation in A549 cells

A549 cells treated with FTY720 (20μM, 2hr) show no significant changes in the ceramide levels in A549 cells after treatment. Data represents means ± SD from three independent experiments, analyzed by paired student's t-test (n=3, p=0.14).

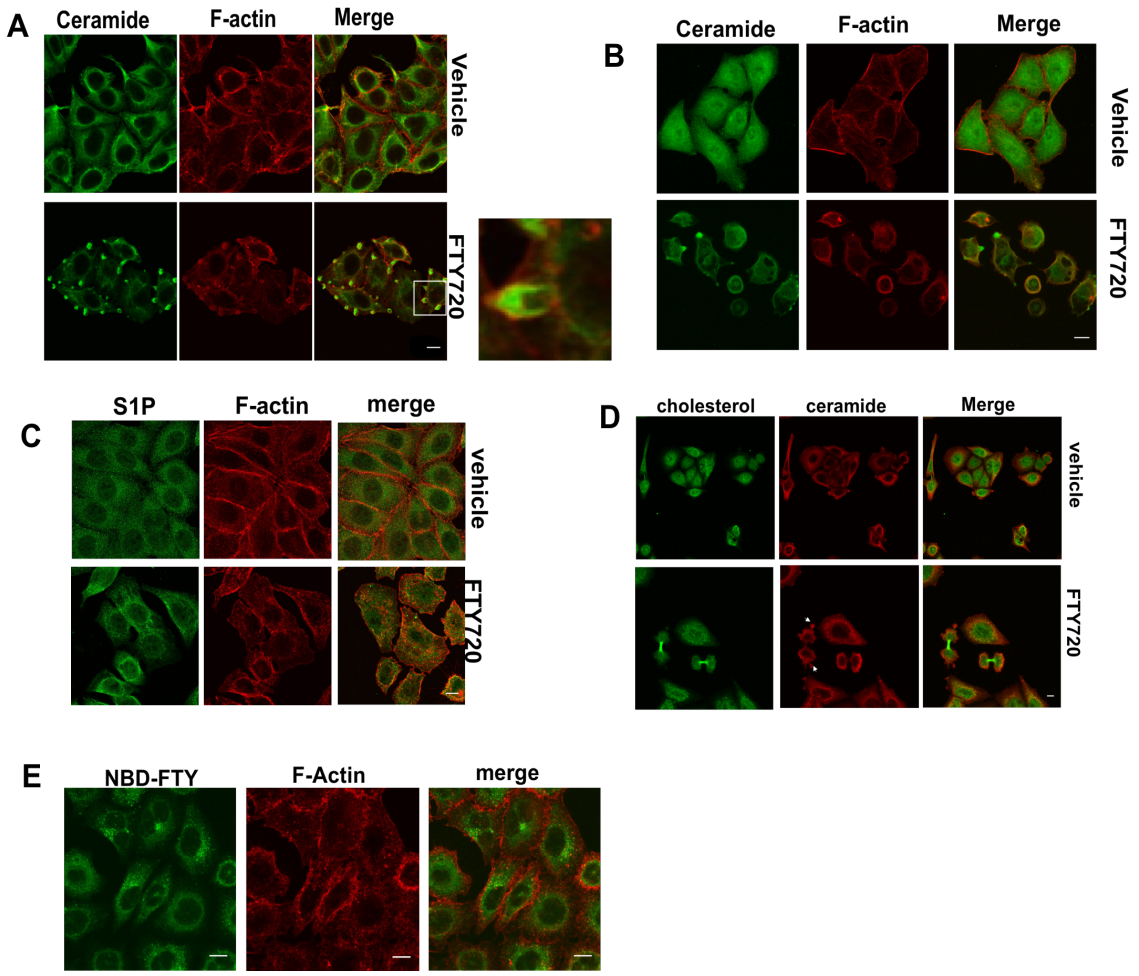

Figure 13 : FTY720 induces ceramide-enriched membrane macrodomains

A. A549 cells were treated for 2hr, with 20μM FTY720, stained for ceramide and F-actin (Rhodamine phalloidin) and imaged using laser scanning confocal microscopy, evidence of ceramide-enriched macrodomains in the plasma membrane. Right panel at the bottom represents a zoom-out of the framed area. Scale bar represents 100 μm. **B.** A549 cells treated with FTY720 (20μM, 2hr) stained with a different ceramide antibody (Rabbit anti-ceramide) and F-actin also show the ceramide-enriched membrane macrodomains. **C**. A549 cells treated with FTY720 (20μM, 2hr) and stained for S1P using anti S1P antibody (1:100) and in **D,** cholesterol using anti-cholesterol antibody (1:100) as controls for ceramide antibody staining. **E.** A549 cells treated with NBD-labeled FTY720 (20μM, 2hr) showed no fluorescence (FTY720) accumulation on the plasma membrane

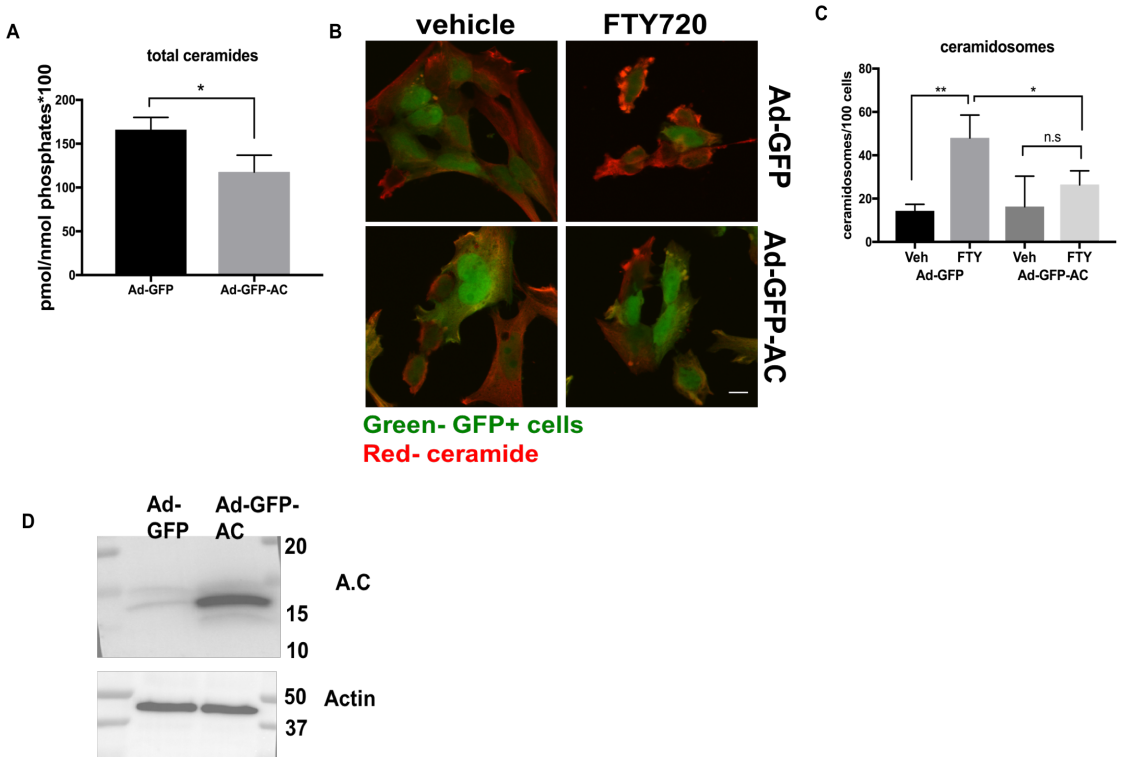

Figure 14 : FTY720-induced macrodomains are specifically made up of ceramide

A. Effects of AC overexpression on cells' lipidomics profile was determined by LC/MS/MS, there was significant decrease in total ceramide levels. Data represents means ± SD from three independent experiments, analyzed by paired student t-test (n=3, *P=0.047). **B.** Ad-GFP-AC was over-expressed in H1341 cells, the cells were treated with 20 µM FTY720 48 hr post-transduction and stained for ceramide-enriched membrane pores. This is quantified in **C.** Data are means ± SD from three independent experiments, analyzed by paired student t-test (n=3 *P=0.02. **P=0.03). **D.** Western blot shows AC expression compared to Ad-GFP control.

3. Ceramide-enriched macrodomains are novel structures

The ceramide-enriched macrodomains were not detectable in the Golgi, ER, early endosomes, caveolin-enriched lipid microdomains, or exosomes in response to FTY720 in these cells **(Figure 15 A)**. In addition, the macrodomains were only induced by FTY720 and its non-phosphorylatable analogues. This was studied by exposing A549 cells to other sphingolipids, such as myriocin (as FTY720 is a myriocin analogue), sphingosine, S1P and lysophosphatidic acid (LPA), all of which, did not induce the ceramide-enriched macrodomains. Exposure of cells to FTY720 and its non-phosphorylatable analogue OSU-2S [160] largely mediated ceramide-enriched membrane pores formation **(Figure 15 B).** In addition, a FTY720-mimetic selected from the ChemBridge library in silico (compound 5) was also able to induce ceramide-enriched membrane pores, suggesting that ceramidosome formation is not dependent on selective FTY720 exposure.

As expected, phosphorylated FTY720 (P-FTY720) did not induce ceramidosomes **(Figure 15 B).** We confirmed this by knocking down sphingosine kinase 2 (SPHK2 or SK2), the key enzyme that phosphorylates FTY720 to P-FTY720. Knocking down SK2 had no effect on ceramidosomes formation compared to controls, scrambled (SCR)-shRNA-transfected and vehicle-treated cells **(Figure 16 A-B).** FTY720 and P-FTY720 levels were measured in A549 cells using mass spectrometry-based lipidomics [142] **(Figure 16 C)** and data showed significant decrease in P-FTY720 with SK2 knockdown, further confirming that ceramidosomes were induced by FTY720 but not P-FTY720. **Figure 16 D.** shows the mRNA expression levels of SK2 after knockdown with shRNA.

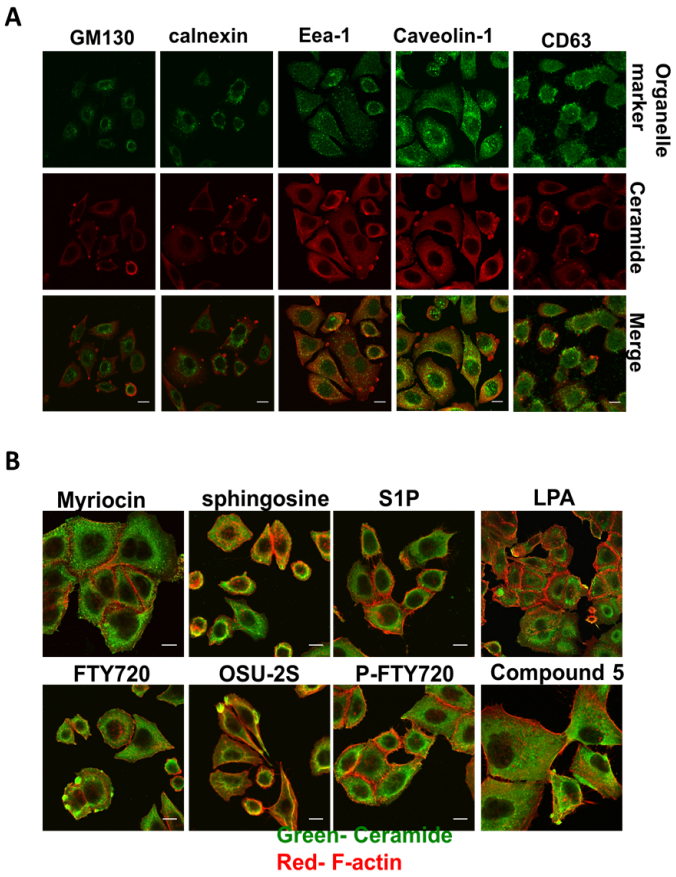

Figure 15 : Ceramide enriched-macrodomains are novel structures and are induced by FTY720 and its non-phosphorylatable analogues

A. A549 cells were treated with FTY720 and stained for ceramide and different organelle markers GM130 (golgi) calnexin (ER), Eea1(Early endosomal markers), caveolin-1 (caveolin-1-enriched lipid rafts), CD63 (Exosomes). Ceramide-enriched membrane pores did not co-localize with any of the stained organelles. **B**. A549 cells were treated with different lipid compounds (20 µM), ceramide and F-actin (Rhodamine phalloidin) were labeled to check evidence of ceramide-enriched membrane pores with immunofluorescence.

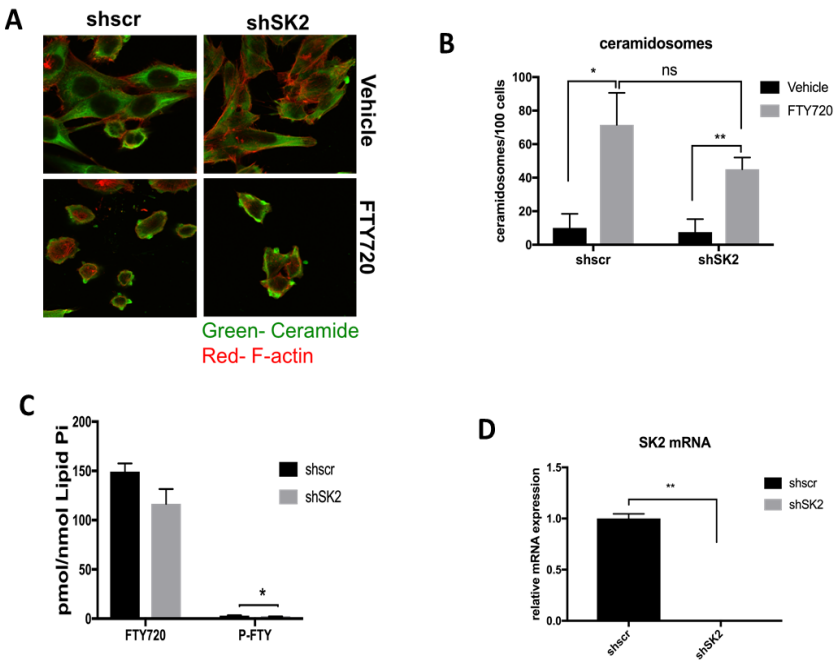

Figure 16 : SK2 knockdown does not affect FTY720-induced ceramide-enriched macrodomains

A. H1341 cells with stable SK2 knockdown were stained for ceramide-enriched membrane pores. The ceramide-enriched macrodomains are quantified in **B,** using ImageJ. Data represents means ± SD from three independent experiments, analyzed by paired student t-test (n=3, ns= not significant *P=0.05, **P=0.04). **C.** Lipidomics analysis of the level of FTY720 and P-FTY720 in H1341 cells with SK2 stable knockdown. Data represents means ± SD from three independent experiments, analyzed by paired student t-test (n=3, **P<0.0001) **D**. qRT-PCR data shows the level of SK2 mRNA after knockdown. Data represents means ± SEM from three independent experiments, analyzed by paired student t-test (n=3, **P<0.0001).

4. Different cell lines respond differently to FTY720 to form Ceramide-enriched membrane pores

During our experiments, we found that H1341 cells required almost tenfold less FTY720 to induce ceramide-enriched pores compared to A549. In H1341 cells, induction of ceramidosomes was detected with 0.1-1 μM FTY720 for 60 min as opposed to 10μM in A549 cells **(Figure 17 A-C)**, showing cell specificity and unique response to FTY720. Interestingly, while ceramide-enriched membrane pores formation in response to FTY720 was evident in multiple cancer lines including H1650 (non-small cell lung cancer, NSCLC), H1341 (small cell lung cancer, SCLC) and 22A (head and neck squamous cell carcinoma, HNSCC) **(Figure 18 A),** they were not detected in non-cancerous skin keratinocytes, normal human lung fibroblasts (NHLF) and NIH3T3 mouse embryonic fibroblasts **(Figure 18 B).** Collectively, these data suggest that FTY720 and FTY720 mimetics, but not P-FTY720, mediate the formation of ceramidosomes in various cancer cells, but not in non-cancerous keratinocytes or fibroblasts, in a dose and time-dependent manner preceding blebbing, lysis of the plasma membrane and necroptosis. The mechanisms mediating these differences between cell lines remain to be investigated. Given the novelty and specificity of these ceramide-enriched membrane pores formed by FTY720, we herein coin the name “ceramidosomes” for them.

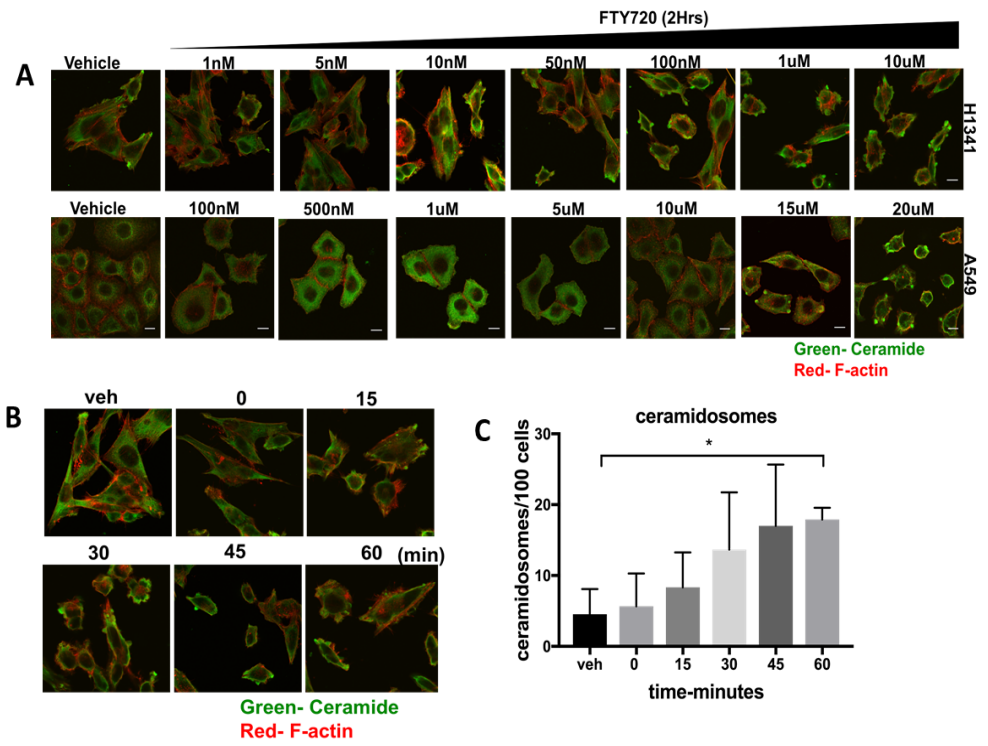

Figure 17 : FTY720 dose titration shows different sensitivity between H1341 and A549 lung cancer cells

A. H1341 and A549 cells were treated with increasing concentrations of FTY720 for two hours and stained with anti-ceramide antibody and Rhodamine phalloidin to check evidence of ceramide-enriched membrane pores with immunofluorescence. **B**. A time course experiment was carried out in H1341 cells. The cells were treated with 10 nM FTY720 for different time periods and stained with anti-ceramide antibody and rhodamine phalloidin to check evidence of ceramide-enriched membrane pores with immunofluorescence. The ceramide-enriched membrane pores are quantified in **C.** Data represent means ± SD from three independent experiments, analyzed by paired student t-test (n=3 *P=0.01).

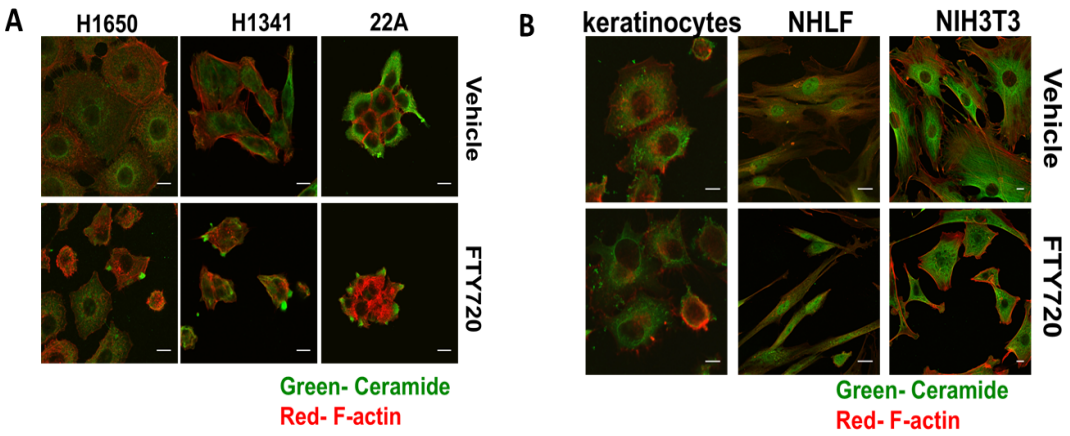

Figure 18 : Cancer cells but not non-cancerous cell form ceramide-enriched membrane macrodomains

A. Multiple cancer cell line were treated with Vehicle (DMSO) or 20 μM FTY720 for 2 hr and stained for ceramide and F-actin. **B.** Non-cancerous cells (keratinocytes, normal human lung fibroblast (NHLF) and NIH3T3) were treated with FTY720 (20μM for 2hr) or vehicle and showed no evidence of ceramide-enriched membrane pores.

5. Ceramide in FTY720-induced ceramidosomes is mainly C16-ceramide

To investigate the source of the ceramide enrichment in membrane pores in response to FTY720, we generated A549 cells stably expressing shRNAs against enzymes that catalyze ceramide generation. We knocked down neutral sphingomyelinase, SMase (nSM1-3), serine pamitoyl transferases, SPT (SPT1-3), and Ceramide synthases, CerS1, CerS2, CerS4, CerS5, and CerS6 using lentiviral particles. We omitted CerS3 because of its selective expression in skin and testes [161]. ShRNA-dependent knockdown of nSMases **(Figure 19 A)** or SPT enzymes **(Figure 19 B-D)** had no effect on ceramidosomes formation with/without FTY720.

Interestingly, knockdown of ceramide synthase 5 or 6, which generate C16-ceramide, but not CerS1, CerS2, or CerS4, abrogated ceramidosomes and protected cells from necroptosis in response to FTY720 **(Figure 20 A-B)**, (mRNA levels are shown in **Figure 20 C)**. Reduction of C16-ceramide by silencing CerS5 and/or CerS6 was confirmed by lipidomics compared to Scr-shRNA-transfected controls **(Figure 20 D)**. Thus, these data suggest that ceramidosomes mainly contain C16-ceramide generated by CerS5 and/or CerS6 in response to FTY720. The fact that the SPT enzymes did not affect ceramidosomes formation suggests a possible role for the salvage pathway in generating the C16 ceramide generation for ceramidosomes formation.

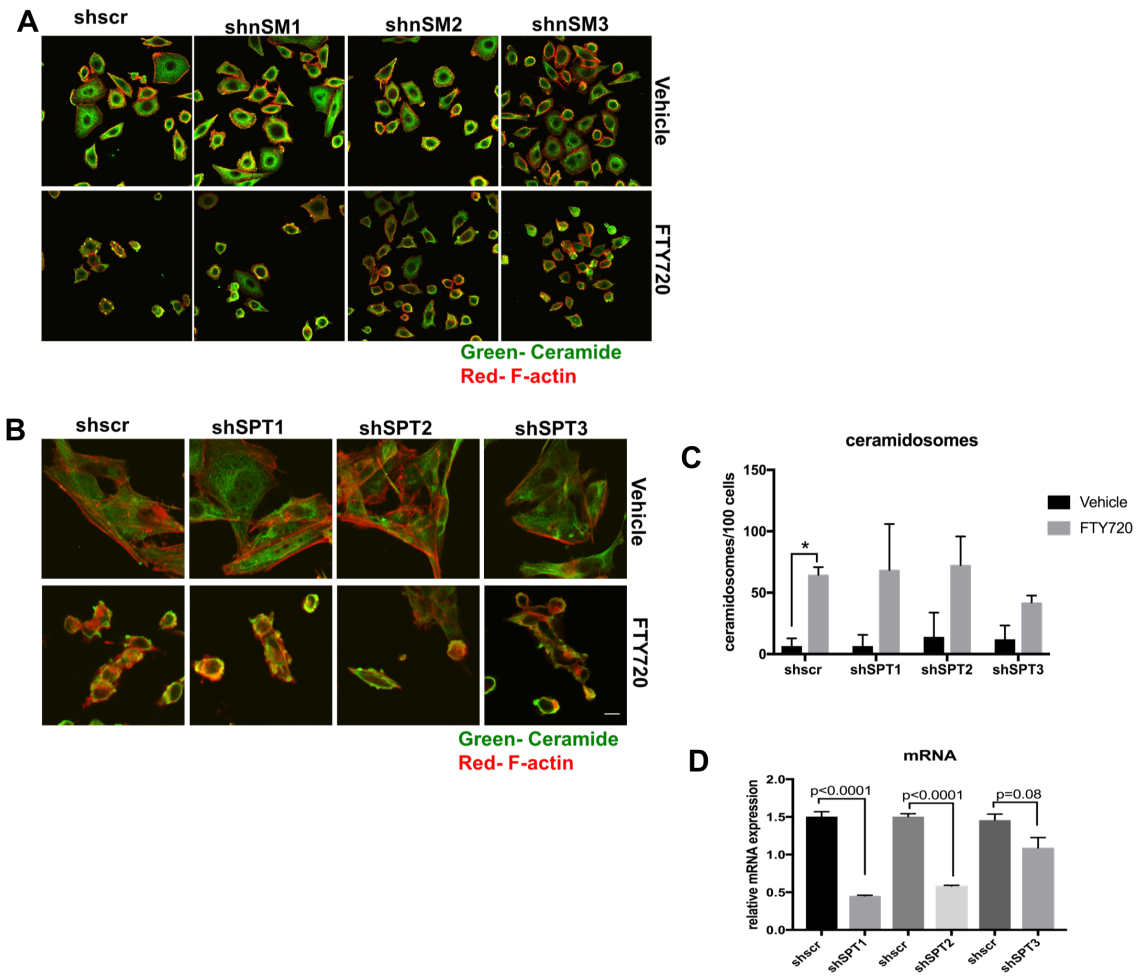

Figure 19 : Sphingomyelinases and serine pamitoyl transferases are not involved in ceramidosomes formation

A. The effects of genetic loss of SMases were studied in A549 cells with stable knockdown of different nSMases. Knocking down nSMases did not abrogate ceramide-enriched membrane pores. **B**. H1341 cells with stable SPT knockdown were stained for ceramide-enriched membrane pores. Knocking down SPT did not significantly abrogate ceramide-enriched macrodomains. This is quantified in **C**. Data represents means ± SD from three independent experiments, analyzed by paired student t-test (n=3, *P=0.01). **D**. mRNA expression levels in the shSPT stable knockdown cells were determined by qRT-PCR. Data represents mean ± SEM from three independent experiments, analyzed by paired student t-test (n=3, *P=0.046).

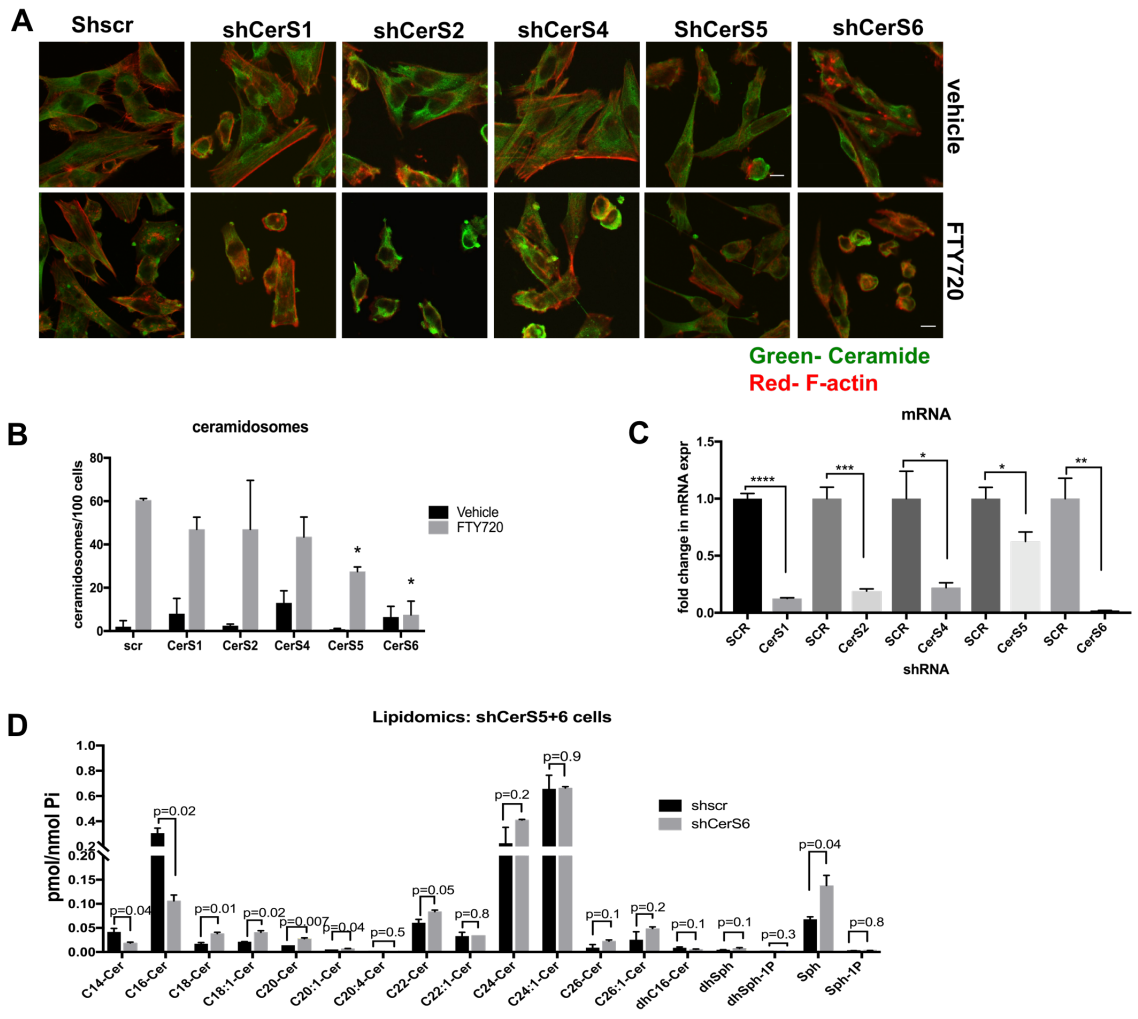

Figure 20 : C16 ceramide in ceramidosomes is generated by CerS5 and CerS6

A. Effects of genetic loss of ceramide synthases on ceramidosomes formation were measured using immunofluorescence with ceramide antibody and Rhodamine phalloidin (F-actin) in H1341 cells with CerS1 CerS2, CerS4, CerS5, CerS6 shRNA, compared to scramble (shscr) shRNA. ceramide-enriched membrane pores were manually quantified **B.** Data represent means ± SD from three independent experiments. Analyzed by student t-test (n=3, *P<0.05) Scale bar represents 100 µm. **C**. mRNA expression levels in the shCerS 1, 2, 4, 5, 6 stable knock-down cells were determined by qRT-PCR. Data represents mean ± SEM from three independent experiments, analyzed by paired student t-test (n=3, *P=0.04**,** **P=0.005, ***P=0.001, ****P<0.0001). **D.** Lipidomics analysis was carried out in H1341 cells with stable CerS5 and 6 knock-down. Data are means ± SD from three independent experiments, analyzed by paired student t-test (n=3).

6. Ceramidosomes mediate RIPK1-dependent necroptosis

Because our previous studies indicated FTY720-mediated necroptosis was dependent on RIPK1, but not RIPK3 [65], we assessed whether RIPK1 played any role in the formation of ceramidosomes in response to FTY720. To determine if RIPK1 is localized within ceramide-enriched membrane pores, we first measured the co-localization of RIPK1 and ceramide by immunofluorescence using anti-RIPK1 and anti-ceramide antibodies. FTY720 exposure induced the co-localization of RIPK1 and ceramide compared to vehicle-treated controls within plasma membrane **(Figure 21 A).** This co-localization between RIPK1 and ceramide was also detectable by immunogold TEM using gold labeled anti-RIPK1 (labeled with 10 nm gold particles) and anti-ceramide (labeled with 1.4 nm gold particles) antibodies **(Figure 21 B**) and proximity ligation assay (PLA) using anti RIPK1 and anti-ceramide antibodies **(Figure 21 C-D)** in response to FTY720 compared to vehicle-treated controls. Thus, these data suggest that RIPK1 is co-localized with ceramide at the plasma membrane within ceramidosomes in response to FTY720-mediated stress.

Then, to determine if RIPK1 was necessary for ceramidosome formation, we measured the effects of RIPK1 knockdown on ceramidosomes in response to FTY720. ShRNA-mediated knockdown of RIPK1 prevented ceramidosomes formation in response to FTY720 **(Figure 22 A-B),** (protein expression in panel **C)**, and protected cells from necroptosis compared to Scr-shRNA-transfected and vehicle-treated cells **(Figure 22 D).**

In contrast, knocking down RIPK3 using shRNA had no effect on ceramidosome formation **(Figure 23 A-B)** or cell death **(Figure 23 C).** (mRNA levels are shown in

Figure 23 D). Given that RIPK3 is known to activate MLKL, which induces membrane pores for the execution of necroptosis [61, 162], we also measured the effects of MLKL inhibition on ceramide-enriched membrane pores formation, using a pharmacological inhibitor necrosulfonamide (NSA) [162]. NSA-mediated MLKL inhibition had no effect on FTY720-mediated ceramidosome formation **(Figure 23 E-F)** or necroptosis as tested by trypan blue assay **(Figure 23 G).**

As an additional control, we also explored other known pore-forming proteins that could be involved in the execution of FTY720-mediated necroptosis. To achieve this, we investigated the effects of purinergic receptor protein (P2X7), which is known to form membrane pores in response to cytotoxic stress such as increased ATP accumulation [163]. Our data showed that pharmacological inhibition of P2X7 using inhibitor AZ10606120 [164] had no effect on induction of ceramidosomes **(Figure 24 A-B)** or necroptosis, **(Figure 24 C)** in the presence of FTY720. Thus, these data are consistent with our previous findings, indicating that while RIPK3 and MLKL were dispensable, RIPK1 is necessary for FTY720-induced ceramidosome formation and necroptosis.

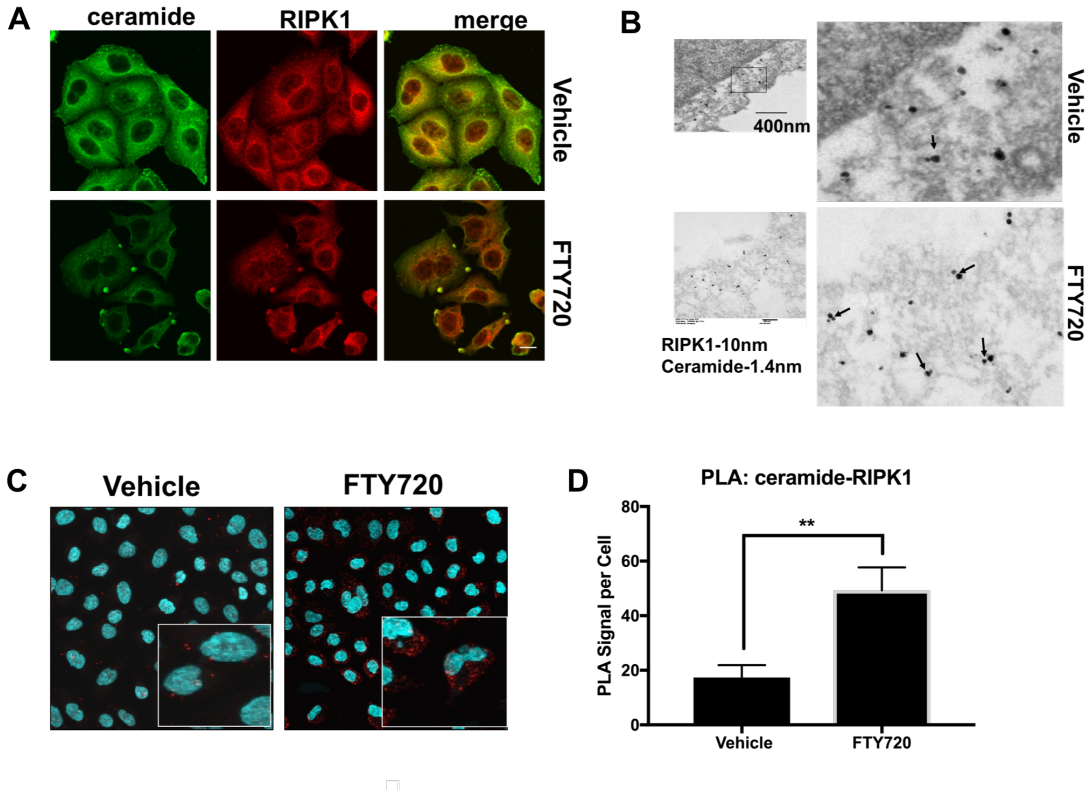

Figure 21 : RIPK1 colocalizes with ceramide in FTY720-induced ceramidosomes

A. Colocalization of RIPK1 and ceramide was measured by confocal microscopy. A549 cells were treated with 20 µM FTY720 for 2 hr and stained with anti-ceramide antibody and anti- RIPK1 antibody and detected by immunofluorescence. Colocalization of RIPK1 and ceramide is evident on the plasma membrane in response to FTY720 treatment. **B**. RIPK1-ceramide colocalization was further detected by immuno-gold TEM. H1341 cells were treated with FTY720 or Vehicle (DMSO). The electron microphotograph shows increased RIPK1 (10 nm gold) association with ceramide (1.4 nm gold) in cells treated with FTY720. **C.** This was confirmed in A549 cells by proximity ligation assay (PLA). Cells treated with FTY720 (20 µM) had increased RIPK1-ceramide association. This is quantified in **D**. Data represent means ± SD from five independent experiments, analyzed by paired student t-test (n=5 **P=0.006).

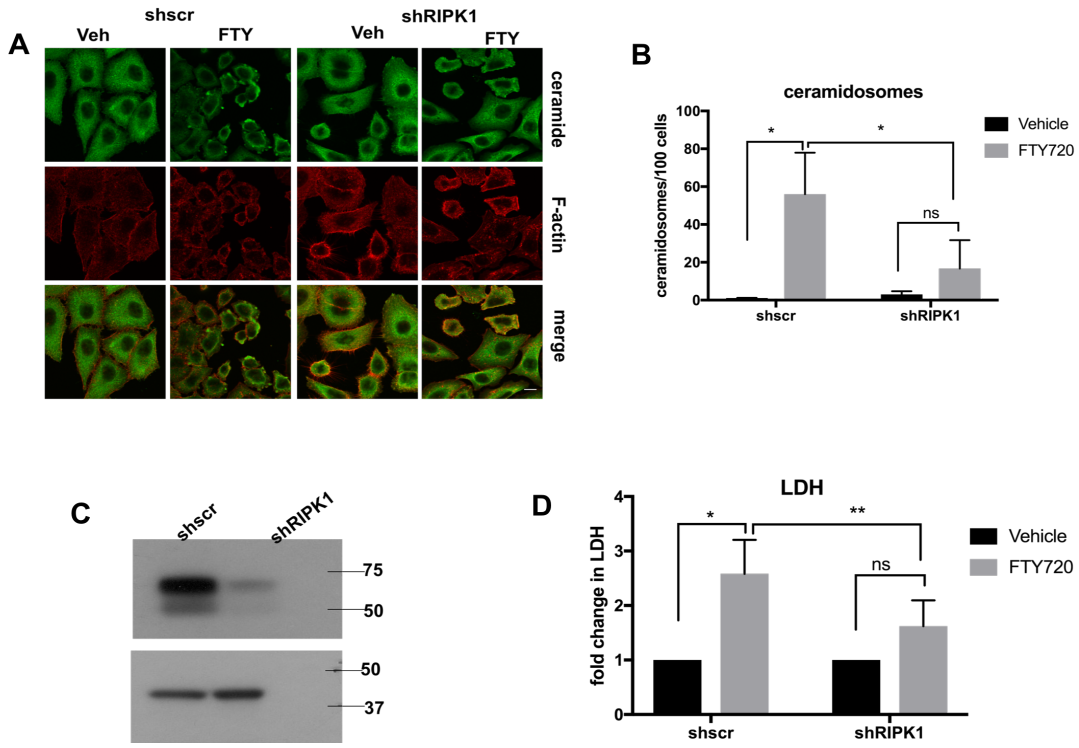

Figure 22 : Knocking down RIPK1 inhibits ceramidosomes formation

A. To study effects of RIPK1 silencing on ceramidosomes formation, A549 cell were stably transfected with lentiviral shRNA against RIPK1. These cells were treated with 20 µM FTY720 or vehicle for 2 hr and stained with anti-ceramide antibody and Rhodamine phalloidin (F-actin). shRIPK1 cells had significantly less ceramidosomes formed as quantified in **B.** Data represent means ± SD from three independent experiments, analyzed by paired student t-test (n=3 *P=0.01). **C.** Western blot shows the RIPK1 expression after knockdown in with RIPK1 shRNA lentiviral particles in A549 cells. RIPK1 was knocked down over 70%. **D.** LDH assay was used to study effect of RIPK1 knockdown on FTY720-induced necroptosis. shRIPK1-A549 cells were less sensitive to FTY720 treatment compared to shscr cells. Data represent means ± SD from three independent experiments, analyzed by paired student t-test (n=3 *P=0.048, **P=0.008, ns=not significant).

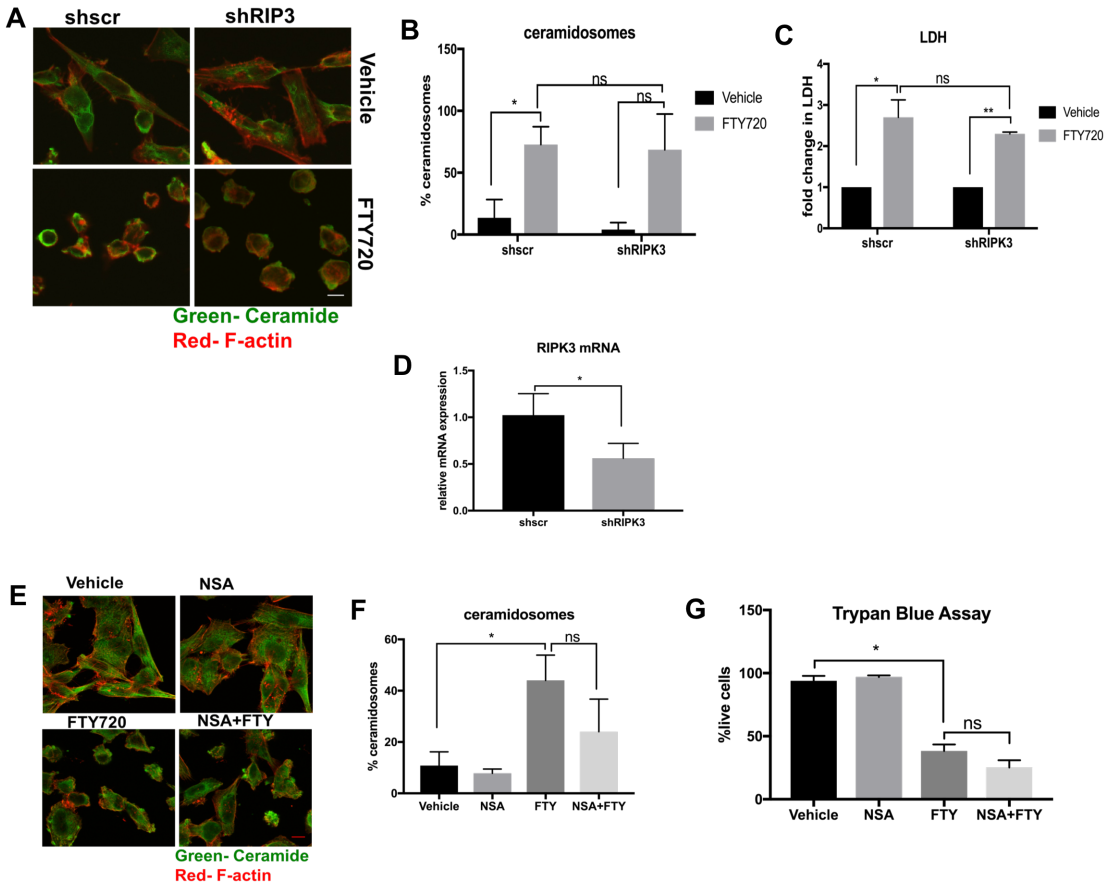

Figure 23 : RIPK3 and MLKL are dispensable in FTY720 induced ceramidosomes formation and necroptosis

A. H1341 cells with stable RIPK3 knockdown were investigated for presence of ceramidosomes with/without FTY720 treatment (10μM 1hr). These were quantified as shown in **B**, Data are means ± SD from three independent experiments, analyzed by paired student t-test (n=3, *P=0.002). **C**. LDH Assay in shRIPK3 cells treated with FTY720 (20μM, 3hr or vehicle control). Data represents means ± SD from three independent experiments, analyzed by paired student t-test (n=3, *P=0.02, **P=0.005). **D**. mRNA expression of RIPK3 in the RIPK3 stable knockdown cells was determined by qRT-PCR. Data represents means ± SEM from three independent experiments, analyzed by paired student t-test (n=3, *P=0.046). **E**. H1341 cells were pretreated with NSA (MLKL inhibitor, 2.5μM for 2hr). The ceramide-enriched pores are quantified in **F**. Data represents means ± SD from three independent experiments, analyzed by paired student t-test (n=3, *P=0.04). **G**. Trypan blue assay was carried out in the NSA pretreated H1341 cells. Data represents means ± SD from three independent experiments, analyzed by paired student t-test (n=3, *P=0.01).

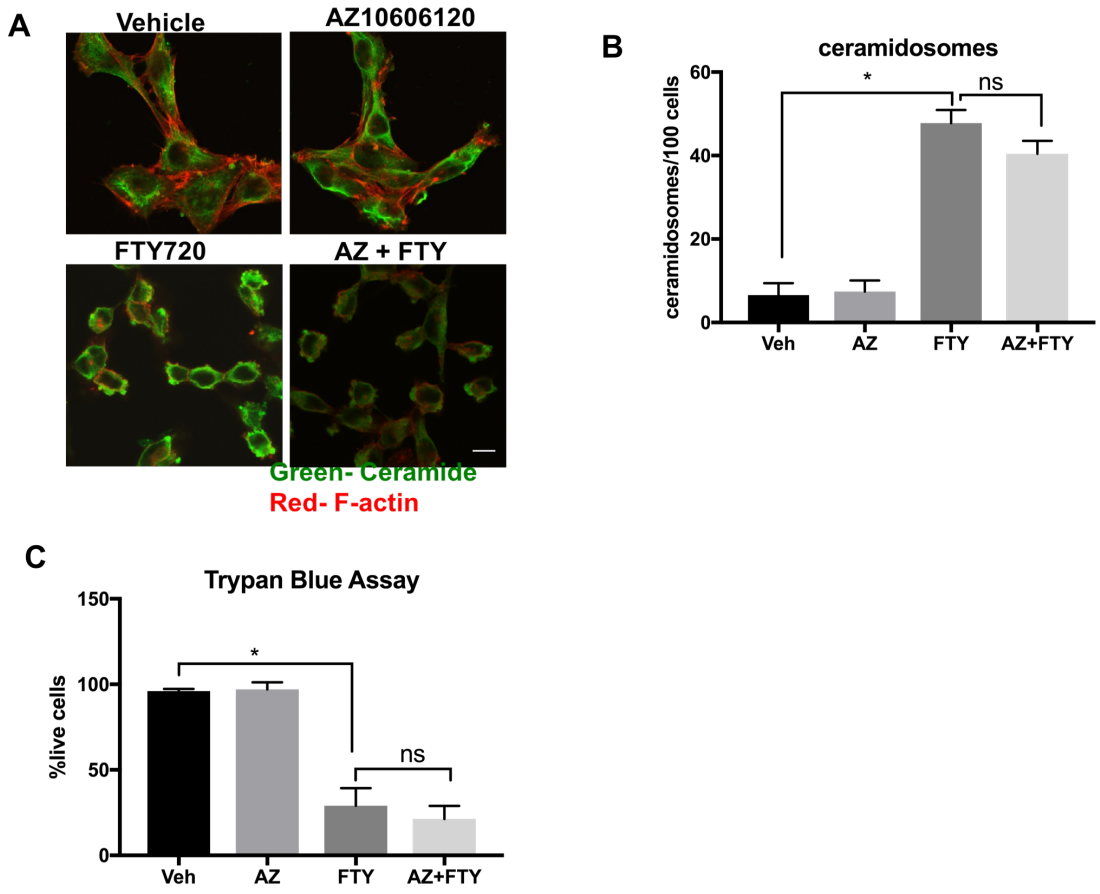

Figure 24 : P2X7 is not involved in FTY720 induced ceramidosomes or necroptosis

A. H1341 cells were pretreated with AZ10606120 (P2X7 inhibitor, 5µM, for 1hr) before treatment with FTY720. The cells were then stained for the ceramidosomes. This is quantified in **B**. Data represents means ± SD from three independent experiments, analyzed by paired student t-test (n=3, *P=0.04). **C.** Trypan blue assay was carried out in the AZ10606120 pretreated cells. Data represents means ± SD from three independent experiments, analyzed by paired student t-test (n=3, *P=0.01).

7. RIPK1 directly binds ceramide to form ceramidosomes

Ceramide-protein interaction is important for various crucial biological roles. For instance, ceramide binding to LC3BII targets autophagolysosomes to the mitochondria to induce lethal mitophagy [7, 8]. Additionally, ceramide has been shown to bind CERT (ceramide transport protein) for trafficking to the golgi for synthesis of sphingomyelin [165]. To investigate if the association between ceramide and RIPK1 was due to their binding, we first measured ceramides by lipidomics after immunoprecipitation of RIPK1 using anti-RIPK1 antibody, and lipid extractions on agarose beads used for pulling down possible RIPK1-ceramide complexes, as we described previously [8, 141] **(Figure 25 A-B).** These data revealed that there was an increase only in C16-ceramide in FTY720 treated cell extracts bound to RIPK1 compared to controls (vehicle-treated). Of note, FTY720 did not affect RIPK1 expression levels **(Figure 25 C).** In reciprocal studies, binding of ceramide with RIPK1 was measured *in-vitro* using biotinylated C6-ceramide and recombinant human RIPK1, which were isolated by avidin-conjugated agarose beads. The amount of RIPK1 bound to biotin-ceramide was measured by ELISA using anti-RIPK1 antibody. It was found that C6-ceramide bound to RIPK1 with a Kd of 1.9 nM **(Figure 25 D),** and the stoichiometry of RIPK1-ceramide binding was found as 1:2.4, calculated as we described previously [141]. These findings further confirmed ceramide-RIPK1 binding and indicate that at least *in-vitro*, RIPK1- ceramide binding is independent of the fatty acid chain length of ceramide. In addition, formation of dimers of RIPK1 upon FTY720 exposure was detected using non-denaturing western blot analysis **(Figure. 25 E).** These biochemical data were then used for *in silico* modeling of RIPK1-ceramide complex, containing RIPK1 dimer associated with four molecules of

C16-ceramide **(Figure. 25 F).** Molecular docking and simulations were done using the already existing X-ray crystal structure of RIPK1 [166] (PDB: 4NEU and 5HX6). The top ranked model of the RIPK1-ceramide complex identified potential residues of RIPK1 that were important for ceramide binding, including D147, N148 and N169 residues.

To confirm and validate the model for RIPK1-ceramide binding, we performed site directed mutagenesis to generate D147A, N148A and N169A conversions and measured their effects on co-localization with ceramide at the plasma membrane and necroptosis. The WT-RIPK1-GFP was co-localized with ceramide at the plasma membrane, whereas the association between ceramide and D147A-RIPK1-GFP or N169A-RIPK1 at the plasma membrane was reduced compared to WT-RIPK1 in response to FTY720 **(Figure 26 A-B).** Interestingly, N186A mutants, which was identified as a weak ceramide interacting residue, co-localized largely with ceramide in response to FTY720 **(Figure 26 A-B).** Live cell imaging of these mutants with PI dye after FTY720 treatment further showed the protective effect of the N169A mutant **(Figure 27 A-B).** The loss of ceramide binding of the N169A-RIPK1 was confirmed using biotin-C6-ceramide and partially purified N169A-RIPK1-GFP, as described above, which showed no binding **(Figure 28 A-B).** Thus, these data suggest that RIPK1-ceramide binding plays a key role for the generation of ceramidosomes and induction of necroptosis after FTY720-mediated cellular stress.

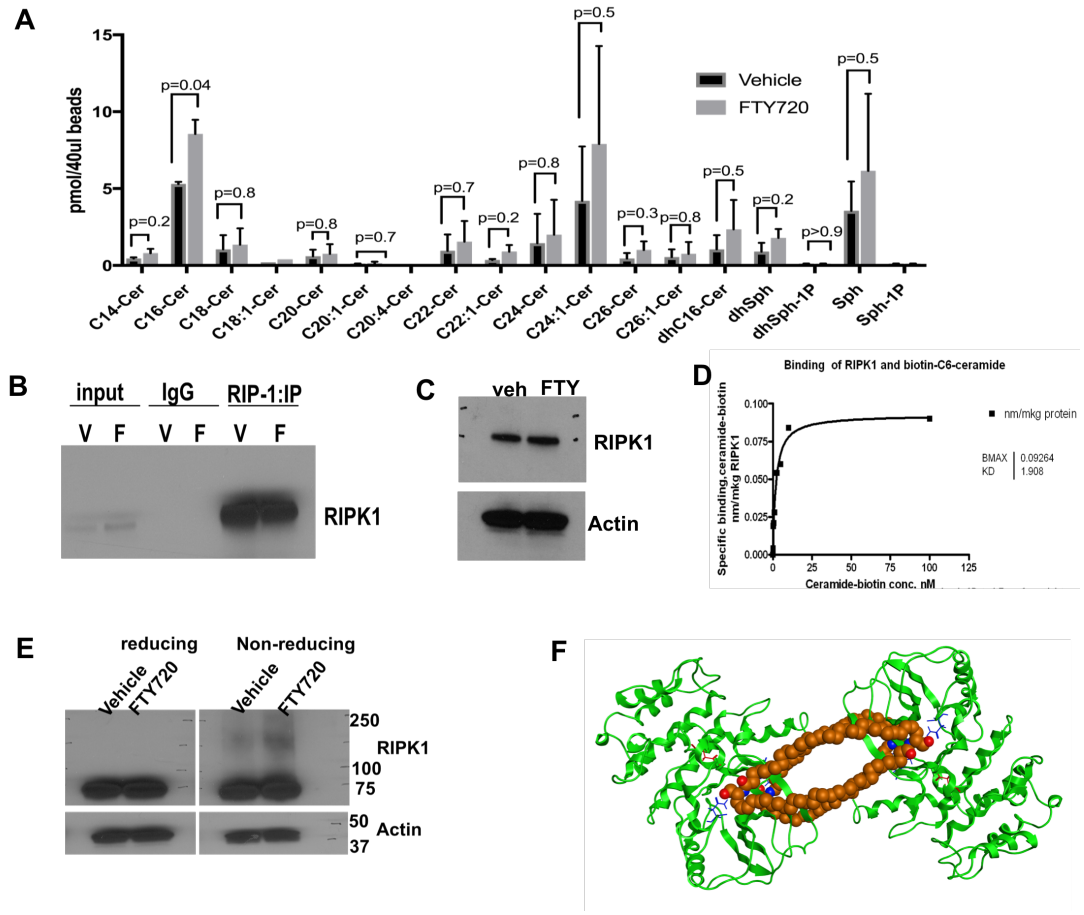

Figure 25 : RIPK1 binds Ceramide in response to FTY720

A. Lipidomics analysis of agarose beads after RIPK1 pull down show significant binding of endogenous C16-ceramide to RIPK1. Data are means ± SD from three independent experiments, analyzed by paired student t-test (n=3, p =0.04) in response to FTY720. **B**. Western blot showing RIPK1 after pull down with anti-RIPK1 antibody and agarose beads in DMSO (vehicle) versus treated (FTY720) cells. **C**. Western blot analysis of H1341 cells treated with FTY720 shows no change RIPK1 relative protein abundance compared to vehicle treated cells. **D.** *In-vitro* ceramide binding assay with purified recombinant human RIPK1 show binding to biotinylated C6-ceramide with a Kd of ~1.908 nM. **E**. Western blot with anti-RIPK1 antibody shows the formation of RIPK1 dimers in non-reducing conditions in cells treated with FTY720 compared to vehicle-treated cells. **F**. Molecular model of RIPK1 and ceramide showed RIPK1 dimers with 4 ceramide molecules. Molecular images were prepared using MOE.

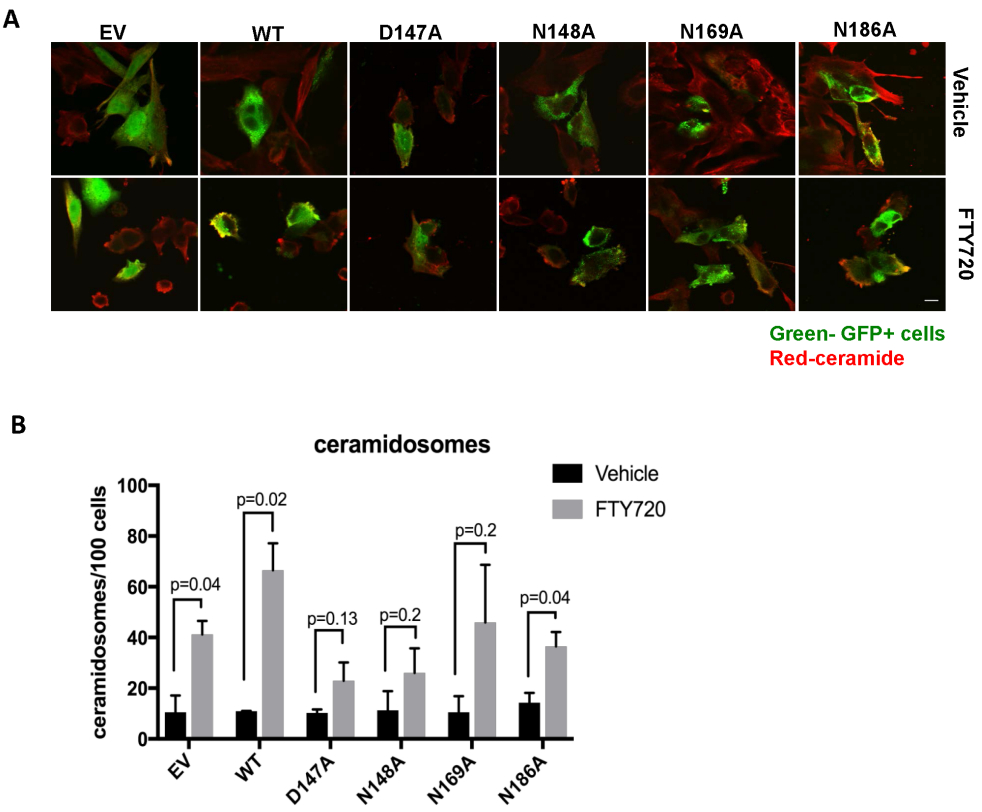

Figure 26 : RIPK1-ceramide binding is crucial for ceramidosomes formation and necroptosis

A. Confocal images showing ceramide-enriched membrane pores formation with the RIPK1 mutants over-expressed in shRIPK1 cells. **B**. quantification of ceramidosomes in **A**. Data represents means ± SD from three independent experiments, analyzed by paired student t-test (n=3 *P<0.05).

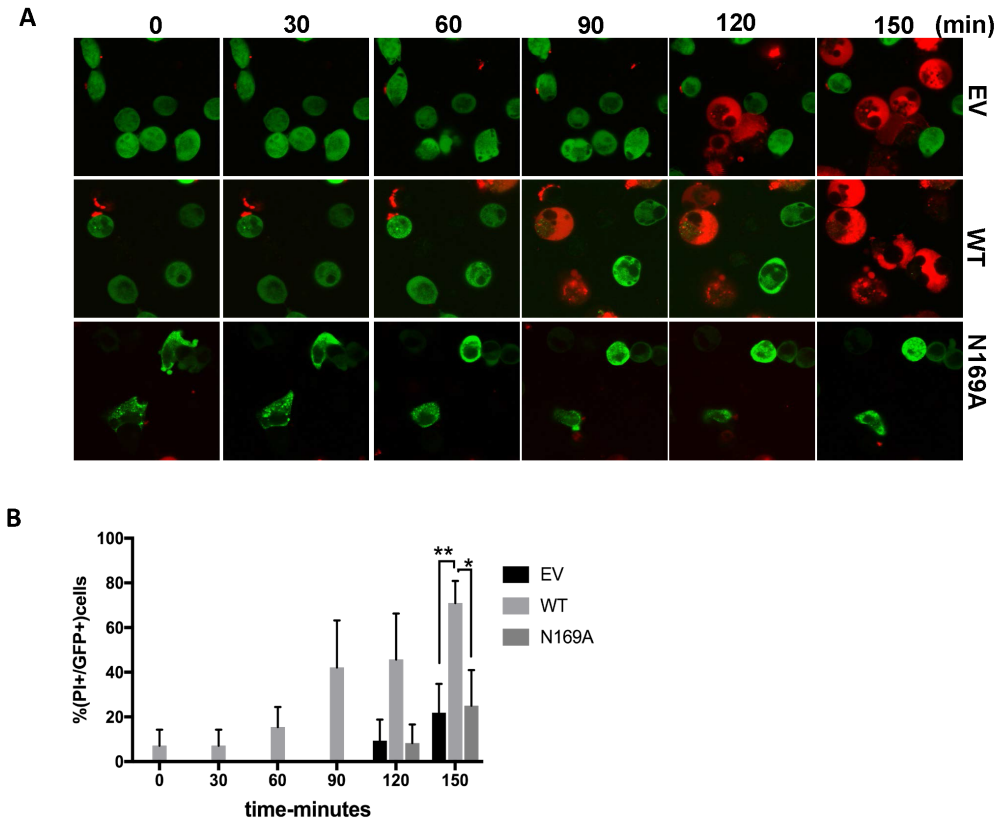

Figure 27 : N169A RIPK1 mutant protects cells from FTY720-induced cell death

A. To determine effect of the RIPK1 mutants on cell death, live cell imaging experiment was carried out on shRIPK1 cells with EV, WT RIPK1 or N169A RIPK1 over-expression. Cells with mutant RIPK1 showed a delay in PI dye inclusion, quantified in **B.** Data represents means ± SD from three independent experiments, analyzed by paired student t-test (n=3 *P=0.05, **P=0.02).

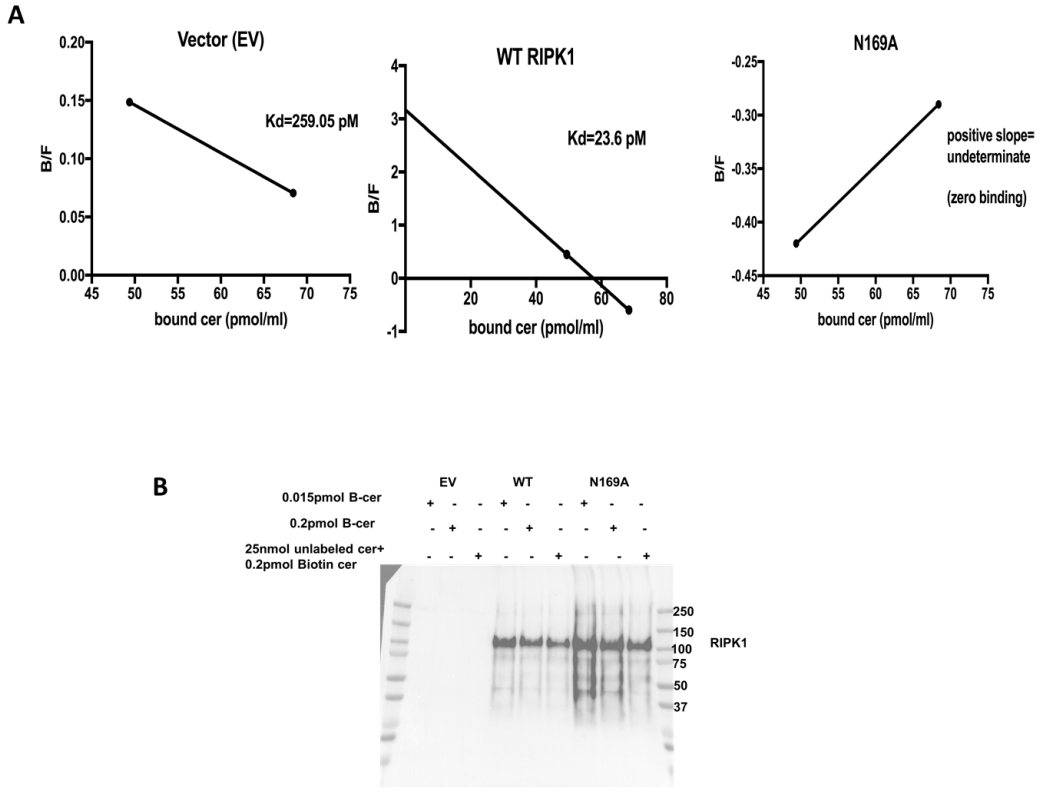

Figure 28 : *In-vitro* RIPK1 mutants-ceramide binding assay

A. *In-vitro* binding assay of partially purified empty vector (EV), WT or N169A RIPK1 using biotinylated C6 ceramide. Data represents means from three independent experiments. **B**. Western blot analysis shows the expression of WT and N169A RIPK1 after pull down for use in the *in-vitro* ceramide binding assay with biotinylated-C6-ceramide.

8. The ceramide-RIPK1 complex is trafficked to PM through vesicular trafficking

Transport of "cargo", including lipids and lipid complexes intracellularly from their site of synthesis to target sites can occur in vesicular and non-vesicular fashion [167]. Vesicular trafficking is known to be dependent on temperature, with low temperatures inhibiting vesicular trafficking [168]. This factor can be used to distinguish between vesicular and non-vesicular trafficking.

To determine whether ceramide-RIPK1 complexes are translocated to the plasma membrane via vesicular or non-vesicular trafficking, we treated A549 cells with FTY720 at 37°C or at 4°C, and measured ceramide-RIPK1-enriched membrane pores. The data demonstrated that while ceramidosomes were formed in cells incubated at 37°C in response to FTY720, incubation of cells at 4°C largely prevented the formation of ceramidosomes at the plasma membrane. Interestingly, when cells that were incubated initially at 4°C were later transferred to 37°C, formation of ceramidosomes was restored **(Figure 29 A-B)**, indicating the involvement of temperature sensitive trafficking, which is usually indicative of vesicular transport. This was confirmed by pretreating A549 cells with a known vesicular trafficking inhibitor, Brefeldin A (10 μg/mL) [169] for 24 hr before FTY720 exposure, which prevented ceramide-RIPK1 complex transport to the plasma membrane **(Figure 29 C-D).**

We found non-muscle myosin IIA (NMIIA) was critical for the ceramidosomes trafficking because blebbistatin pretreatment attenuated the formation of ceramidosomes **(Figure 29 E).** However, pharmacologic inhibitors of kinesin spindle protein (ARRY520) [170], kinesin (K858) [171] and Dynein (ciliobrevin) [172], had no effect on the formation of ceramide-RIPK1-enriched pores after FTY720-mediated stress **(Figure 29 E).**

Interestingly, the vesicular trafficking of the ceramide-RIPK1 complex was also dependent on an intact actin cytoskeleton, because inhibiting actin polymerization using Latruculin A (Lat A) [173] attenuated ceramidosome formation **(Figure 29 F-G).** Thus, these data suggest that NMIIA is key for the transport of ceramide-RIPK1 complex to the plasma membrane, and that the ceramide-RIPK1-NMIIA complex integrates ceramidosomes to form a membrane macrodomain and subsequent membrane pores leading to FTY720-induced necroptosis.

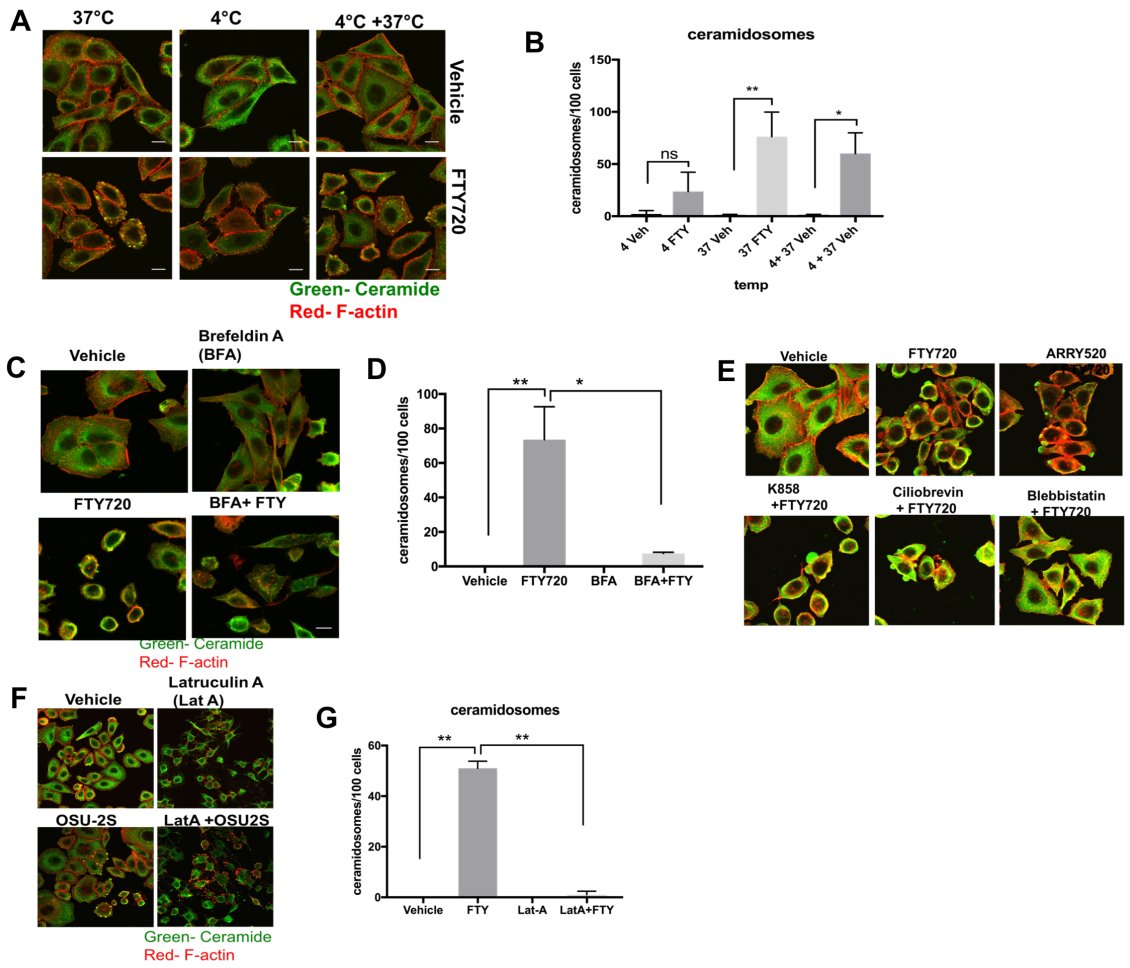

Figure 29 : Ceramidosomes are trafficked to the plasma membrane via vesicular trafficking

A. Shows cells treated with Vehicle/ FTY720 and incubated at 4º C or 37º C for two hours or 4º C followed by 37º C. This is quantified in panel **B,** Data are means ± SD from three independent experiments, analyzed by paired student t-test (n=3, ns=not significant *P =0.007, **P=0.005). **C.** A549 cells were pretreated with Brefeldin A (10µg/µl for 24hr) before FTY720 treatment. The cells were then stained for ceramide and F-actin as shown. This is quantified in panel **D**. Data are means ± SD from three independent experiments, analyzed by paired student t-test (n=3, *P =0.04, **P=0.03). **E**. Pharmacological inhibitors against Kinesin or dynein or NMIIA were used to pretreat A549 cells before treatment with FTY720 and immunofluorescence staining for ceramide-enriched pores. **F**. A549 cells were pretreated with latrunculin A and treated with FTY720 for 1 hr. Ceramide- enriched pores are quantified in **G.** Data represent means ± SD from three independent experiments, analyzed by paired student t-test (n=3, **P=0.002).

9. NMIIA traffics RIPK1-ceramide complex to the plasma membrane

Non-muscle myosin IIA, NMIIA, coded by the MYH9 gene is known to bind and traffic Golgi glycosyltransferase to the ER [174]. Not only has NMIIA been implicated in intracellular vesicle trafficking [175, 176] but also, it has been shown to be important in tissue folding in *D. melanogaster* [177], suggesting a conserved role of this protein in both mammalian and lower organism level. Interestingly, MYH9 knock out is embryonic lethal in mice [178] and *D. melanogaster* [179, 180] .

Based on the observation that blebbistatin, an inhibitor of NMIIA, also protected ceramide-enriched pores, we then hypothesized that NMIIA, recently identified as a tumor suppressor protein [181, 182], might be key for the trafficking of the ceramide-RIPK1 complex to the plasma membrane to form ceramidosomes in response to FTY720. To test this hypothesis, we first measured the co-localization of NMIIA with ceramide and RIPK1 using immunofluorescence. FTY720 exposure induced the co-localization of NMIIA with ceramide and RIPK1 **(Figure 30 A-B)** compared to vehicle-treated controls. This was confirmed with tri-color colocalization of ceramide-RIPK1 and NMIIA **(Figure 30 C).** The co-localization of NMIIA and RIPK1 within ceramidosomes at the plasma membrane in response to FTY720 was also consistent in TEM studies performed using gold labeled anti-NMIIA (labeled with 1.4 nm gold particles) and anti-RIPK1 (labeled with 10 nm gold particles) **(Figure 30 D).**

Interestingly, PLA analysis showed that while NMIIA associated highly with RIPK1 **(Figure 31 A-B),** there was almost no detectable interaction between NMIIA and ceramide **(Figure 31 C-D).** Thus, these data suggest that FTY720-mediated

ceramidosomes are transported to the plasma membrane by NMIIA via RIPK1-NMIIA association.

Next, we determined whether NMIIA knockdown inhibited the formation of ceramidosomes in response to FTY720. NMIIA knockdown reduced the formation of ceramidosomes (80%) in response to FTY720 compared to shscr-transfected and vehicle-treated controls **(Figure 32 A-B).** Down-regulation of NMIIA using shRNA also protected A549 cells from FTY720-mediated necroptosis compared to controls **(Figure 32 C)**. The expression levels of NMIIA after knockdown are shown in **Figure 32 D.**

Using the tricolor Zstack confocal image, we generated a three-dimensional (3D) image of the ceramide-RIPK1-NMIIA complex at the plasma membrane using the using ImarisCell software **(Figure 33).**

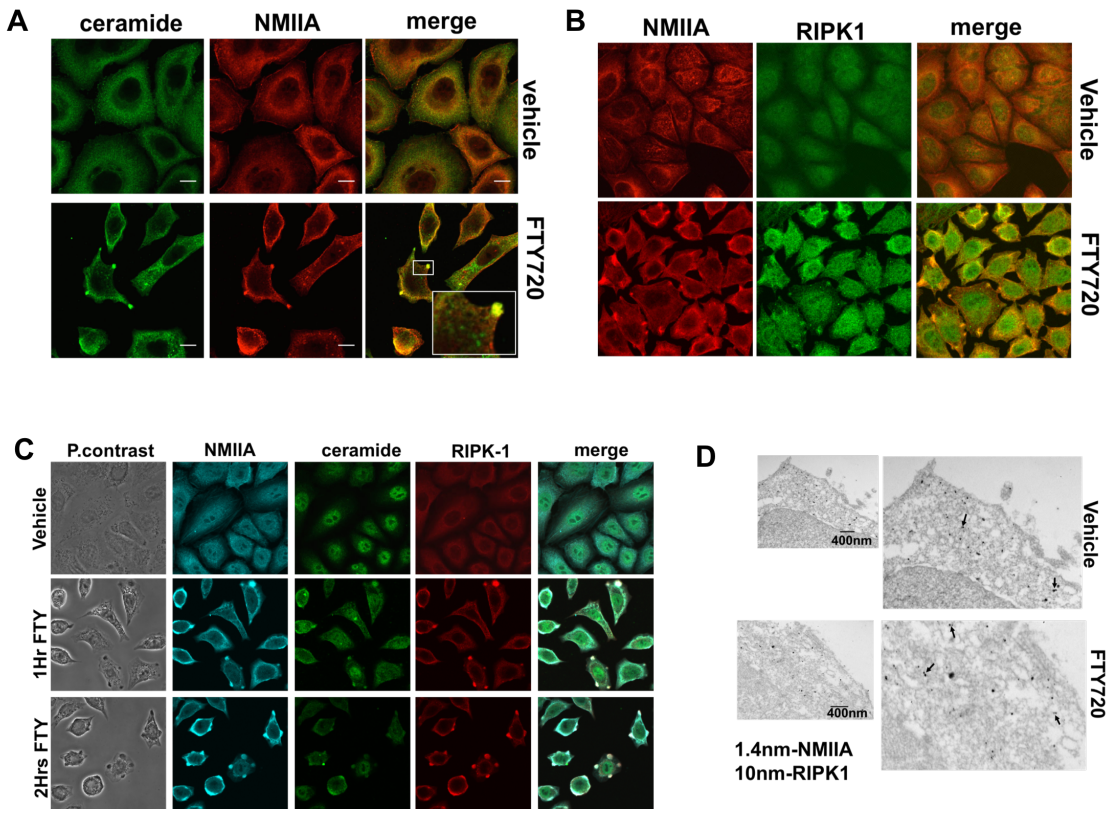

Figure 30 : NMIIA colocalizes with ceramide and RIPK1 on the plasma membrane in response to FTY720

A. Colocalization of NMIIA with ceramide in ceramide-enriched membrane pores was detected by immunofluorescence using anti-ceramide and anti-NMIIA antibodies (Insert on bottom right shows a zoom-out of the framed area). **B** Colocalization of RIPK1 and NMIIA in ceramide-enriched membrane pores was detected by immunofluorescence using anti-ceramide and anti-RIPK1 antibodies. **C**. Tricolor immuno-fluorescence of A549 cells with NMIIA, RIPK1, and ceramide antibodies shows the colocalization of the three at the plasma membrane in response to FTY720. **D**. Immuno-gold TEM show colocalization of NMIIA (1.4 nm) and RIPK1 (10 nm) in H1341 cells treated with FTY720.

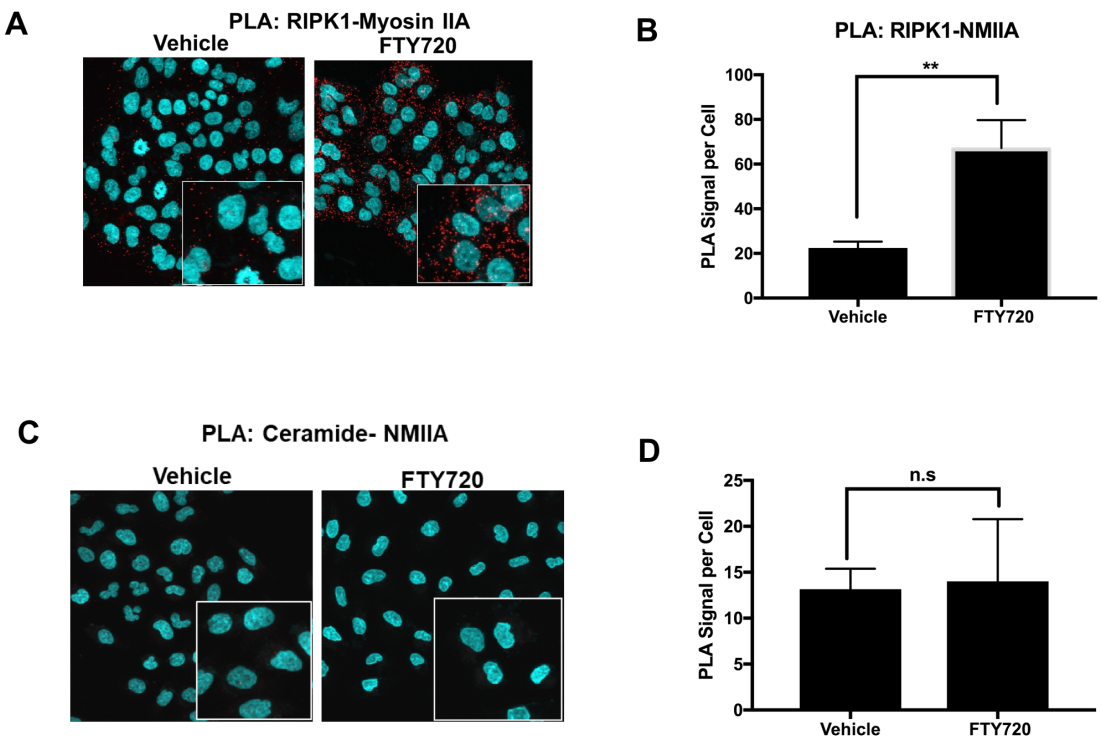

Figure 31 : NMIIA interacts with RIPK1 in the RIPK1-ceramide-NMIIA complex

A. PLA assay in A549 cells detects RIPK1 and NMIIA increased association in response to FTY720. PLA assay is quantified in **B.** Data represent means ± SD from three independent experiments, analyzed by paired student t-test (n=5 **P=0.004). **C**. PLA assay did not show interaction between ceramide-NMIIA interaction in response to FTY720. The detected PLA signal is quantified in **D**. Data represent means ± SD from three independent experiments, analyzed by paired student t-test (n=5 ns=not significant).

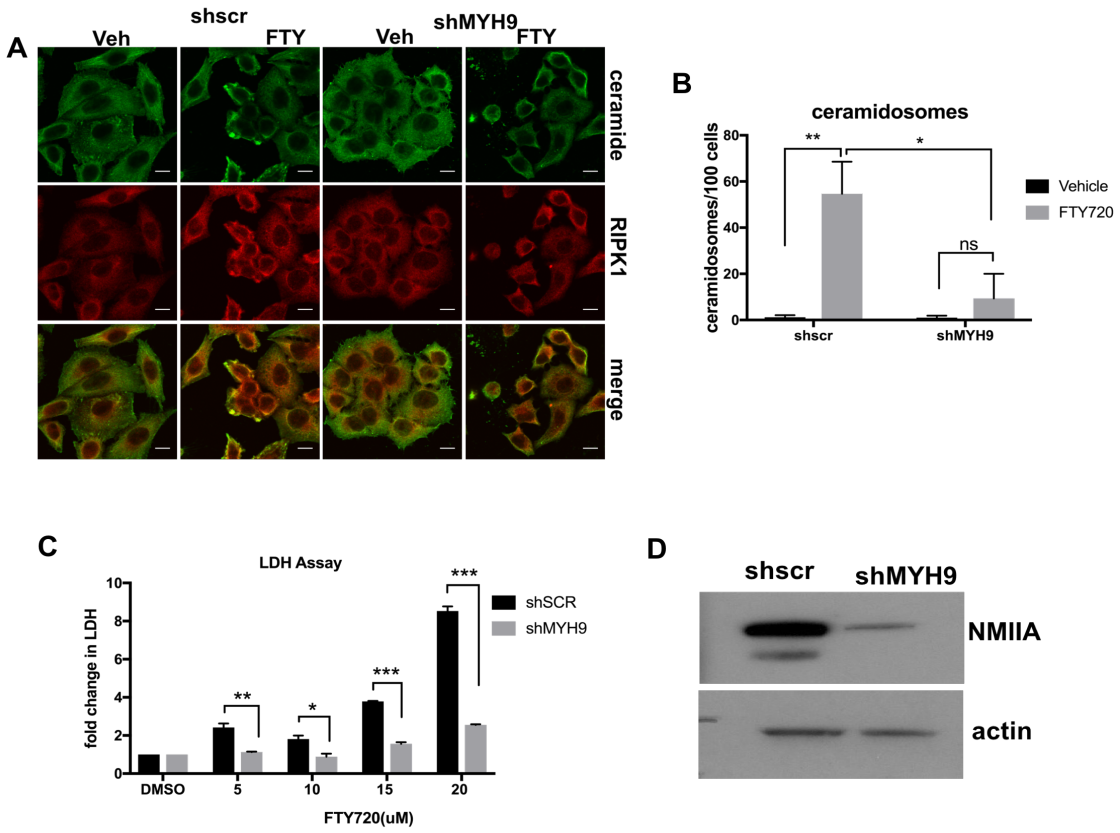

Figure 32 : NMIIA inhibits ceramidosomes formation and protects cells from cell death

A. A549 cells with stable NMIIA knockdown (shMYH9) were stained for ceramide-enriched membrane pores using anti-ceramide and anti-RIPK1 antibodies. This is quantified in **B.** Data represent means ± SD from three independent experiments, analyzed by paired student t-test (n=3 *P=0.01, **P=0.003). **C**. LDH assay in stable shMYH9 cells treated with increasing doses of FTY720 show significant protection from FTY720 induced cell death. Data represent means ± SD from three independent experiments, analyzed by paired student t-test (n=3 *P=0.004, **P=0.01, ***P≤0.0008). **D**. Western blot of A549 cells with stable knockdown of NMIIA.

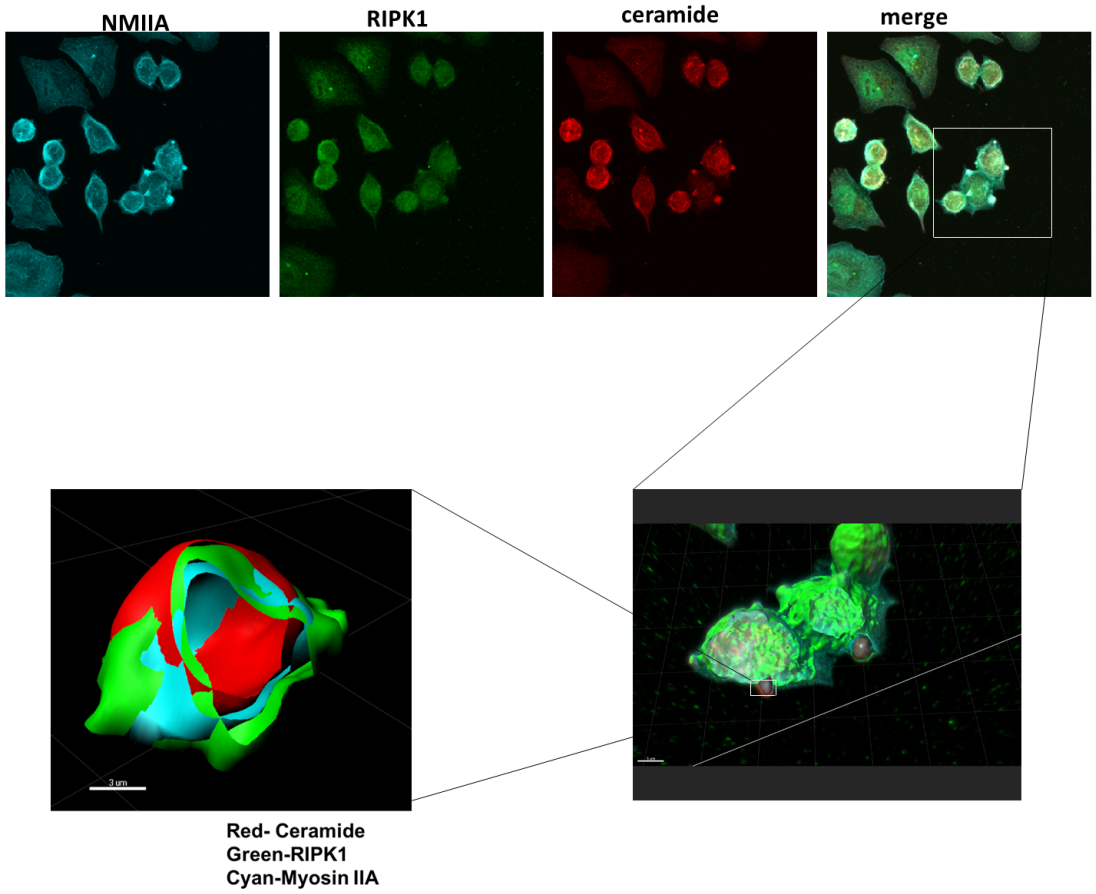

Figure 33 : 3D model of ceramidosome

ImarisCell model (derived from a Zstack confocal image) shows the spatial interaction of components of ceramidosomes

10. NMIIA interacts with RIPK1 for the trafficking of the RIPK1-ceramide complex to the PM

Because our studies suggest that trafficking of ceramide-RIPK1 complex to the plasma membrane was facilitated by NMIIA via its interaction with RIPK1, we then generated a model of the NMIIA-RIPK1 interaction, containing the RIPK1-ceramide complex using molecular modeling and simulations **(Figure 34 A-B).** This model (the top ranked model among various others) suggested a few possible residues of RIPK1 that might be involved in NMIIA interaction, including L112, C256, R258, L293, and E295 **(Figure. 34 B).** We then confirmed this model by measuring the effects of WT-RIPK1-GFP compared to various mutants of RIPK1 with L112A, C256A, R258A, L293A, or E295A conversions with the GFP tag on NMIIA interaction using immunofluorescence **(Figure 35 A-B).** Western blotting **(Figure 35 C)** shows the expression of the mutants after overexpression. The data showed that alterations of RIPK1-NMIIA interaction due to R258, L293A or E295A mutations on RIPK1 limited the formation of ceramidosomes in response to FTY720. We picked L293A mutant for live cell imaging using YOPRO-1 and PI and the mutation also protected cells from FTY720-mediated necroptosis compared to the cells expressing WT-RIPK1-GFP **(Figure 36 A-B).**

To visualize the ceramide-RIPK1-NMIIA complex (ceramidosome) that forms large pores on the plasma membrane in response to FTY720, we isolated ceramidosomes from the plasma membrane by using the method for the isolation of giant plasma membrane vesicles (GPMV) [183]. This method induces the vesiculation of the plasma membrane ("pinching off" of plasma membrane), including FTY720-induced ceramidosomes, which we can further study using different applications. **Figure 37 A**

shows an image of how the GPMV appear, when induced in A549-GFP cells. We treated H1341 cells with 10μM FTY720/vehicle and isolated the GPMV from both conditions. After isolation, the GPMVs were fixed and labeled using gold-labeled anti-ceramide, anti-RIPK1 or anti-NMIIA antibodies for visualization by TEM **(Figure 37 B).** The TEM images of these GPMVs demonstrate that while ceramide surrounds the inner channel, RIPK1 and NMIIA appear to have a general distribution within these vesicles consistent with the molecular modeling **(Figure 34 A)** and the three-dimensional image **(Figure 33).** Overall, these data suggest that RIPK1-NMIIA interaction, involving R258/L293/E295 residues of RIPK1, plays a key role for the transport of ceramide-RIPK1 complex to the plasma membrane for the formation of ceramidosomes and large membrane pores, involved in the execution of FTY720-mediated necroptosis.

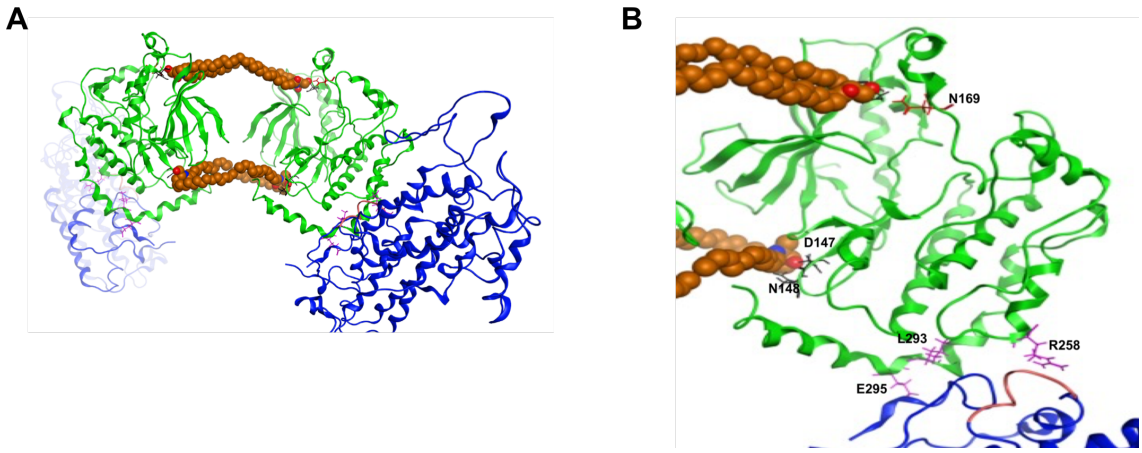

Figure 34 : Ceramidosome model showing key residues for interaction

A. Predicted model of ceramidosomes, showing ceramide, RIPK1, and NMIIA, (brown, green and blue respectively). The right panel **(B)** highlights the residues predicted to be key for RIPK1 and ceramide, as well as RIPK1-NMIIA binding.

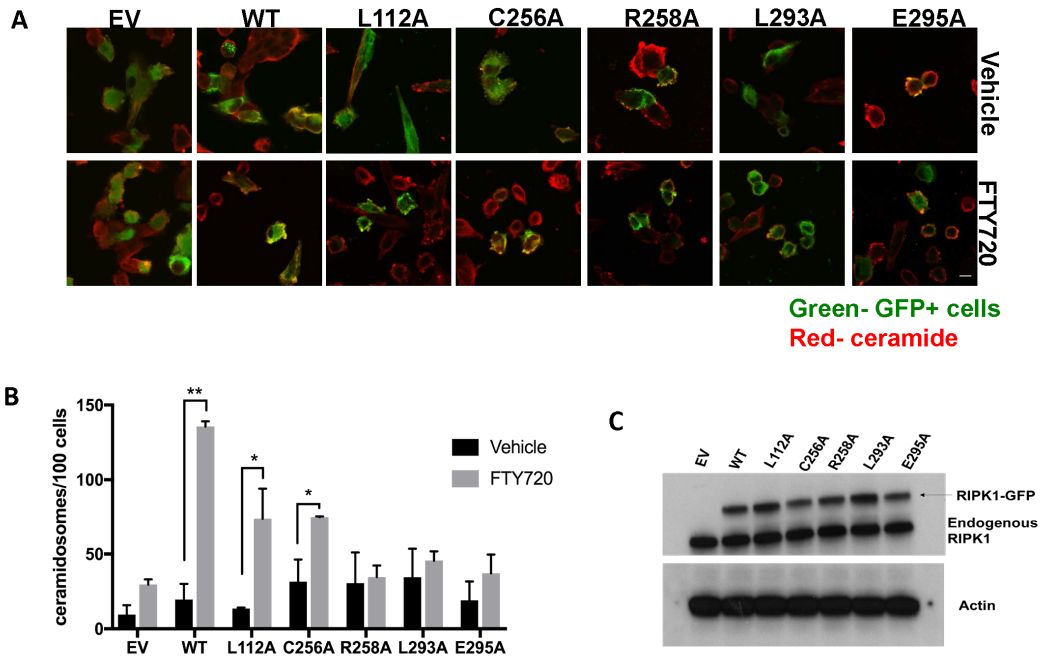

Figure 35 : R258, L293 and E295 residues in RIPK1 are important for RIPK1-NMIIA binding

A. RIPK1 mutants were overexpressed in shRIPK1 cells, the cells were then stained for ceramidosomes. These are quantified in **B**. Data represent means ± SD from three independent experiments, analyzed by paired student t-test (n=3 *P=0.05, **P=0.005). **C.** Western blot showing the expression of the RIPK1 mutants in H1341 cells.

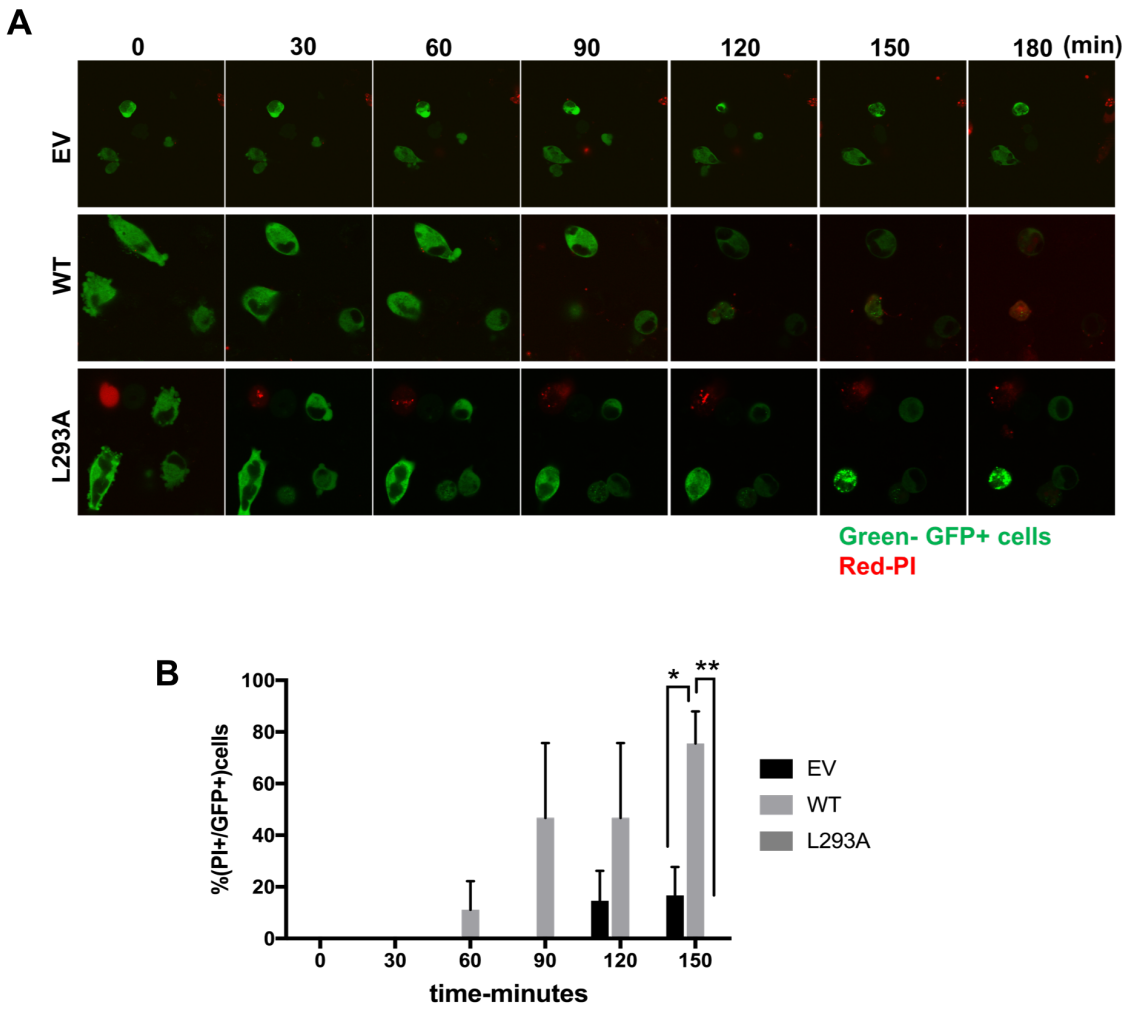

Figure 36 : L293A mutant protects cells from FTY720-induced cell death

A. To determine effect of the RIPK1 mutants on cell death, RIPK1 mutant L293A, was overexpressed in shRIPK1 H1341 cells. The cells were then treated with 20μM FTY720 and monitored over time for inclusion of propidium iodide dye with confocal live cell imaging. This is quantified in **B**. Data represents means ± SD from three independent experiments, analyzed by paired student t-test (n=3 *P=0.02, **P=0.004)**.**

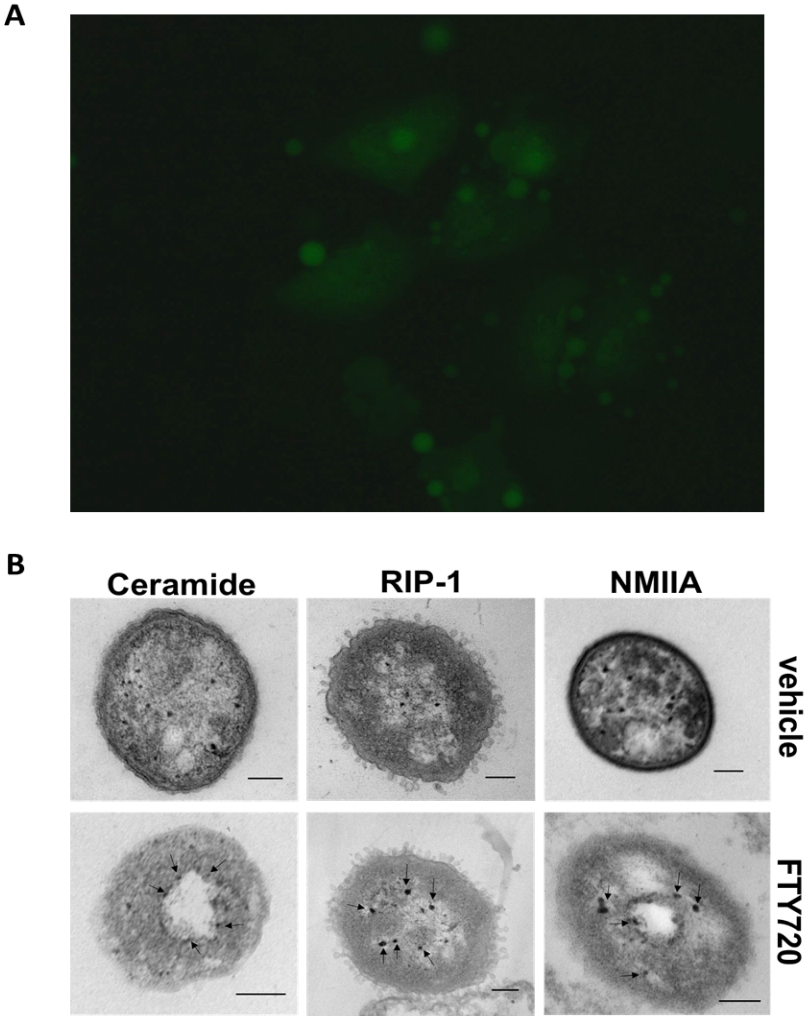

Figure 37 : Isolated ceramidosomes show ceramide, RIPK1 and NMIIA staining

A. Image shows induced plasma membrane "pinching off" (GPMV) in A549-GFP cells. Ceramidosomes were isolated through this method. **B**. Isolated ceramidosomes were stained for ceramide, RIPK1, NMIIA staining, in immunogold TEM. scale bar represents 200 nm.

CHAPTER FOUR: DISCUSSION AND FUTURE DIRECTIONS

DISCUSSION

In this study, our data demonstrate that the ceramide-RIPK1-NMIIA complex forms large membrane pores at the plasma membrane, which are referred to here as ceramidosomes. The formation of ceramidosomes in response to FTY720-mediated stress resulted in plasma membrane blebbing, leading to compromised membrane integrity and necroptosis in cancer cells. FTY720/ceramidosome-mediated necroptosis was RIPK1-dependent, however, unlike canonical necroptosis, RIPK3 and MLKL were dispensable in this process. We suggest that in place of MLKL, ceramidosomes are serving as the "executioner" in FTY720-mediated necroptosis, a term used to describe MLKL in canonical necroptosis, for its pore forming function [184, 185, 186].

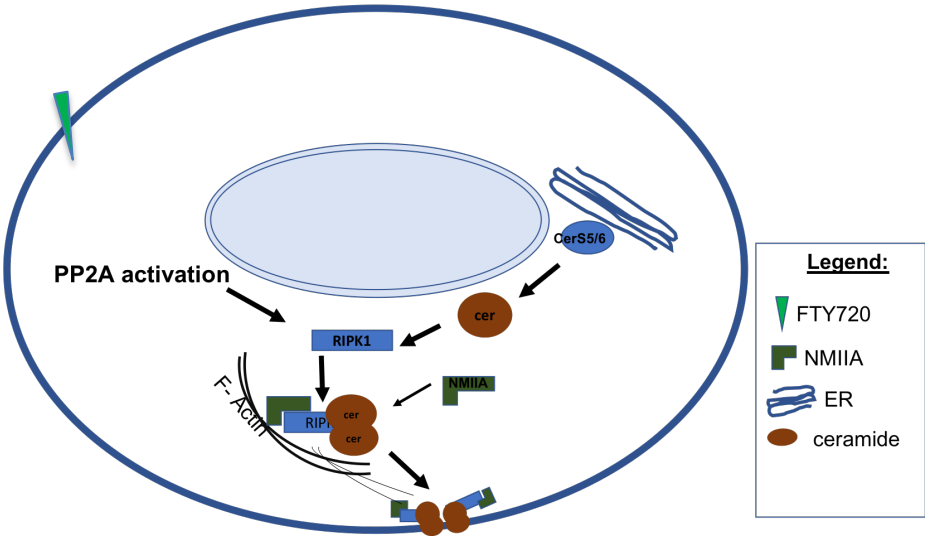

Figure 38 : Graphical abstract

PP2A activation by FTY720/OSU-2S leads to the dimerization of RIPK1 and binding to C16 ceramide. This complex is then trafficked to the plasma membrane by NMIIA, where it forms pores on the plasma membrane and result in cell death. In non-pathological setting, the ceramidosome complex could be serving more of regulatory channel role than a pore signaling for cell death.

It has been known that ceramide induced necroptosis in response to TNF-alpha-mediated stress in L929 cells, which is protected by hydrolysis of ceramide by acid ceramidase [187]. Studies by *Lang et. al*., also suggested that ceramide-mediated necroptosis played a key role in hyperosmotic-induced cell death in erythrocytes (suicidal death of erythrocytes, eryptosis), which was associated with membrane blebbing and necrosis [188]. However, the mechanisms by which ceramide induces membrane blebbing and necroptosis have been unknown. A recent study showed that ceramide nanoliposomes induced MLKL-dependent necroptosis in ovarian cancer cells [189]. Our data suggest that FTY720-mediated necroptosis is dependent on the formation of novel ceramide-enriched membrane pores (ceramidosomes), which are made up of ceramide-RIPK1/NMIIA complex. Ceramidosome-mediated necroptosis appears to be distinct from canonical necroptosis, as RIPK3 and MLKL were dispensable for this process in response to FTY720-induced stress.

Although ceramide was modeled to form lipid channels *in vitro*, and these ceramide channels were reported to exist at the mitochondrial membrane, which are disassembled by anti-apoptotic Bcl-2 family proteins [190, 191], whether ceramide channels in mitochondria play any roles in the regulation of cell death remain unknown. To this end, our studies demonstrate that FTY720-mediated ceramidosomes are formed intracellularly with the involvement of ceramide-RIPK1 association and are then trafficked to the plasma membrane through actin filaments by NMIIA. It has been shown that NMIIA is involved in the trafficking of protein cargo to various biological

membranes with distinct functions such as controlling exocytosis or positioning of organelles in cells [192, 193]. Our data are also consistent with the tumor suppression function of NMIIA [194], as its genetic deletion resulted in squamous cell carcinoma development in mice through inactivation of p53 signaling, similar to the prevention of ceramidosome-mediated necroptosis by shRNA-mediated NMIIA knockdown in response to FTY720 in lung cancer cells. However, whether ceramidosomes were formed in other cell types without any external stress stimuli were unknown.

To address this, we used *D. melanogaster* as a model organism, specifically ovaries as they contain multiple types of cells at various stages of development. The data suggested that ceramidosomes formed in germline stem cells, and that inhibition of ceramidosome formation using siRNA-mediated knockdown of *zipper* stunted ovary development potentially by inhibition of germline stem cell signaling without affecting their survival. Our data suggested that ceramidosomes can also form without any external stress stimuli, at least in the early stages of oogenesis, selectively in the germline stem cells in *D. melanogaster*. A limitation for this study however, is that there is no true orthologue of RIPK1 in *D. melanogaster*. RIPK1, closest "relative" in *D. melanogaster* is imd [195], which functions in inflammation signaling similarly to mammalian RIPK1, however, imd only has a death domain, which we have previously found [65] and have confirmed in the experiments described in this thesis, dispensable in FTY720-induced necroptosis. There could be other protein (s) in *D. melanogaster* that could serve a similar role to RIPK1 in ceramidosomes formation, but this remains to be investigated.

Inhibition of ceramide synthesis or knockdown of NMIIA *(zipper)* limited ceramidosome formation and ovary development, suggesting important roles for ceramidosomes in germline stem cells signaling during oogenesis.

Although we have shown the presence of ceramidosomes in *D. melanogaster* ovaries, the mechanisms by which ceramidosomes regulate oogenesis are unknown and need to be determined. It is known that there are nanotubes in the *D. melanogaster* testes, which mediate niche stem cell signaling [196]. It remains unknown whether ceramidosomes play similar roles in ovaries. It is possible that ceramidosomes might play a role in the regulation of germ line stem cell niche organization by enhancing EGFR signaling, as demonstrated previously by the involvement of nuclear pores and lamina [197, 198].

Thus, this thesis presents a novel lipid-multiprotein complex, involving ceramide-RIPK1 and NMIIA complex, which is trafficked to the membrane to form pores, ceramidosomes, inducing membrane rupture and necroptosis in response to FTY720 in lung cancer cells, or in germline stem cell signaling *de novo* regulating oogenesis.

FUTURE DIRECTIONS

In our previous study, we found that FTY720 induced a non-canonical type of necroptosis that was independent of RIPK3 and MLKL. This begged the question of the downstream targets of RIPK1 in FTY720-induced necroptosis. With knowledge from literature indicating ceramide's ability to form membrane pores and FTY720 ability to modulate ceramide signaling in cells we pursued this possibility in necroptosis. In this study, we have focused on the effects of FTY720 on ceramide generation and localization during necroptosis. Our studies have elucidated that in small cell (SCLC) and non-small cell lung cancer (NSCLC) cell lines, FTY720 does not significantly affect ceramide generation but does induce the formation of ceramidosomes, as discussed earlier. Although the findings of this study are novel and answer important questions about FTY720-induced necroptosis in lung cancer, there are still some unanswered questions that could be investigated in future research.

We also showed, in our initial studies, that PP2A activation mediated cell death was mitigated by RIPK1 knockdown [65], this indicated that RIPK1 acted downstream of PP2A activation. Although this dissertation study explores what occurs downstream of RIPK1, the mechanisms of exactly how PP2A activates RIPK1 remain elusive. Our preliminary proximity ligation assay (PLA) studies show that there is a significant increase in the association between PP2A and RIPK1 in response to FTY720, however, whether this association is direct binding, and whether PP2A dephosphorylation of RIPK1 mediates its non-canonical necroptotic activity remains unknown.

In this study, we have also demonstrated the novel role of NMIIA in trafficking ceramidosomes to the plasma membrane and how critical this role is in mediating cell

death. However, there remain myriad unanswered questions about NMIIA activation during FTY720-induced necroptosis. In our other unpublished data, we have also found out that NMIIA is a target of PP2A. This, we observe by proximity ligation studies which show increased PP2A and NMIIA association, as well as SILAC mass spectrometry studies. These findings bring about more questions about exactly how PP2A modulates NMIIA and how this affects NMIIA role in ceramidosomes trafficking and necroptosis.

Additionally, this brings about the main question, of how PP2A activates both NMIIA and RIPK1 to induce necroptosis. Different possibilities could be investigated here; 1) Does PP2A dephosphorylate RIPK1? Is RIPK1 a direct target of PP2A? 2)Is PP2A indirectly activating RIPK1 via NMIIA? And if so, how is this occurring and which residues on NMIIA are dephosphorylated by PP2A. Answers to these intriguing questions will allow for better understanding of this mechanism and this could be manipulated to affect necroptosis in cancer cells versus non-cancerous cells.

Moreover, we have shown the varying responses of different cell lines to the same concentration of FTY720. Further studies could be carried out to find out the mechanism behind the different sensitivities among the cell lines. In our preliminary studies to investigate this, we examined the proteins that could bind FTY720 to either enhance or lessen its potency in the different cell lines, hence leading to the different responses to the same dose of FTY720. To study this, we treated A549 and H1341 cells with biotin-tagged FTY720, lysed the cells pulled down the FTY720-bound proteins with streptavidin-coated agarose beads and run the samples on a gradient polyacrylamide gel. The gel was then stained with coomassie blue dye. We observed one band that was more

prominent in H1341 cells treated with Biotin FTY720 **(Figure 39 A)** compared to A549 cells. This band was excised and analyzed by mass spectrometry.

Interestingly, we found that in H1341 cells, compared to A549 cells, Biotin tagged FTY720 bound to caldesmon, a protein known to inhibit myosin-actin interaction in cells **(Figure 39 B**). FTY720 binding caldesmon could be enhancing NMIIA movement along actin filaments (by inhibiting the inhibitor), to promote more ceramidosomes on the plasma membrane and more cell death, hence making these cells more sensitive to FTY720 compared to A549 cells. This experiment could be confirmed and further investigated to better understand why this phenomenon is occurring in one cell line and not the other. Answers to these questions will have clinical relevance as they could potentially predict which type of cancer would respond more ceramidosome-inducing, necroptotic triggering chemotherapeutic agents.

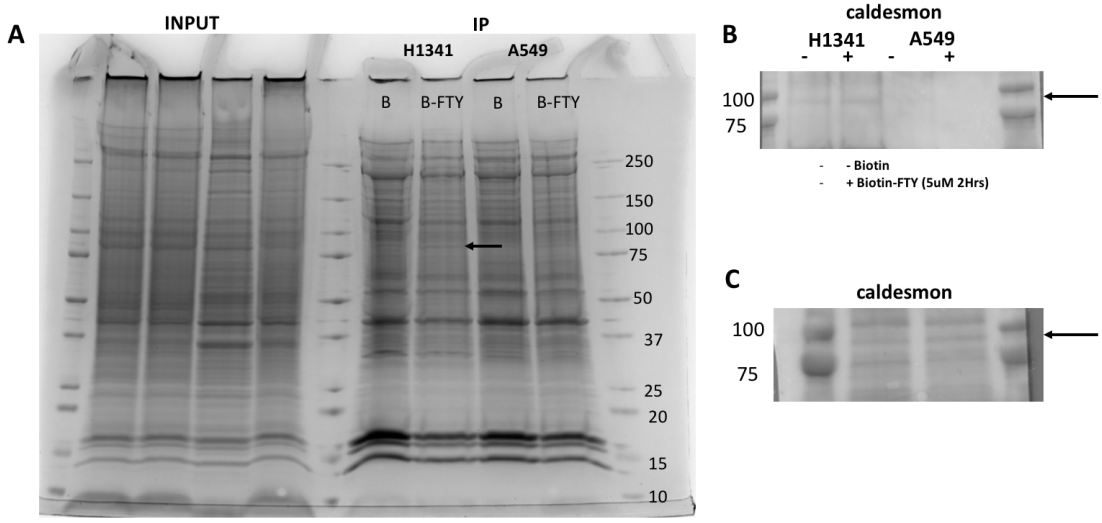

Figure 39 : Biotin-FTY720 binds caldesmon in H1341 cells

A. Coomassie blue staining of H1341 and A549 cells (treated with Biotin-FTY720/Biotin) after IP with avidin-coated beads. **B.** Expression of caldesmon, one of the proteins identified from mass spectrometry analysis of the band indicated by the black arrow in A, in H1341 and A549 after IP with avidin-coated beads. **C.** Expression of caldesmon in H1341 and A549 cells without FTY720 treatment

In our studies, we have seen that ceramidosomes were only evident in cancer cell lines and not in non-cancer cell lines that we looked at. This lack of ceramidosomes formation in these cell lines also correlated with their response to FTY720. Cells that did not form ceramidosomes also required a lot more FTY720, almost twice as much to induce cell death. We still do not why non-cancerous cells did not form ceramidosomes in response to FTY720. This intriguing phenomenon in cells could be further investigated to understand the implications of this phenomenon in future cancer treatment. Could making normal cells more resistant to ceramidosomes formation reduce the side-effects typically seen in patients undergoing chemotherapy?

Our study showed us that ceramidosomes formed large membrane pores and appeared to be highly organized and well structured. Because of this and ceramide's implication in stem cells differentiation and development in non-pathological conditions [130, 131], we decided to investigate whether ceramidosomes were also formed in physiological condition without FTY720 exposure or any exogenous stress stimuli. To determine this, we elected to use *D. melanogaster* ovaries due to the presence of various stages of developmental process and stem cell types [149, 199, 200]. We isolated ovary tissues from *D. melanogaster* and performed immunofluorescence using anti-ceramide and a germline stem cell marker, 1B1 [201]. Interestingly, ceramide-enriched macrodomains were detected colocalized with the germline stem cell marker **(Figure 40 A)**, which also marks structures in the germline stem cells known as spectrosomes/fusomes [202], known to be key in synchronizing germline stem cells differentiation by sharing of intracellular contents.

To further examine the role of ceramide membrane pores/macrodomains in the ovary development, we analyzed the effects of the inhibition of ceramide synthesis using fumonisin B1 (FB1) on the formation of ceramide-enriched macrodomains and ovary development. the data showed significant decrease in ceramide and 1B1 co-localization without affecting the survival of GSC **(Figure 40 B-C),** indicating a possible key role of ceramide in GSC signaling.

To determine if ceramidosome play any functional roles in the ovary development, we obtained *zipper* (NMIIA homologue) [203] RNAi flies and drove RNAi using Nos RNAi driver. We then determined the effects of *zipper* knockdown on the formation of ceramide pores/macrodomains and ovary development. Remarkably,

siRNA-mediated knockdown of *zipper* inhibited the formation of ceramide-enriched macrodomains in ovaries, and resulted in a defective ovary development in insects, leading to a sterile phenotype **(Figure 41 A-B).** Overall, these data suggest that ceramidosome, at least containing ceramide and NMIIA homologue *zipper*, are possibly formed *de novo* without any external drug treatment or stress stimuli selectively in GSC found in the early developmental stages of ovaries. We suggest that ceramidosomes could be playing a key role in oogenesis at least in *D. melanogaster*.

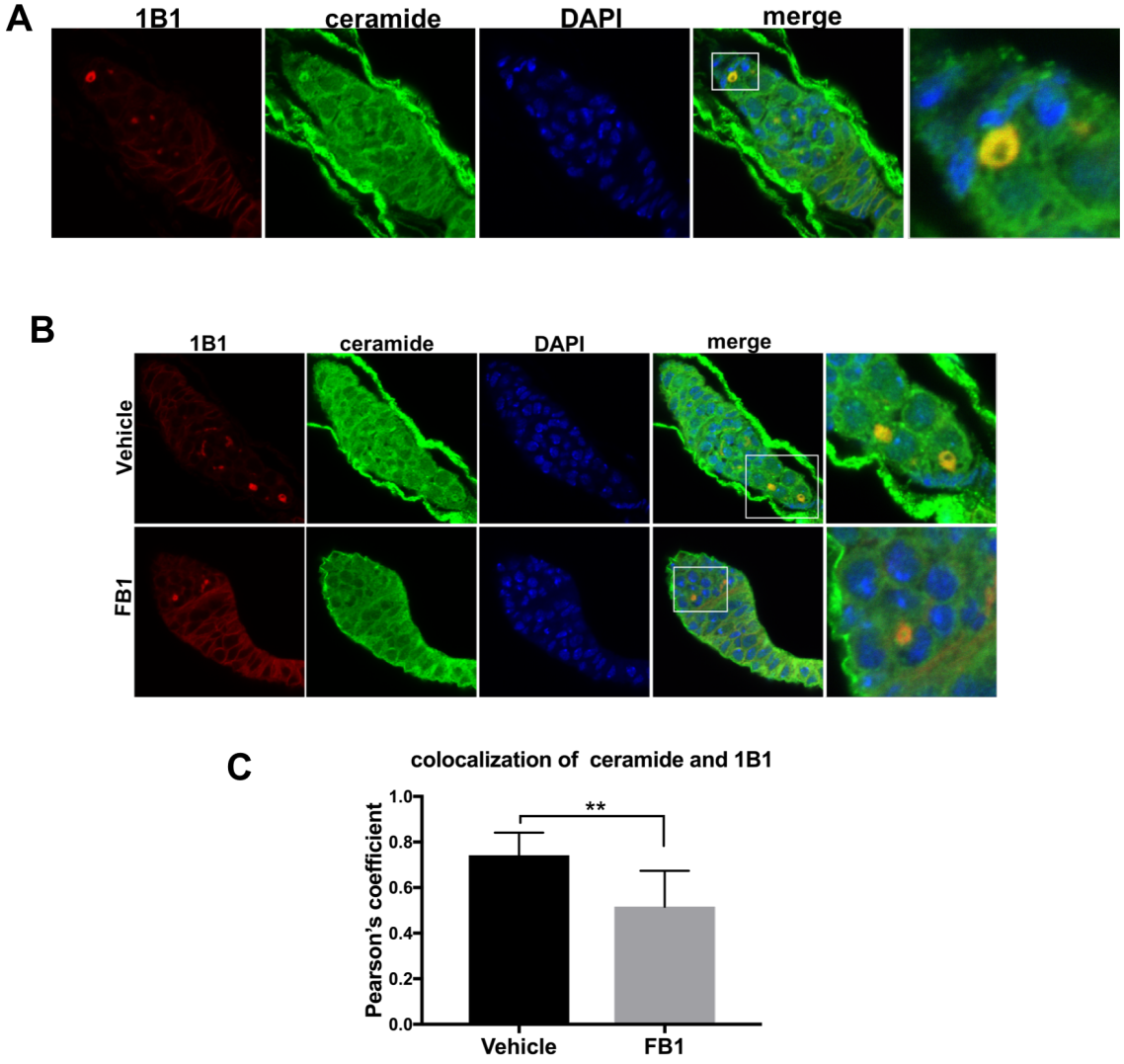

Figure 40 : Ceramide colocalizes with germline stem cell marker in *D. melanogaster* ovaries and this is inhibited by FB1

A. Isolated ovarioles from *D. melanogaster* were stained for ceramide and stem cell marker (1B1) using the respective antibodies**.** The rightmost panel shows a zoomed-out picture of the framed area. **B**. Isolated ovaries from *D. melanogaster* exposed to FB1 (100 μM)/Vehicle were stained for ceramide and 1B1. There was decreased co-localization between ceramide and 1B1 in the flies exposed to FB1 the rightmost panels show zoomed-out pictures of the framed areas. Quantification of 1B1 and ceramide colocalization is shown in **C**.

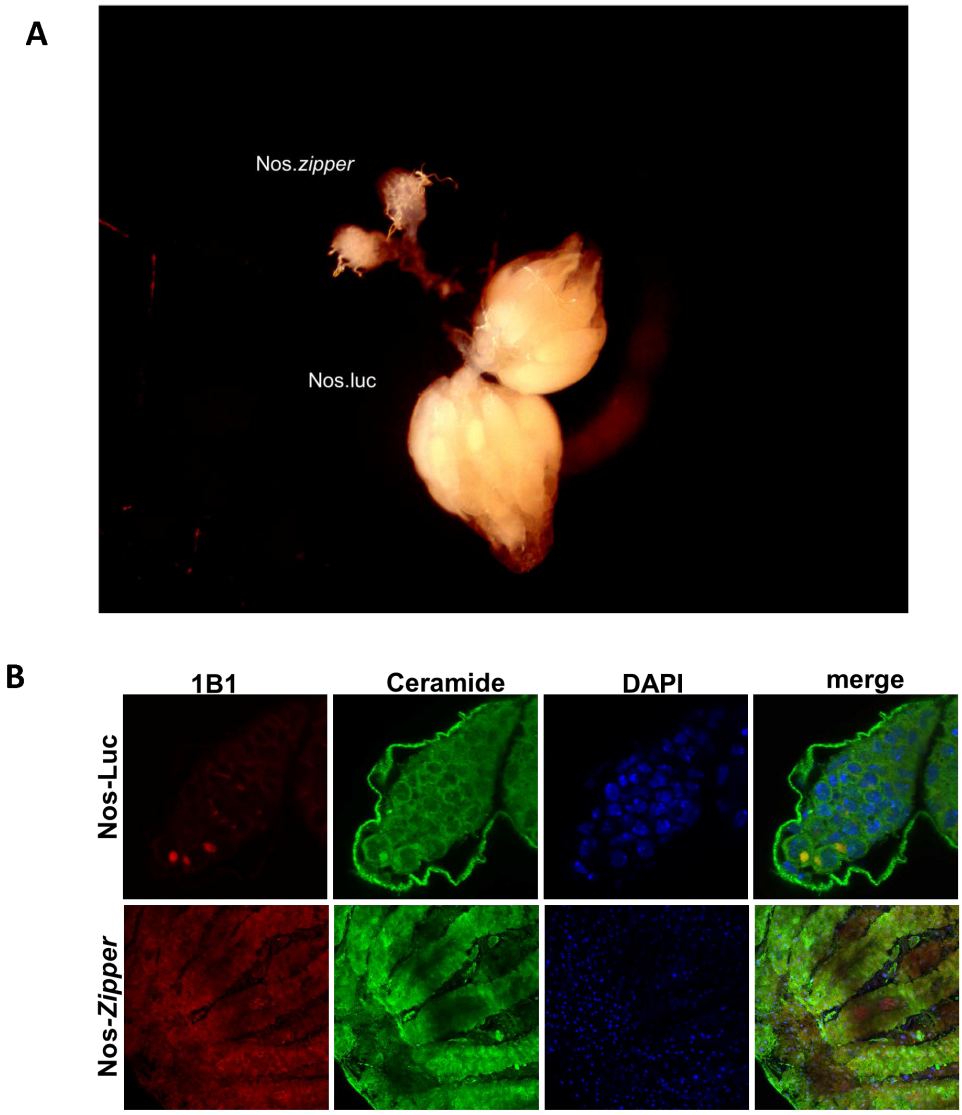

Figure 41 : Knocking down NMIIA (*zipper*) in *D. melanogaster* leads to a sterile phenotype

A. To investigate the effect of genetic loss of *zipper* (NMIIA), ovarioles isolated from *zipper* RNAi flies were stained for ceramide and stem cell marker (1B1). **A.** shows *zipper* RNAi flies had stunted ovary development compared to Nos.Luciferase RNAi (control). **B.** shows 1B1 and ceramide staining in the germarium in Nos.Luciferase ovarioles (top panel) compared to the whole ovary in the Nos.*zipper* RNAi flies (bottom panel).

Given that ceramidosomes (identified by ceramide antibody) were colocalized in with spectrosomes/fusomes in germlines stem cells and knocking down a key component of ceramidosomes led to defective ovary development, our data suggest that ceramidosomes could be involved in the trafficking of non-polar molecules like sterols between cells, especially germline stem cells during the early stages of oogenesis. However, further studies to understand if this is what is going on, need to be carried out.

As before-mentioned, FTY720 is currently being used to treat multipole sclerosis. Compared to this role, the dose required to induce cancer cell death is quite high compared to the dose typically required to induce immune suppression in MS. Predictably, the side effects for this would be deleterious to cancer patients. This necessitates the need for analogues of FTY720 that are more potent at lower does than FTY720 and possibly have less side-effects. Additionally, non-phosphorylatable analogues of FTY720 would be more clinically relevant for cancer treatment as they will induce tumor suppression without the immune suppression driven by P-FTY720.

Appendix

Inorganic Phosphates (Pi) Analysis

Day 1

**make Ashing buffer 9:1:40 (10N H_2SO_4: 70% $HClO_4$: H_2O) (make a lot to keep at bench for future use)

**Make 10mM NaH_2PO_4 if you don't have this already (make a lot to keep at bench for future use)

Protocol

Add 1 mL chloroform and 2 mL methanol, vortex

Add 800µl ddH2O, vortex

Add 1 mL chloroform, vortex

Add 1 mL ddH2O vortex

Spin 3000 rpm 5 minutes

** in the mean-time take fresh glass tubes (duplicates for each sample) and label them

Using glass pipet, insert into bottom clear phase and take 1 mL, divide into two tubes (0.5 mL each tube)

Dry under nitrogen. (turn top knob; silver (just until it's on), then front knob to approximately 100 KPa. Insert pipets in tubes dry completely

** in the meantime, make standards with NaH_2PO_4

Stock solution to keep at the bench is 10 mM

For standards, dilute and aliquot of 10 mM to make 1 mM and then dilute the 1mM to make 0.1mM. Use the 1mM and 0.1mM stock solutions to make standards

Follow table below:

Concentration (in nmoles)	Volume from stock (in µl)	Stock solution
0	n/a	n/a
1	10	0.1mM
3	30	0.1mM
5	50	0.1mM
10	10	1mM
20	20	1mM
40	40	1mM
60	60	1mM
80	80	1mM

Add 600 µl ashing buffer to samples and standards, vortex well

Put samples in cold heating block in the hood, then set it to 160°C for O/N (16-24 hrs)

Day 2

Prepare fresh ascorbic acid (9%) and ammonium molybdate (0.9%)

**1.8 g Ascorbic acid in 20 mL ddH2O

**225 mg ammonium molybdate in 25 mL

Turn on water bath 45°C

Add 0.9 mL ddH_2O, vortex well

Add 500 µl 0.9% ammonium molybdate, vortex well

Add 200µl 9% ascorbic acid, vortex

Incubate in water bath at 45°C for 30 minutes (check every 10 minutes for color development, if purple color develops before the 30 minutes, take the samples out of the water bath)

Add 200µl of each sample and standard per well in a 96 well plate and read at 600 nm

**To calculate amount of phosphates from the colorimetric readings, make linear curve from the standards, using the equation, plug and chug. The value you get, multiple by 4 then again by 4 if you received 1mL dried lipids from the core.

LIST OF REFERENCES

1. Ogretmen, B. Sphingolipid metabolism in cancer signalling and therapy. *Nat Rev Cancer* **18**, 33-50 (2018).

2. Taniguchi, M. *et al.* Regulation of autophagy and its associated cell death by "sphingolipid rheostat": reciprocal role of ceramide and sphingosine 1-phosphate in the mammalian target of rapamycin pathway. *J Biol Chem* **287**, 39898-39910 (2012).

3. Ogretmen, B. & Hannun, Y.A. Biologically active sphingolipids in cancer pathogenesis and treatment. *Nat Rev Cancer* **4**, 604-616 (2004).

4. Venkataraman, K. *et al.* Upstream of growth and differentiation factor 1 (uog1), a mammalian homolog of the yeast longevity assurance gene 1 (LAG1), regulates N-stearoyl-sphinganine (C18-(dihydro)ceramide) synthesis in a fumonisin B1-independent manner in mammalian cells. *J Biol Chem* **277**, 35642-35649 (2002).

5. Senkal, C.E. *et al.* Role of human longevity assurance gene 1 and C18-ceramide in chemotherapy-induced cell death in human head and neck squamous cell carcinomas. *Mol Cancer Ther* **6**, 712-722 (2007).

6. Thomas, R.J. *et al.* HPV/E7 induces chemotherapy-mediated tumor suppression by ceramide-dependent mitophagy. *EMBO Mol Med* **9**, 1030-1051 (2017).

7. Dany, M. *et al.* Targeting FLT3-ITD signaling mediates ceramide-dependent mitophagy and attenuates drug resistance in AML. *Blood* **128**, 1944-1958 (2016).

8. Sentelle, R.D. *et al.* Ceramide targets autophagosomes to mitochondria and induces lethal mitophagy. *Nat Chem Biol* **8**, 831-838 (2012).

9. Laviad, E.L. *et al.* Characterization of ceramide synthase 2: tissue distribution, substrate specificity, and inhibition by sphingosine 1-phosphate. *J Biol Chem* **283**, 5677-5684 (2008).

10. Sassa, T., Suto, S., Okayasu, Y. & Kihara, A. A shift in sphingolipid composition from C24 to C16 increases susceptibility to apoptosis in HeLa cells. *Biochimica et biophysica acta* **1821**, 1031-1037 (2012).

11. Mizutani, Y., Kihara, A. & Igarashi, Y. LASS3 (longevity assurance homologue 3) is a mainly testis-specific (dihydro)ceramide synthase with relatively broad substrate specificity. *Biochem J* **398**, 531-538 (2006).

12. Ebel, P. *et al.* Ceramide synthase 4 deficiency in mice causes lipid alterations in sebum and results in alopecia. *Biochem J* **461**, 147-158 (2014).

13. Gencer, S. *et al.* TGF-beta receptor I/II trafficking and signaling at primary cilia are inhibited by ceramide to attenuate cell migration and tumor metastasis. *Sci Signal* **10** (2017).

14. Gosejacob, D. *et al.* Ceramide Synthase 5 Is Essential to Maintain C16:0-Ceramide Pools and Contributes to the Development of Diet-induced Obesity. *J Biol Chem* **291**, 6989-7003 (2016).

15. Senkal, C.E. *et al.* Alteration of ceramide synthase 6/C16-ceramide induces activating transcription factor 6-mediated endoplasmic reticulum (ER) stress and apoptosis via perturbation of cellular Ca2+ and ER/Golgi membrane network. *J Biol Chem* **286**, 42446-42458 (2011).

16. Thomas, R.L., Jr., Matsko, C.M., Lotze, M.T. & Amoscato, A.A. Mass spectrometric identification of increased C16 ceramide levels during apoptosis. *J Biol Chem* **274**, 30580-30588 (1999).

17. Senkal, C.E., Ponnusamy, S., Bielawski, J., Hannun, Y.A. & Ogretmen, B. Antiapoptotic roles of ceramide-synthase-6-generated C16-ceramide via selective regulation of the ATF6/CHOP arm of ER-stress-response pathways. *FASEB J* **24**, 296-308 (2010).

18. Karahatay, S. *et al.* Clinical relevance of ceramide metabolism in the pathogenesis of human head and neck squamous cell carcinoma (HNSCC): attenuation of C(18)-ceramide in HNSCC tumors correlates with lymphovascular invasion and nodal metastasis. *Cancer Lett* **256**, 101-111 (2007).

19. Zhao, L. *et al.* A deficiency of ceramide biosynthesis causes cerebellar purkinje cell neurodegeneration and lipofuscin accumulation. *PLoS Genet* **7**, e1002063 (2011).

20. Holliday, M.W., Jr., Cox, S.B., Kang, M.H. & Maurer, B.J. C22:0- and C24:0-dihydroceramides confer mixed cytotoxicity in T-cell acute lymphoblastic leukemia cell lines. *PLoS One* **8**, e74768 (2013).

21. Pewzner-Jung, Y. *et al.* A critical role for ceramide synthase 2 in liver homeostasis: II. insights into molecular changes leading to hepatopathy. *J Biol Chem* **285**, 10911-10923 (2010).

22. Jennemann, R. *et al.* Loss of ceramide synthase 3 causes lethal skin barrier disruption. *Hum Mol Genet* **21**, 586-608 (2012).

23. Russo, S.B. *et al.* Ceramide synthase 5 mediates lipid-induced autophagy and hypertrophy in cardiomyocytes. *J Clin Invest* **122**, 3919-3930 (2012).

24. Ebel, P. *et al.* Inactivation of ceramide synthase 6 in mice results in an altered sphingolipid metabolism and behavioral abnormalities. *J Biol Chem* **288**, 21433-21447 (2013).

25. Dany, M. & Ogretmen, B. Ceramide induced mitophagy and tumor suppression. *Biochimica et biophysica acta* **1853**, 2834-2845 (2015).

26. Tan, S.F., Pearson, J.M., Feith, D.J. & Loughran, T.P., Jr. The emergence of acid ceramidase as a therapeutic target for acute myeloid leukemia. *Expert Opin Ther Targets* **21**, 583-590 (2017).

27. Spiegel, S. & Milstien, S. Sphingosine-1-phosphate: an enigmatic signalling lipid. *Nat Rev Mol Cell Biol* **4**, 397-407 (2003).

28. Schnaar, R.L. & Kinoshita, T. Glycosphingolipids, in *Essentials of Glycobiology*. (eds. rd *et al.*) 125-135 (Cold Spring Harbor (NY); 2015).

29. D'Angelo, G., Capasso, S., Sticco, L. & Russo, D. Glycosphingolipids: synthesis and functions. *FEBS J* **280**, 6338-6353 (2013).

30. Singh, P., Paila, Y.D. & Chattopadhyay, A. Role of glycosphingolipids in the function of human serotonin(1)A receptors. *J Neurochem* **123**, 716-724 (2012).

31. Wijesinghe, D.S., Lamour, N.F., Gomez-Munoz, A. & Chalfant, C.E. Ceramide kinase and ceramide-1-phosphate. *Methods Enzymol* **434**, 265-292 (2007).

32. Huitema, K., van den Dikkenberg, J., Brouwers, J.F. & Holthuis, J.C. Identification of a family of animal sphingomyelin synthases. *EMBO J* **23**, 33-44 (2004).

33. Watters, R.J. *et al.* Targeting glucosylceramide synthase synergizes with C6-ceramide nanoliposomes to induce apoptosis in natural killer cell leukemia. *Leuk Lymphoma* **54**, 1288-1296 (2013).

34. D'Angelo, G. *et al.* Vesicular and non-vesicular transport feed distinct glycosylation pathways in the Golgi. *Nature* **501**, 116-120 (2013).

35. Simanshu, D.K. *et al.* Non-vesicular trafficking by a ceramide-1-phosphate transfer protein regulates eicosanoids. *Nature* **500**, 463-467 (2013).

36. Maceyka, M. & Spiegel, S. Sphingolipid metabolites in inflammatory disease. *Nature* **510**, 58-67 (2014).

37. Huang, W.C. *et al.* Sphingosine-1-phosphate phosphatase 2 promotes disruption of mucosal integrity, and contributes to ulcerative colitis in mice and humans. *FASEB J* **30**, 2945-2958 (2016).

38. Zamora-Pineda, J., Kumar, A., Suh, J.H., Zhang, M. & Saba, J.D. Dendritic cell sphingosine-1-phosphate lyase regulates thymic egress. *J Exp Med* **213**, 2773-2791 (2016).

39. Sun, Y. & Peng, Z.L. Programmed cell death and cancer. *Postgraduate medical journal* **85**, 134-140 (2009).

40. Elmore, S. Apoptosis: A Review of Programmed Cell Death. *Toxicologic pathology* **35**, 495-516 (2007).

41. Obeid, L.M., Linardic, C.M., Karolak, L.A. & Hannun, Y.A. Programmed cell death induced by ceramide. *Science* **259**, 1769-1771 (1993).

42. Colombini, M. Ceramide channels and mitochondrial outer membrane permeability. *J Bioenerg Biomembr* **49**, 57-64 (2017).

43. Chang, K.T. *et al.* Ceramide channels: destabilization by Bcl-xL and role in apoptosis. *Biochimica et biophysica acta* **1848**, 2374-2384 (2015).

44. Stiban, J., Fistere, D. & Colombini, M. Dihydroceramide hinders ceramide channel formation: Implications on apoptosis. *Apoptosis* **11**, 773-780 (2006).

45. Stiban, J. & Perera, M. Very long chain ceramides interfere with C16-ceramide-induced channel formation: A plausible mechanism for regulating the initiation of intrinsic apoptosis. *Biochimica et biophysica acta* **1848**, 561-567 (2015).

46. White-Gilbertson, S. *et al.* Ceramide synthase 6 modulates TRAIL sensitivity and nuclear translocation of active caspase-3 in colon cancer cells. *Oncogene* **28**, 1132-1141 (2009).

47. Hanahan, D. & Weinberg, R.A. Hallmarks of cancer: the next generation. *Cell* **144**, 646-674 (2011).

48. Ponnusamy, S. *et al.* Sphingolipids and cancer: ceramide and sphingosine-1-phosphate in the regulation of cell death and drug resistance. *Future oncology (London, England)* **6**, 1603-1624 (2010).

49. Glick, D., Barth, S. & Macleod, K.F. Autophagy: cellular and molecular mechanisms. *J Pathol* **221**, 3-12 (2010).

50. Pattingre, S., Bauvy, C., Levade, T., Levine, B. & Codogno, P. Ceramide-induced autophagy: to junk or to protect cells? *Autophagy* **5**, 558-560 (2009).

51. Spassieva, S.D., Mullen, T.D., Townsend, D.M. & Obeid, L.M. Disruption of ceramide synthesis by CerS2 down-regulation leads to autophagy and the unfolded protein response. *Biochem J* **424**, 273-283 (2009).

52. Scarlatti, F. *et al.* Ceramide-mediated macroautophagy involves inhibition of protein kinase B and up-regulation of beclin 1. *J Biol Chem* **279**, 18384-18391 (2004).

53. Hernandez-Tiedra, S. *et al.* Dihydroceramide accumulation mediates cytotoxic autophagy of cancer cells via autolysosome destabilization. *Autophagy* **12**, 2213-2229 (2016).

54. Corcelle-Termeau, E. *et al.* Excess sphingomyelin disturbs ATG9A trafficking and autophagosome closure. *Autophagy* **12**, 833-849 (2016).

55. Wei, H., Liu, L. & Chen, Q. Selective removal of mitochondria via mitophagy: distinct pathways for different mitochondrial stresses. *Biochimica et biophysica acta* **1853**, 2784-2790 (2015).

56. Dunai, Z., Bauer, P.I. & Mihalik, R. Necroptosis: Biochemical, Physiological and Pathological Aspects. *Pathology & Oncology Research* **17**, 791 (2011).

57. Bertrand, M.J. *et al.* cIAP1 and cIAP2 facilitate cancer cell survival by functioning as E3 ligases that promote RIP1 ubiquitination. *Mol Cell* **30**, 689-700 (2008).

58. Moquin, D.M., McQuade, T. & Chan, F.K. CYLD deubiquitinates RIP1 in the TNFalpha-induced necrosome to facilitate kinase activation and programmed necrosis. *PLoS One* **8**, e76841 (2013).

59. Wertz, I.E. *et al.* De-ubiquitination and ubiquitin ligase domains of A20 downregulate NF-kappaB signalling. *Nature* **430**, 694-699 (2004).

60. Chen, D., Yu, J. & Zhang, L. Necroptosis: an alternative cell death program defending against cancer. *Biochimica et biophysica acta* **1865**, 228-236 (2016).

61. Cai, Z. *et al.* Plasma membrane translocation of trimerized MLKL protein is required for TNF-induced necroptosis. *Nat Cell Biol* **16**, 55-65 (2014).

62. Wang, H. *et al.* Mixed lineage kinase domain-like protein MLKL causes necrotic membrane disruption upon phosphorylation by RIP3. *Mol Cell* **54**, 133-146 (2014).

63. Hildebrand, J.M. *et al.* Activation of the pseudokinase MLKL unleashes the four-helix bundle domain to induce membrane localization and necroptotic cell death. *Proc Natl Acad Sci U S A* **111**, 15072-15077 (2014).

64. Meng, M.B. *et al.* Necroptosis in tumorigenesis, activation of anti-tumor immunity, and cancer therapy. *Oncotarget* **7**, 57391-57413 (2016).

65. Saddoughi, S.A. *et al.* Sphingosine analogue drug FTY720 targets I2PP2A/SET and mediates lung tumour suppression via activation of PP2A-RIPK1-dependent necroptosis. *EMBO Mol Med* **5**, 105-121 (2013).

66. Zhang, X. *et al.* Ceramide Nanoliposomes as a MLKL-Dependent, Necroptosis-Inducing, Chemotherapeutic Reagent in Ovarian Cancer. *Mol Cancer Ther* **17**, 50-59 (2018).

67. Sawai, H., Ogiso, H. & Okazaki, T. Differential changes in sphingolipids between TNF-induced necroptosis and apoptosis in U937 cells and necroptosis-resistant sublines. *Leuk Res* **39**, 964-970 (2015).

68. Salazar, M. *et al.* Cannabinoid action induces autophagy-mediated cell death through stimulation of ER stress in human glioma cells. *J Clin Invest* **119**, 1359-1372 (2009).

69. Yacoub, A. *et al.* PERK-dependent regulation of ceramide synthase 6 and thioredoxin play a key role in mda-7/IL-24-induced killing of primary human glioblastoma multiforme cells. *Cancer Res* **70**, 1120-1129 (2010).

70. Fekry, B., Esmaeilniakooshkghazi, A., Krupenko, S.A. & Krupenko, N.I. Ceramide Synthase 6 Is a Novel Target of Methotrexate Mediating Its Antiproliferative Effect in a p53-Dependent Manner. *PLoS One* **11**, e0146618 (2016).

71. Dbaibo, G.S. *et al.* Retinoblastoma gene product as a downstream target for a ceramide-dependent pathway of growth arrest. *Proc Natl Acad Sci U S A* **92**, 1347-1351 (1995).

72. Phillips, D.C. *et al.* Ceramide-induced G2 arrest in rhabdomyosarcoma (RMS) cells requires p21Cip1/Waf1 induction and is prevented by MDM2 overexpression. *Cell Death Differ* **14**, 1780-1791 (2007).

73. Wang, J., Lv, X.W., Shi, J.P. & Hu, X.S. Mechanisms involved in ceramide-induced cell cycle arrest in human hepatocarcinoma cells. *World Journal of Gastroenterology : WJG* **13**, 1129-1134 (2007).

74. Bose, R. *et al.* Ceramide synthase mediates daunorubicin-induced apoptosis: an alternative mechanism for generating death signals. *Cell* **82**, 405-414 (1995).

75. Park, M.A. *et al.* Vorinostat and sorafenib increase CD95 activation in gastrointestinal tumor cells through a Ca(2+)-de novo ceramide-PP2A-reactive oxygen species-dependent signaling pathway. *Cancer Res* **70**, 6313-6324 (2010).

76. Saddoughi, S.A. *et al.* Results of a phase II trial of gemcitabine plus doxorubicin in patients with recurrent head and neck cancers: serum C(1)(8)-ceramide as a novel biomarker for monitoring response. *Clin Cancer Res* **17**, 6097-6105 (2011).

77. Ch'ang, H.J. *et al.* ATM regulates target switching to escalating doses of radiation in the intestines. *Nat Med* **11**, 484-490 (2005).

78. Rotolo, J. *et al.* Anti-ceramide antibody prevents the radiation gastrointestinal syndrome in mice. *J Clin Invest* **122**, 1786-1790 (2012).

79. Dubois, N. *et al.* Plasma ceramide, a real-time predictive marker of pulmonary and hepatic metastases response to stereotactic body radiation therapy combined with irinotecan. *Radiother Oncol* **119**, 229-235 (2016).

80. Venant, H. *et al.* The Sphingosine Kinase 2 Inhibitor ABC294640 Reduces the Growth of Prostate Cancer Cells and Results in Accumulation of Dihydroceramides In Vitro and In Vivo. *Mol Cancer Ther* **14**, 2744-2752 (2015).

81. Britten, C.D. *et al.* A Phase I Study of ABC294640, a First-in-Class Sphingosine Kinase-2 Inhibitor, in Patients with Advanced Solid Tumors. *Clin Cancer Res* **23**, 4642-4650 (2017).

82. Liu, F. *et al.* Ceramide activates lysosomal cathepsin B and cathepsin D to attenuate autophagy and induces ER stress to suppress myeloid-derived suppressor cells. *Oncotarget* **7**, 83907-83925 (2016).

83. Nair, S. *et al.* Clonal Immunoglobulin against Lysolipids in the Origin of Myeloma. *N Engl J Med* **374**, 555-561 (2016).

84. Pandey, M.K. *et al.* Complement drives glucosylceramide accumulation and tissue inflammation in Gaucher disease. *Nature* **543**, 108-112 (2017).

85. Sofi, M.H. *et al.* Ceramide synthesis regulates T cell activity and GVHD development. *JCI Insight* **2** (2017).

86. Senkal, C.E. *et al.* Potent antitumor activity of a novel cationic pyridinium-ceramide alone or in combination with gemcitabine against human head and neck

squamous cell carcinomas in vitro and in vivo. *J Pharmacol Exp Ther* **317**, 1188-1199 (2006).

87. Beckham, T.H. *et al.* LCL124, a cationic analog of ceramide, selectively induces pancreatic cancer cell death by accumulating in mitochondria. *J Pharmacol Exp Ther* **344**, 167-178 (2013).

88. Liu, X. *et al.* Targeting of survivin by nanoliposomal ceramide induces complete remission in a rat model of NK-LGL leukemia. *Blood* **116**, 4192-4201 (2010).

89. Rahmaniyan, M., Curley, R.W., Jr., Obeid, L.M., Hannun, Y.A. & Kraveka, J.M. Identification of dihydroceramide desaturase as a direct in vitro target for fenretinide. *J Biol Chem* **286**, 24754-24764 (2011).

90. Hullin-Matsuda, F. *et al.* Limonoid compounds inhibit sphingomyelin biosynthesis by preventing CERT protein-dependent extraction of ceramides from the endoplasmic reticulum. *J Biol Chem* **287**, 24397-24411 (2012).

91. Pastukhov, O. *et al.* The ceramide kinase inhibitor NVP-231 inhibits breast and lung cancer cell proliferation by inducing M phase arrest and subsequent cell death. *Br J Pharmacol* **171**, 5829-5844 (2014).

92. Cheng, J.C. *et al.* Radiation-induced acid ceramidase confers prostate cancer resistance and tumor relapse. *J Clin Invest* **123**, 4344-4358 (2013).

93. Beckham, T.H. *et al.* Acid ceramidase induces sphingosine kinase 1/S1P receptor 2-mediated activation of oncogenic Akt signaling. *Oncogenesis* **2**, e49 (2013).

94. Tirodkar, T.S. *et al.* Expression of Ceramide Synthase 6 Transcriptionally Activates Acid Ceramidase in a c-Jun N-terminal Kinase (JNK)-dependent Manner. *J Biol Chem* **290**, 13157-13167 (2015).

95. Cohen, J.A. *et al.* Oral fingolimod or intramuscular interferon for relapsing multiple sclerosis. *N Engl J Med* **362**, 402-415 (2010).

96. Kappos, L. *et al.* A placebo-controlled trial of oral fingolimod in relapsing multiple sclerosis. *N Engl J Med* **362**, 387-401 (2010).

97. Neviani, P. *et al.* PP2A-activating drugs selectively eradicate TKI-resistant chronic myeloid leukemic stem cells. *J Clin Invest* **123**, 4144-4157 (2013).

98. Ponnusamy, S. *et al.* Communication between host organism and cancer cells is transduced by systemic sphingosine kinase 1/sphingosine 1-phosphate signalling to regulate tumour metastasis. *EMBO Mol Med* **4**, 761-775 (2012).

99. Li, M.H. *et al.* Antitumor Activity of a Novel Sphingosine-1-Phosphate 2 Antagonist, AB1, in Neuroblastoma. *J Pharmacol Exp Ther* **354**, 261-268 (2015).

100. Kapitonov, D. *et al.* Targeting sphingosine kinase 1 inhibits Akt signaling, induces apoptosis, and suppresses growth of human glioblastoma cells and xenografts. *Cancer Res* **69**, 6915-6923 (2009).

101. Schnute, M.E. *et al.* Modulation of cellular S1P levels with a novel, potent and specific inhibitor of sphingosine kinase-1. *Biochem J* **444**, 79-88 (2012).

102. Kennedy, P.C. *et al.* Characterization of a sphingosine 1-phosphate receptor antagonist prodrug. *J Pharmacol Exp Ther* **338**, 879-889 (2011).

103. Pal, S.K. *et al.* A phase 2 study of the sphingosine-1-phosphate antibody sonepcizumab in patients with metastatic renal cell carcinoma. *Cancer* **123**, 576-582 (2017).

104. Lewis, C.S., Voelkel-Johnson, C. & Smith, C.D. Suppression of c-Myc and RRM2 expression in pancreatic cancer cells by the sphingosine kinase-2 inhibitor ABC294640. *Oncotarget* **7**, 60181-60192 (2016).

105. Cohen, J.A. *et al.* Oral fingolimod or intramuscular interferon for relapsing multiple sclerosis. *N Engl J Med* **362**, 402-415 (2010).

106. Kappos, L. *et al.* A placebo-controlled trial of oral fingolimod in relapsing multiple sclerosis. *N Engl J Med* **362**, 387-401 (2010).

107. Hisano, Y., Kobayashi, N., Kawahara, A., Yamaguchi, A. & Nishi, T. The sphingosine 1-phosphate transporter, SPNS2, functions as a transporter of the phosphorylated form of the immunomodulating agent FTY720. *J Biol Chem* **286**, 1758-1766 (2011).

108. Kihara, A. & Igarashi, Y. Production and release of sphingosine 1-phosphate and the phosphorylated form of the immunomodulator FTY720. *Biochimica et biophysica acta* **1781**, 496-502 (2008).

109. Liang, J. *et al.* Sphingosine-1-phosphate links persistent STAT3 activation, chronic intestinal inflammation, and development of colitis-associated cancer. *Cancer Cell* **23**, 107-120 (2013).

110. Velmurugan, B.K. *et al.* PP2A deactivation is a common event in oral cancer and reactivation by FTY720 shows promising therapeutic potential. *J Cell Physiol* **233**, 1300-1311 (2018).

111. Cristobal, I. *et al.* PP2A inhibition is a common event in colorectal cancer and its restoration using FTY720 shows promising therapeutic potential. *Mol Cancer Ther* **13**, 938-947 (2014).

112. Beider, K. *et al.* The Sphingosine-1-Phosphate Modulator FTY720 Targets Multiple Myeloma via the CXCR4/CXCL12 Pathway. *Clin Cancer Res* **23**, 1733-1747 (2017).

113. Yasui, H. *et al.* FTY720 induces apoptosis in multiple myeloma cells and overcomes drug resistance. *Cancer Res* **65**, 7478-7484 (2005).

114. Zhang, L., Wang, H., Ding, K. & Xu, J. FTY720 induces autophagy-related apoptosis and necroptosis in human glioblastoma cells. *Toxicol Lett* **236**, 43-59 (2015).

115. Li, Y. *et al.* Combination treatment of FTY720 and cisplatin exhibits enhanced antitumour effects on cisplatin-resistant non-small lung cancer cells. *Oncol Rep* **39**, 565-572 (2018).

116. Martin, J.L. *et al.* Inhibition of basal-like breast cancer growth by FTY720 in combination with epidermal growth factor receptor kinase blockade. *Breast cancer research : BCR* **19**, 90 (2017).

117. Marvaso, G. *et al.* Sphingosine analog fingolimod (FTY720) increases radiation sensitivity of human breast cancer cells in vitro. *Cancer Biol Ther* **15**, 797-805 (2014).

118. Schiffmann, S. *et al.* Inhibitors of specific ceramide synthases. *Biochimie* **94**, 558-565 (2012).

119. Huang, W.C. *et al.* Glucosylceramide synthase inhibitor PDMP sensitizes chronic myeloid leukemia T315I mutant to Bcr-Abl inhibitor and cooperatively induces glycogen synthase kinase-3-regulated apoptosis. *FASEB J* **25**, 3661-3673 (2011).

120. Tonelli, F. *et al.* FTY720 and (S)-FTY720 vinylphosphonate inhibit sphingosine kinase 1 and promote its proteasomal degradation in human pulmonary artery smooth muscle, breast cancer and androgen-independent prostate cancer cells. *Cellular signalling* **22**, 1536-1542 (2010).

121. Bandhuvula, P., Tam, Y.Y., Oskouian, B. & Saba, J.D. The immune modulator FTY720 inhibits sphingosine-1-phosphate lyase activity. *J Biol Chem* **280**, 33697-33700 (2005).

122. Jin, Y., Zollinger, M., Borell, H., Zimmerlin, A. & Patten, C.J. CYP4F enzymes are responsible for the elimination of fingolimod (FTY720), a novel treatment of

relapsing multiple sclerosis. *Drug metabolism and disposition: the biological fate of chemicals* **39**, 191-198 (2011).

123. Mechtcheriakova, D. *et al.* FTY720-phosphate is dephosphorylated by lipid phosphate phosphatase 3. *FEBS Lett* **581**, 3063-3068 (2007).

124. Yamanaka, M., Anada, Y., Igarashi, Y. & Kihara, A. A splicing isoform of LPP1, LPP1a, exhibits high phosphatase activity toward FTY720 phosphate. *Biochem Biophys Res Commun* **375**, 675-679 (2008).

125. Berdyshev, E.V. *et al.* FTY720 inhibits ceramide synthases and up-regulates dihydrosphingosine 1-phosphate formation in human lung endothelial cells. *J Biol Chem* **284**, 5467-5477 (2009).

126. Lahiri, S. *et al.* Ceramide synthesis is modulated by the sphingosine analog FTY720 via a mixture of uncompetitive and noncompetitive inhibition in an Acyl-CoA chain length-dependent manner. *J Biol Chem* **284**, 16090-16098 (2009).

127. Bailey, L.J., Alahari, S., Tagliaferro, A., Post, M. & Caniggia, I. Augmented trophoblast cell death in preeclampsia can proceed via ceramide-mediated necroptosis. *Cell Death Dis* **8**, e2590 (2017).

128. Thomas, R.J. *et al.* HPV/E7 induces chemotherapy-mediated tumor suppression by ceramide-dependent mitophagy. *EMBO Mol Med* (2017).

129. Marfia, G. *et al.* Autocrine/paracrine sphingosine-1-phosphate fuels proliferative and stemness qualities of glioblastoma stem cells. *Glia* **62**, 1968-1981 (2014).

130. Bieberich, E. Ceramide in stem cell differentiation and embryo development: novel functions of a topological cell-signaling lipid and the concept of ceramide compartments. *J Lipids* **2011**, 610306 (2011).

131. Bieberich, E. Ceramide and sphingosine-1-phosphate signaling in embryonic stem cell differentiation. *Methods Mol Biol* **874**, 177-192 (2012).

132. He, Q. *et al.* Primary cilia in stem cells and neural progenitors are regulated by neutral sphingomyelinase 2 and ceramide. *Mol Biol Cell* **25**, 1715-1729 (2014).

133. Konig, A. & Shcherbata, H.R. Visualization of adult stem cells within their niches using the Drosophila germline as a model system. *Methods Mol Biol* **1035**, 25-33 (2013).

134. Wodarz, A. Establishing cell polarity in development. *Nat Cell Biol* **4**, E39-44 (2002).

135. Pellettieri, J. & Seydoux, G. Anterior-posterior polarity in C. elegans and Drosophila--PARallels and differences. *Science* **298**, 1946-1950 (2002).

136. Peng, J.C., Valouev, A., Liu, N. & Lin, H. Piwi maintains germline stem cells and oogenesis in Drosophila through negative regulation of Polycomb group proteins. *Nat Genet* **48**, 283-291 (2016).

137. Ji, Y. & Tulin, A.V. Poly(ADP-ribose) controls DE-cadherin-dependent stem cell maintenance and oocyte localization. *Nat Commun* **3**, 760 (2012).

138. Fast, E.M. *et al.* Wolbachia enhance Drosophila stem cell proliferation and target the germline stem cell niche. *Science* **334**, 990-992 (2011).

139. Bauer, R. *et al.* Schlank, a member of the ceramide synthase family controls growth and body fat in Drosophila. *EMBO J* **28**, 3706-3716 (2009).

140. Ables, E.T., Hwang, G.H., Finger, D.S., Hinnant, T.D. & Drummond-Barbosa, D. A Genetic Mosaic Screen Reveals Ecdysone-Responsive Genes Regulating Drosophila Oogenesis. *G3 (Bethesda)* **6**, 2629-2642 (2016).

141. Panneer Selvam, S. *et al.* Binding of the sphingolipid S1P to hTERT stabilizes telomerase at the nuclear periphery by allosterically mimicking protein phosphorylation. *Sci Signal* **8**, ra58 (2015).

142. Bielawski, J. *et al.* Comprehensive quantitative analysis of bioactive sphingolipids by high-performance liquid chromatography-tandem mass spectrometry. *Methods Mol Biol* **579**, 443-467 (2009).

143. Levental, K.R. & Levental, I. Giant plasma membrane vesicles: models for understanding membrane organization. *Curr Top Membr* **75**, 25-57 (2015).

144. Levental, K.R. & Levental, I. Isolation of giant plasma membrane vesicles for evaluation of plasma membrane structure and protein partitioning. *Methods Mol Biol* **1232**, 65-77 (2015).

145. Vilar, S., Cozza, G. & Moro, S. Medicinal chemistry and the molecular operating environment (MOE): application of QSAR and molecular docking to drug discovery. *Curr Top Med Chem* **8**, 1555-1572 (2008).

146. Harris, P.A. *et al.* Discovery of Small Molecule RIP1 Kinase Inhibitors for the Treatment of Pathologies Associated with Necroptosis. *ACS Med Chem Lett* **4**, 1238-1243 (2013).

147. Harris, P.A. *et al.* DNA-Encoded Library Screening Identifies Benzo[b][1,4]oxazepin-4-ones as Highly Potent and Monoselective Receptor Interacting Protein 1 Kinase Inhibitors. *J Med Chem* **59**, 2163-2178 (2016).

148. Wei, Z., Liu, X., Yu, C. & Zhang, M. Structural basis of cargo recognitions for class V myosins. *Proc Natl Acad Sci U S A* **110**, 11314-11319 (2013).

149. Karam, J.A., Parikh, R.Y., Nayak, D., Rosenkranz, D. & Gangaraju, V.K. Co-chaperone Hsp70/Hsp90-organizing protein (Hop) is required for transposon silencing and Piwi-interacting RNA (piRNA) biogenesis. *J Biol Chem* **292**, 6039-6046 (2017).

150. Krishnamurthy, K., Dasgupta, S. & Bieberich, E. Development and characterization of a novel anti-ceramide antibody. *Journal of lipid research* **48**, 968-975 (2007).

151. Tsapras, P., Sagona, A.P. & Nezis, I.P. Immuno-Gold Labeling of Drosophila Follicles for Transmission Electron Microscopy, in *Oogenesis: Methods and Protocols*. (ed. I.P. Nezis) 97-103 (Springer New York, New York, NY; 2016).

152. Sorge, R.E. *et al.* Genetically determined P2X7 receptor pore formation regulates variability in chronic pain sensitivity. *Nat Med* **18**, 595-599 (2012).

153. Allingham, J.S., Smith, R. & Rayment, I. The structural basis of blebbistatin inhibition and specificity for myosin II. *Nat Struct Mol Biol* **12**, 378-379 (2005).

154. Tepper, A.D. *et al.* Sphingomyelin hydrolysis to ceramide during the execution phase of apoptosis results from phospholipid scrambling and alters cell-surface morphology. *J Cell Biol* **150**, 155-164 (2000).

155. Trajkovic, K. *et al.* Ceramide triggers budding of exosome vesicles into multivesicular endosomes. *Science* **319**, 1244-1247 (2008).

156. Cowart, L.A., Szulc, Z., Bielawska, A. & Hannun, Y.A. Structural determinants of sphingolipid recognition by commercially available anti-ceramide antibodies. *Journal of lipid research* **43**, 2042-2048 (2002).

157. Visentin, B. *et al.* Validation of an anti-sphingosine-1-phosphate antibody as a potential therapeutic in reducing growth, invasion, and angiogenesis in multiple tumor lineages. *Cancer Cell* **9**, 225-238 (2006).

158. Ohno-Iwashita, Y. *et al.* Cholesterol-binding toxins and anti-cholesterol antibodies as structural probes for cholesterol localization. *Subcell Biochem* **51**, 597-621 (2010).

159. Dworski, S. *et al.* Acid Ceramidase Deficiency is characterized by a unique plasma cytokine and ceramide profile that is altered by therapy. *Biochimica et biophysica acta* **1863**, 386-394 (2017).

160. Omar, H.A. *et al.* Antitumor effects of OSU-2S, a nonimmunosuppressive analogue of FTY720, in hepatocellular carcinoma. *Hepatology* **53**, 1943-1958 (2011).

161. Rabionet, M. *et al.* Male germ cells require polyenoic sphingolipids with complex glycosylation for completion of meiosis: a link to ceramide synthase-3. *J Biol Chem* **283**, 13357-13369 (2008).

162. Sun, L. *et al.* Mixed lineage kinase domain-like protein mediates necrosis signaling downstream of RIP3 kinase. *Cell* **148**, 213-227 (2012).

163. Schilling, W.P., Wasylyna, T., Dubyak, G.R., Humphreys, B.D. & Sinkins, W.G. Maitotoxin and P2Z/P2X(7) purinergic receptor stimulation activate a common cytolytic pore. *Am J Physiol* **277**, C766-776 (1999).

164. Allsopp, R.C., Dayl, S., Schmid, R. & Evans, R.J. Unique residues in the ATP gated human P2X7 receptor define a novel allosteric binding pocket for the selective antagonist AZ10606120. *Sci Rep* **7**, 725 (2017).

165. Hanada, K. *et al.* Molecular machinery for non-vesicular trafficking of ceramide. *Nature* **426**, 803-809 (2003).

166. Najjar, M. *et al.* Structure guided design of potent and selective ponatinib-based hybrid inhibitors for RIPK1. *Cell Rep* **10**, 1850-1860 (2015).

167. Lev, S. Nonvesicular lipid transfer from the endoplasmic reticulum. *Cold Spring Harb Perspect Biol* **4** (2012).

168. Iwasa, A. *et al.* Cellular uptake and subsequent intracellular trafficking of R8-liposomes introduced at low temperature. *Biochimica et Biophysica Acta (BBA) - Biomembranes* **1758**, 713-720 (2006).

169. Ogretmen, B. *et al.* Biochemical mechanisms of the generation of endogenous long chain ceramide in response to exogenous short chain ceramide in the A549 human lung adenocarcinoma cell line. Role for endogenous ceramide in mediating the action of exogenous ceramide. *J Biol Chem* **277**, 12960-12969 (2002).

170. Zhu, X., Ma, Y. & Liu, D. Novel agents and regimens for acute myeloid leukemia: 2009 ASH annual meeting highlights. *J Hematol Oncol* **3**, 17 (2010).

171. Nakai, R. *et al.* K858, a novel inhibitor of mitotic kinesin Eg5 and antitumor agent, induces cell death in cancer cells. *Cancer Res* **69**, 3901-3909 (2009).

172. Sainath, R. & Gallo, G. The dynein inhibitor Ciliobrevin D inhibits the bidirectional transport of organelles along sensory axons and impairs NGF-mediated regulation of growth cones and axon branches. *Dev Neurobiol* **75**, 757-777 (2015).

173. Wang, Y.H. *et al.* DNA damage causes rapid accumulation of phosphoinositides for ATR signaling. *Nat Commun* **8**, 2118 (2017).

174. Petrosyan, A., Ali, M.F., Verma, S.K., Cheng, H. & Cheng, P.W. Non-muscle myosin IIA transports a Golgi glycosyltransferase to the endoplasmic reticulum by binding to its cytoplasmic tail. *Int J Biochem Cell Biol* **44**, 1153-1165 (2012).

175. Lin, P. *et al.* Nonmuscle myosin IIA facilitates vesicle trafficking for MG53-mediated cell membrane repair. *Faseb j* **26**, 1875-1883 (2012).

176. Milberg, O. *et al.* Concerted actions of distinct nonmuscle myosin II isoforms drive intracellular membrane remodeling in live animals. *J Cell Biol* **216**, 1925-1936 (2017).

177. Vasquez, C.G., Heissler, S.M., Billington, N., Sellers, J.R. & Martin, A.C. Drosophila non-muscle myosin II motor activity determines the rate of tissue folding. *Elife* **5** (2016).

178. Mhatre, A.N. *et al.* Generation and characterization of mice with Myh9 deficiency. *Neuromolecular medicine* **9**, 205-215 (2007).

179. Young, P.E., Pesacreta, T.C. & Kiehart, D.P. Dynamic changes in the distribution of cytoplasmic myosin during Drosophila embryogenesis. *Development* **111**, 1-14 (1991).

180. Young, P.E., Richman, A.M., Ketchum, A.S. & Kiehart, D.P. Morphogenesis in Drosophila requires nonmuscle myosin heavy chain function. *Genes Dev* **7**, 29-41 (1993).

181. Schramek, D. *et al.* Direct in vivo RNAi screen unveils myosin IIa as a tumor suppressor of squamous cell carcinomas. *Science* **343**, 309-313 (2014).

182. Coaxum, S.D. *et al.* The tumor suppressor capability of p53 is dependent on non-muscle myosin IIA function in head and neck cancer. *Oncotarget* **8**, 22991-23007 (2017).

183. Sezgin, E. *et al.* Elucidating membrane structure and protein behavior using giant plasma membrane vesicles. *Nat Protoc* **7**, 1042-1051 (2012).

184. Galluzzi, L., Kepp, O. & Kroemer, G. MLKL regulates necrotic plasma membrane permeabilization. *Cell Res* **24**, 139-140 (2014).

185. Dondelinger, Y. *et al.* MLKL compromises plasma membrane integrity by binding to phosphatidylinositol phosphates. *Cell Rep* **7**, 971-981 (2014).

186. Gong, Y.N., Guy, C., Crawford, J.C. & Green, D.R. Biological events and molecular signaling following MLKL activation during necroptosis. *Cell Cycle* **16**, 1748-1760 (2017).

187. Strelow, A. *et al.* Overexpression of acid ceramidase protects from tumor necrosis factor-induced cell death. *J Exp Med* **192**, 601-612 (2000).

188. Lang, K.S. *et al.* Involvement of ceramide in hyperosmotic shock-induced death of erythrocytes. *Cell Death Differ* **11**, 231-243 (2004).

189. Zhang, Y., Chen, X., Gueydan, C. & Han, J. Plasma membrane changes during programmed cell deaths. *Cell Res* **28**, 9-21 (2018).

190. Siskind, L.J. & Colombini, M. The lipids C2- and C16-ceramide form large stable channels. Implications for apoptosis. *J Biol Chem* **275**, 38640-38644 (2000).

191. Siskind, L.J. *et al.* Anti-apoptotic Bcl-2 Family Proteins Disassemble Ceramide Channels. *J Biol Chem* **283**, 6622-6630 (2008).

192. Tran, D.T., Masedunskas, A., Weigert, R. & Ten Hagen, K.G. Arp2/3-mediated F-actin formation controls regulated exocytosis in vivo. *Nat Commun* **6**, 10098 (2015).

193. Lin, C. *et al.* Active diffusion and microtubule-based transport oppose myosin forces to position organelles in cells. *Nat Commun* **7**, 11814 (2016).

194. Senol, O. *et al.* miR-200a-mediated suppression of non-muscle heavy chain IIb inhibits meningioma cell migration and tumor growth in vivo. *Oncogene* **34**, 1790-1798 (2015).

195. Kleino, A. *et al.* Peptidoglycan-Sensing Receptors Trigger the Formation of Functional Amyloids of the Adaptor Protein Imd to Initiate Drosophila NF-kappaB Signaling. *Immunity* **47**, 635-647 e636 (2017).

196. Inaba, M., Buszczak, M. & Yamashita, Y.M. Nanotubes mediate niche-stem-cell signalling in the Drosophila testis. *Nature* **523**, 329-332 (2015).

197. Hampoelz, B. *et al.* Pre-assembled Nuclear Pores Insert into the Nuclear Envelope during Early Development. *Cell* **166**, 664-678 (2016).

198. Chen, H., Chen, X. & Zheng, Y. The nuclear lamina regulates germline stem cell niche organization via modulation of EGFR signaling. *Cell Stem Cell* **13**, 73-86 (2013).

199. Gangaraju, V.K. *et al.* Drosophila Piwi functions in Hsp90-mediated suppression of phenotypic variation. *Nat Genet* **43**, 153-158 (2011).

200. Ku, H.Y., Gangaraju, V.K., Qi, H., Liu, N. & Lin, H. Tudor-SN Interacts with Piwi Antagonistically in Regulating Spermatogenesis but Synergistically in Silencing Transposons in Drosophila. *PLoS Genet* **12**, e1005813 (2016).

201. Lee, S., Zhou, L., Kim, J., Kalbfleisch, S. & Schock, F. Lasp anchors the Drosophila male stem cell niche and mediates spermatid individualization. *Mech Dev* **125**, 768-776 (2008).

202. Huynh, J.-R. Fusome as a Cell-Cell Communication Channel of Drosophila Ovarian Cyst, in *Cell-Cell Channels* 217-235 (Springer New York, New York, NY; 2006).

203. Aldaz, S., Escudero, L.M. & Freeman, M. Dual role of myosin II during Drosophila imaginal disc metamorphosis. *Nat Commun* **4**, 1761 (2013).